People's Democratic Republic of Algeria

Ministry of Higher Education and Scientific Research

University of Echahid Hamma Lakhdar-El-Oued

FACULTY OF TECHNOLOGY

DEPARTEMENT OF MECHANICAL ENGINEERING

Ph.D Thesis

Presented to fulfill the requirements to obtain

ACADEMIC Ph.D DEGREE

Subject-Field: Sciences and Technology

Option: Mechanical engineering

Specialty: Energetics

Presented by:

Nacer Lebbihiat

30/06/2024

Subject

Modeling and optimization of geothermal heat exchanger performance under Sub-Saharan climate region - Algeria -

Thesis examination committee:

Dr. Ali Boukhari	MCA	University of El Oued	Chairman
Dr. Sidi Mohammed El Amine Bekkouche	MCA	URAER of Ghardaïa	Examiner
Dr. Abdelouahab Benseddik	MCA	URAER of Ghardaïa	Examiner
Pr. Boubaker Benhaoua	Professor	University of El Oued	Examiner
Pr. Abdelmalek Atia	Professor	University of El Oued	Supervisor
Dr. Noureddine Meneceur	MCA	University of El Oued	Co-supervisor

2023/2024

Dedications

This work is dedicated:

To my parents for their love, confidence, and motivation, may this work be a testimony of my deep gratitude.

To my wife and children.

To my brothers and sisters.

To my professors.

To all my family.

To all my friends.

To anyone who ever gave me love, hope and support.

Nacer

Acknowledgments

First and foremost, thank is to the Almighty Allah for endowing us the will and strength to complete this thesis. The gratitude must be also expressed to our respected supervisor Pr. Abdelmalek Atia, associate professor, Department of mechanical engineering, University of El-Oued, for his substantial guidance, support and care delivered throughout the process of carrying out this research. he will always be a source of inspiration.

Also, sincere thanks and appreciation to Dr. Noureddine Meneceur, Associate professor, Department of mechanical engineering, University of El-Oued, for extending his cordial support, guidance during the operation of conducting this research.

My special acknowledges go to Pr. Müslüm Arici (Kocaeli University, Turkey) for his guidance, precious help and valuable advices.

Gratitude must be also expressed to anyone who lay a hand of help accomplishing this research, especially Mr. Abdelhak Keddouda and Dr. Ali Boukhari, and for all professors of the department of the mechanical engineering at the University of El-Oued.

Last but not the least, we would like express our gratitude to our friends, families and our beloved ones for their continuous support, patience and confidence which made this work see the light on this day.

Table of contents

List of tables

List of figures

Nomenclature

A	Heat exchange area	(m^2)
C_p	Air specific heat.	$(\mathrm{J.kg^{-1}K^{-1}})$
D	Diameter of heat exchanger.	(m)
d	Pipe diameter.	(m)
d^*	Dimensionless pipe diameter.	$(-)$
$\Delta\mathrm{T}$	Temperature difference.	$(°\mathrm{C})$
ΔTLM	Log mean temperature drop.	$(°\mathrm{C})$
E	Effectiveness	$(-)$
f	Friction factor	$(-)$
k	Thermal conductivity.	$(\mathrm{W.m^{-1}K^{-1}})$
L	Length.	(m)
$\dot{m}$	Air mass flow rate	$(\mathrm{kg.s^{1}})$
P	Pressure.	$(\mathrm{N.m^{-2}})$
P^*	Dimensionless pressure.	$(-)$
$\dot{Q}$	Heat exchange rate	(W)
R	Total thermal resistance	$(°\mathrm{C.mW^{-1}})$
T	Temperature.	$(°\mathrm{C})$
T^*	Dimensionless Temperature.	$(-)$
t	Pipe thickness / time.	$(\mathrm{m})/\ (s)$
t^*	Dimensionless pipe thickness.	$(-)$
U	Overall heat transfer coefficient.	$(\mathrm{W.m^{-2}°C^{-1}})$
$\mathrm{u,v,w}$	Velocity components.	$(\mathrm{m.s^{1}})$
$\mathrm{u^*,\ v^*,\ w^*}$	Dimensionless velocity components.	$(-)$
$\mathrm{x,y,z}$	Cartesian coordinates.	$(-)$
$\mathrm{x^*,\ y^*,\ z^*}$	Dimensionless Cartesian coordinates.	(m)
Z	Depth.	(m)

Greek Symbols

ρ	Density	$(\mathrm{kg.m^{-3}})$
μ	Dynamic viscosity.	$(\mathrm{kg.m^{-1}.s^{-1}})$
α	Thermal diffusivity.	$(\mathrm{m^2.s^{-1}})$

Dimensionless numbers

Re	Reynolds number.	$(-)$

Subscripts

act	Actual.
avg	Average.
c	Curved pipe.
in	Inlet.
max	Maximum.
out	Outlet.
s	Straight pipe.
so	Soil.
$\mathrm{i, n, p}$	Indices

Abbreviations

EAHE	Earth Air Heat Exchanger.
GAHE	Ground Air Heat Exchanger.
GSHP	Ground Source Heat Pump.
H	Hour.
HER	Heat Exchange Rate.
HGAHE	Helical Ground Air Heat Exchanger.
MAE	Mean Absolute Error.
MAPE	Mean Absolute Percentage Error.
MLR	Multiple-Linear Regression.
MSE	Mean Squared Error.
RMSE	Root Mean Squared Error.
TPDF	Thermal Performance Derating Factor.

GENERAL INTRODUCTION

GENERAL INTRODUCTION

CONTEXT

Climate change, caused by greenhouse gases such as CO_2 generated from burning of fossil fuels, has become an important concern for the global scientific community. Worldwide total population growth, along with the rising needs has further increased the energy demand, bringing about depletion of fossil fuels at a higher rate. As a direct consequence of this, both developed and developing countries are now looking for alternative energy source. The importance of concept of energy security, sustainable development and low carbon technologies have been increasing on both political and social agendas [1, 2].

Recently, international climate negotiations, legislations, and policies on the renewable energy utilization increased with the aim of increasing the share of renewable energies to meet the increasing energy demand. Under the Paris Agreement, 109 parties had provided quantified renewable energy goals [3]. Energy consumption of fossil fuels and its negative effect on the climate change can be decreased considerably by the exploitation of renewable energy sources. Renewable energy systems employ naturally available resources, which are persistently replenished through natural resources, such as wind, solar and wave energy, geothermal heat, and tidal movements. The renewable systems contributed, by 24.5 % to generation of electricity and 19.3 % to global energy consumption in 2016, which proven their importance in the worldwide energy utilization [4].

Algeria's commitment to the environment, energy security and climate change mitigation under the Paris Agreement has proven in all levels of government, communicating the utmost importance of utilizing more renewable and sustainable energy resources available as an alternative solution to lessen the dependence on limited fossil fuel reserves. Algeria participates in many renewable energy programs such as the Mediterranean Renewable Energy Program (MEDREP), which is managed by the Mediterranean Center for Renewable Energies (MEDREC) of Tunisia for the purpose of delivering sustainable energy services to populations, particularly in rural areas, and help to mitigate climate change by promoting the utilization of renewable energy in the region [5].

Geothermal energy, which is environmentally friendly, green, reliable, and sustainable, is classified as one of the important types of renewable energies. It is basically the heat generated and stored beneath the crust of Earth, originating from the formation of the planet.

However, geothermal energy generally refers to the part of the Earth’s heat that can be found from the shallow ground and employed for various industrial applications such as electricity generation, space heating/cooling, and aquaculture, and for domestic and therapeutic applications such as bathing and swimming [6, 7]. A number of techniques are used to harness the geothermal energy potential, all of which exert to utilize the thermal energy stored within the Earth. Basically, shallow and deep geothermal techniques are employed to exploit respectively low and high enthalpy resources [8, 9].

Shallow geothermal approaches try to extract thermal energy from the Earth's crust's top layers. The methods used to extract shallow geothermal energy are generally referred to as 'ground air heat exchanger' systems. The systems are well suited for using low entropy systems to offer space heating and/or cooling. The energy government figures showed the proportion of energy used to provide space heating and cooling in South Algeria which can be classified as desert climate (hot and arid) with an average ambient temperature around 45°C during summer months. Therefore, the achievement of indoor thermal comfort whilst minimizing energy consumption in buildings under desert climates is a key challenge which highlights the potential significance of ground air heat exchanger systems as an alternative to traditional fossil fuels, which are currently used for space heating and cooling. The use of ground air heat exchanger systems can help to decrease energy loads on the national grid while simultaneously increasing energy diversity.

PROBLEMATIC

Ground air heat exchanger (GAHE) can be deployed to cool or warm air for building air conditioning, therefore decreasing the energy requirement for ventilation purposes passively, and contributes in a cleaner built environment. The GAHEs use the earth's undisturbed temperature as a heat source. When air passes across the ducts, thermal energy is transmitted from air to ground or from ground to air depends to the air temperature relative to the soil temperature which remains more than the outdoor air temperature during winter, and lower in summer, for air heating/cooling based on the seasonal energy needs.

Previous research has shown that GAHE systems have a significant potential for providing cooling and heating effect as well as a viable solution for taking the advantage of the underground temperature. However, several researchers reveal that among the main problems hindering the spreading of the GAHE is the large installation area as well as the excavation cost required for long pipes to attain the desired amount of heat transfer. Thus, various researchers have studied non-straight pipe configurations in the aim of achieving extra tube length per unit trench length to assure the desired amount of heat exchange rate.

According to the literature, it has been identified that the helical-pipe configuration requires a lesser ground space for installing longer pipes. The helical-coil layout has been extensively studied by various researchers in the ground source heat pump (GSHP) system. However, this configuration still has not been examined in real applications of GAHE system under Saharan climate.

STUDY OBJECTIVES

The aim of the research presented is to advance knowledge regarding the ground air heat exchanger behavior under Saharan climate using a proposed helical-coil layout. This has been achieved through the field-scale monitoring of a newly installed system and the development of a numerical model capable of simulating the helical ground air heat exchanger (HGAHE) system behavior.

- To review geothermal energy utilization in Algeria and around the globe as well as to propose countermeasures and solutions to promote geothermal energy development in Algeria.

- To conduct a real in-situ experimental set up of the proposed helical configuration of ground air heat exchanger for summer cooling under arid climate.

- To establish a transient numerical model of the HGAHE system and validated against the experimental data.

- To assess the thermal behavior of helical-coil layout GAHE experimentally under Saharan climate.

- To analyze thermal performance of the proposed helical shaped GAHE system numerically using ANSYS Fluent.

- To investigate the influence of different important operating and geometric parameters using the validated numerical model.

THESIS ORGANIZATION

Chapter I contains a literature review salient to the work contained in this thesis. The literature review has been split broadly into two sections inspecting; i) the existing literature and current practices of the Algeria's geothermal resources are reviewed and geothermal energy use and latest technologies around the world have been summarized. This section elucidates the influencing factors in the development of geothermal energy in Algeria and suggests the development roadmap and a number of measures that can enhance the development of this significant energy source. ii) reviewed the design aspects of GAHE systems. In particular are discussed the classification and types of GAHEs such as open or closed loop systems, vertical or horizontal, U-tube or helical. Furthermore, the possible applications as well as the recent research trends of the GAHE systems have been addressed.

The design and implementation of the in-situ experimental set up of the proposed helical configuration of ground air heat exchanger are presented in Chapter II. The experimental methodology and sensors selected for use are presented along with details regarding the thermal performance modeling of the HGAHE system

Mathematical formulations for the coupled heat and mass model used in this thesis are presented in Chapter III. Moreover, numerical procedure, boundary conditions as well as solution techniques implemented within the current work is presented.

Chapter IV presents the results and discussion of the work contained in this thesis. The results and discussion have been split broadly into three sections; i) experimental analyzes of the thermal performance of the proposed helical ground air heat exchanger for cooling purposes under Saharan climate. ii) the developed model is validated against the experimental data, later on, the numerically simulated has been applied to assess the thermal behavior of the helical-coil layout GAHE computationally. iii) the transient numerical model of the HGAHE system has been employed to investigate the influence of different important operating and geometric parameters. Furthermore, along with the parametric results, multiple regression method has been used to propose effective model to predict thermal performance of the HGAHE system. Thus, the obtained results from this work can be used as a valuable guidance to achieve an optimized design of HGAHE systems.

CHAPTER I : LITERATURE REVIEW

I.1 Introduction

This chapter will focus on research which has been conducted within the scope of the current thesis. The review has been sub-divided into two sections. The first section reviews the available literature and current practices on the Algeria's geothermal resources and discusses the development roadmap. Moreover, geothermal energy use and up to date technologies around the globe have been summarized. The main obstacles to the development and utilization of geothermal energy in Algeria are analyzed, and possible utilization opportunities are addressed. Besides, countermeasures and solutions to promote the development and utilization of geothermal energy in the country are proposed. The second section reviewed the recent research trends of the GAHE systems. In particular are discussed the classification and types of GAHEs such as open or closed loop systems, as well as the various configurations and their advantageous and disadvantageous. Furthermore, the possible applications as well as the research gab and limitation have been addressed.

I.2 Geothermal energy

Basically, it is the heat generated and stored beneath the crust of Earth originating from the formation of the planet. However, geothermal energy generally refers to the part of the Earth's heat that can be found from the shallow ground and employed for various industrial applications. Geothermal energy is a clean, reliable and environmentally friendly source, which can contribute to social sustainable development and help to protect the global environment [7].

I.2.1 Around the globe

Geothermal energy is one of the world's top priorities as an alternative source for reducing worldwide fossil-fuel dependence and its environmental issues such as the emission of global greenhouse gases. The world geothermal resource evaluation estimated that around 68 % of the total resources have temperatures below 130 °C, which is suitable for direct use applications and the rest of the share (32 %) has temperatures above 130 °C, which is suitable for power generation [10]. In the following subsections geothermal energy use and latest technologies will be discussed.

I.2.1.1 Current status

Geothermal energy use is classified into two groups based on the geothermal resource temperature: direct-use and power generation. For the direct use group, there are a total of 82 countries reporting direct utilization of geothermal energy with an estimated installed capacity at 70,885 MW_t globally, at a growth rate of 7.9 % per year. The worldwide thermal energy use, estimated at 592,638 TJ/year, is growing with a compound rate of 6.9 % per year. The leading country in the direct usage of geothermal energy is China with 17,870 MW_t installed thermal capacity accounting for 25.2 % of the world capacity. Nine categories of direct utilization have been identified, namely, heat pumps, bathing and swimming, space heating, greenhouses heating, aquaculture, industrial uses, space cooling and snow melting, agricultural crop drying and other uses. The top 10 countries in direct use and the distribution of the worldwide geothermal direct use applications are shown in Figure I.1 and Figure I.2, respectively [11, 12].

It has been reported that the installed capacity of the ground-source (geothermal) heat pumps worldwide is 50,258 MW_t and the yearly energy use is 326,848 TJ. Geothermal heat pumps have the highest installed capacity (about 70.90 %) and the largest energy use (accounting for 55.15 %) worldwide. Majority of the ground-source heat pumps are implemented in North America, Europe, and China. The number of countries adopted geothermal heat pump is nearly doubled between 2000 and 2015 (from 26 to 48 installations). However, the worldwide installed capacity for bathing and swimming is 9,143 MW_t and the annual energy use is 119,611 TJ/year, which represents 20.2 % of the total annual energy use. The largest annual energy consuming country for this category is China, which is followed by Japan, Turkey, Brazil, and Mexico. The global installed capacity in space heating sector is 7,602 MW_t with yearly energy use of 88,668 TJ/year, while Turkey being the most user in space heating application. For greenhouses heating, the worldwide installed capacity is 1,972 MW_t and energy use of 29,038 TJ/year. Turkey is the leading country in the yearly energy use of this category. For aquaculture sector, the total installed capacity is 696 MW_t and 11,953 TJ/year of energy use, where USA being the main country in terms of yearly energy use. Industrial uses category accounts for worldwide installed capacity of 614 MW_t and yearly energy use of 10,454 TJ/year. In the other hand, the snow melting worldwide installed capacity is 307 MW_t and 2,323 TJ/year of annual energy use. Whereas, the total worldwide installed capacity for space cooling is 53 MW_t and annual energy use is 273 TJ/year. Agricultural crop drying global installed capacity and annual energy use are 161 MW_t and 2030 TJ/year, respectively, while China being the largest user of this category. The other usage category includes desalination, spirulina cultivations, animal farming, and sterilization of bottles. The worldwide installed capacity is 79 MW_t and annual energy use is 1,440 TJ/year, where the New Zealand is the top ranking country in this sector [11].

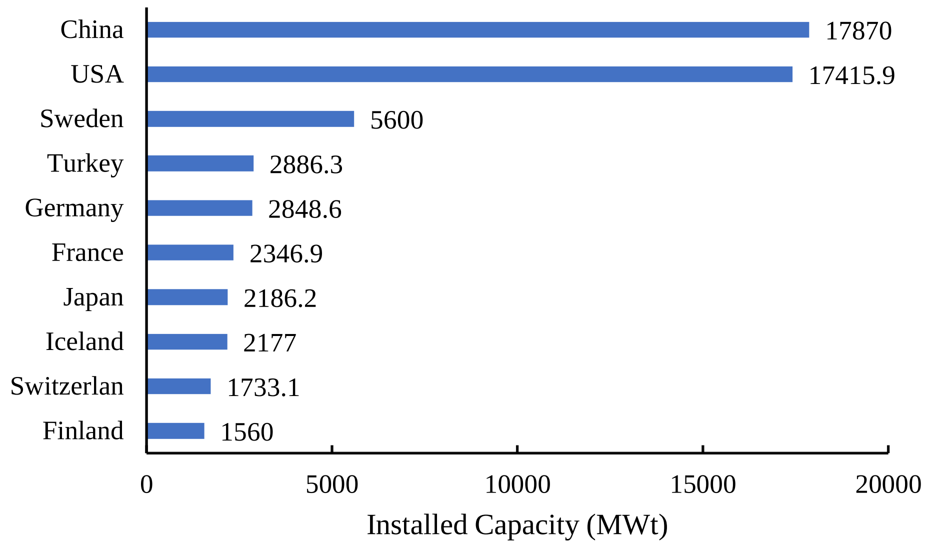

Figure I.1: Top 10 countries in geothermal direct use in the globe [11].

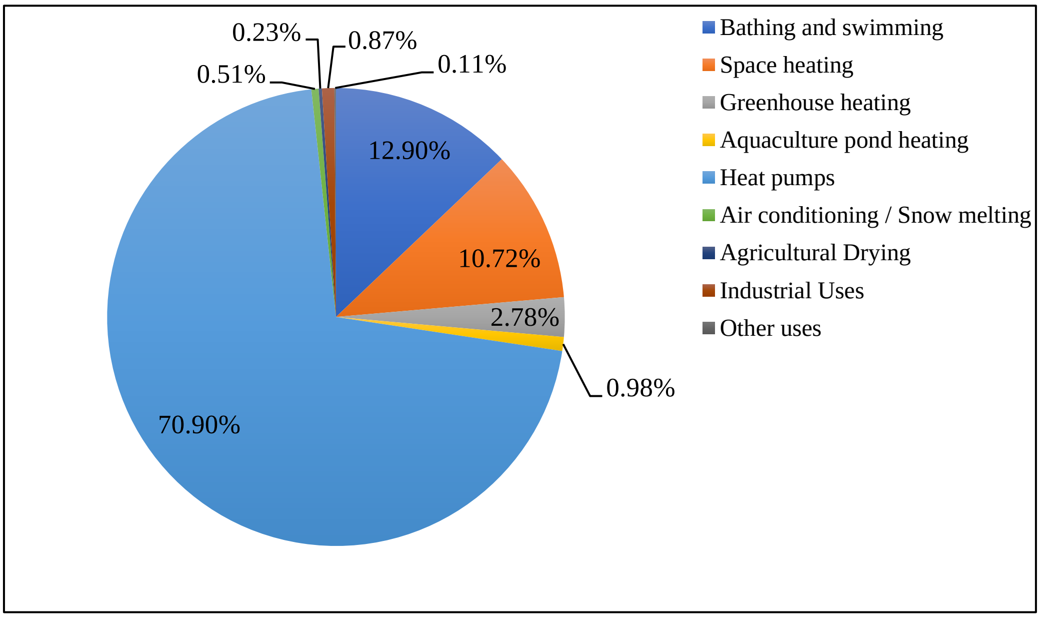

Figure I.2: Distribution of worldwide installed capacity of direct use applications (MWt) [11].

For power generation group, there are roughly 26 countries using geothermal energy for electricity production with an estimated worldwide installed capacity of geothermal power generation at 12.729 MW_e. The leader country in geothermal power production is the USA with 3,450 MW_e installed capacity accounting for 28.8 % of the world capacity. The top 10 countries in geothermal power generation are shown in Figure I.3. The share of the total installed capacity per the standard technology plant classification is defined as follows: 41 % single flash, 23 % dry steam, 19 % double flash, 14 % binary, 2 % triple flash, and 1 % back pressure. The total number of units for each category and the installed capacity and energy production average values per unit are presented in Table I.1 [13].

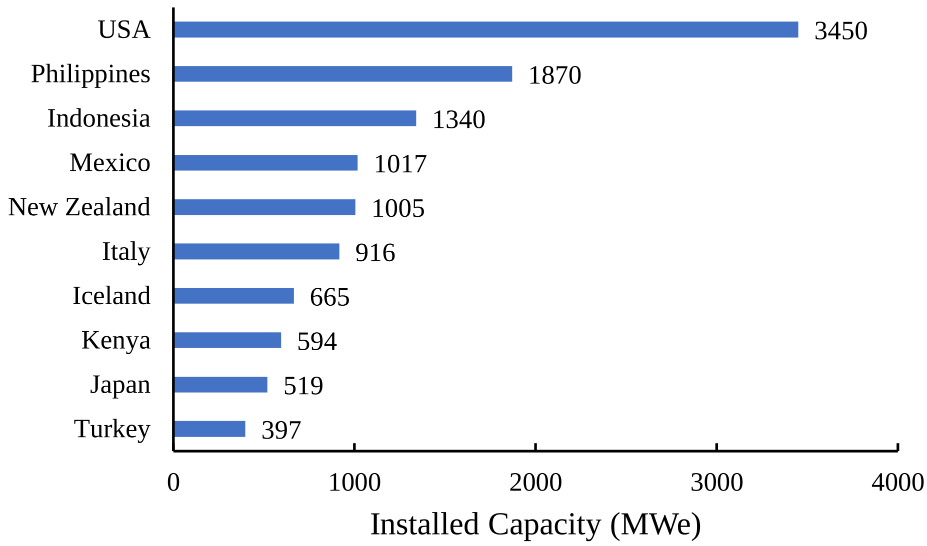

Figure I.3: Top 10 countries in geothermal electricity generation in the globe [11, 13].

Table I.1: The worldwide total number of units for each category and the installed capacity and energy production average values per unit [13].

Plant category	Number of units	Ave. energy (GWh/unit)	Ave. capacity (MW_e/unit)
Binary	279	31	6.3
Single Flash	170	179	30.4
Double Flash	67	231	37.4
Dry Steam	63	253	45.4
Back Pressure	22	76	7
Triple Flash	3	500	90.8

I.2.1.2 Geothermal energy technology

This subsection addresses the up-to-date geothermal power plant (GPP) and direct utilization applications technologies around the globe. For power generation, Valdimarsson [14] states that GPPs can be classified in two groups; binary cycles for geothermal resources of medium and low temperatures and steam cycles for geothermal resources of high temperature. Therefore, the selection of the appropriate technology is mainly based on the exploitable geothermal source type. In this regard, several studies have undertaken the possible technologies and power plant configurations [15, 16]. Today, three major configurations are being used to generate power from geothermal resources [12, 17, 18]:

- Dry steam: This configuration is the most effective among the configurations of higher enthalpy technology which is dedicated for dry hydrothermal reservoirs. The vapor passes directly from the borehole across the coupled turbine-generator unit to produce power.

- Flash steam: This technology is a relatively simple geothermal energy to power conversion when a liquid-dominant mixture is produced from the boreholes of the geothermal reservoir. The flash steam power plant includes two configurations, namely, Single Flash and Double Flash. In the Single Flash configuration, a flash vessel is used to separate the mixture in two distinct phases, vapor and brine, based on the natural density difference between the two fluids. The Double Flash configuration could achieve up to 25 % more electricity production for the same geothermal reservoir. However, this kind of plant is more expensive and complex.

- Binary cycle: This configuration is based on Kalina or Rankine cycles and particularly appropriate when the brine temperature in the hydrothermal reservoir is lower than 150 °C. In this system, the working fluid is preheated and evaporated via exchanging heat by making contact with the hydrothermal heat flow.

Recently, researchers agree that hybrid technologies are other interesting options that could improve the global performance of GPPs. Furthermore, this type of technology can be utilized for low enthalpy hydrothermal resources such as oil and gas fields which present another opportunity to decrease fossil energy usage and carbon dioxide emissions [12, 18].

For the direct use of heat, all of the power cycles discussed above enable of delivering geothermal energy at lower temperatures for direct use applications after power generation. Thus, high enthalpy hydrothermal resources are capable to combine direct use of heat and electricity production. This kind of configuration is known as cascade application which maximizes the heat utilization of the same geothermal fluid through electric and direct use applications [19].

Figure I.4 illustrates geothermal energy applications as per usage [20]. The use of hydrothermal resources in cascade configurations include power production as well as non-electric applications (direct use) of thermal energy proves positive impact on geothermal energy development. In the cascading systems, various temperatures of the same geothermal source are used in staging, the brine is first used in power generation and then for direct use purposes such as industrial applications, bathing and swimming and aquaculture pond. Figure I.5 presents an example of a combined thermal and power configuration in a multiuse cascade system. From this figure, the same high enthalpy geothermal fluid is used to generate power first, then, when it leaves the power plant at temperature of 81 °C, the brine is utilized for district heating application and finally at a lower temperature, the brine is used for other applications of direct use of heat [19].

Ground source heat pumps (GSHP) also play an important role in cooling and heating load of buildings in many countries. Researchers agree that, geothermal heat exchanger has a vital role to achieve high efficiency of the GSHP system. Hence, extensive studies have been carried out in this field. From the literature it has been revealed that, changing the geothermal heat exchanger design such as pipe arrangement, pipe length and pipe diameter could significantly improve the thermal performance of the system. Moreover, the heat exchange rate can be enhanced by increasing thermal conductivity of backfilling material (such as adding moisture, mixture of sand bentonite etc.). However, grout material with high thermal conductivity can cause an increase in thermal interference, which could be prevented by using insulation in various parts of the pipe according to the pipe design. To date, some suggestions to improve the efficiency of the geothermal heat exchanger are under examination such as using nano-fluids as working fluid and phase change material (PCM) in boreholes [21-23].

In this section, status quo and advanced technologies of geothermal energy utilization around the globe have been discussed so that in the next section, the current status and future of geothermal energy in Algeria can be analyzed and the suitable technologies for the country geothermal production can be proposed.

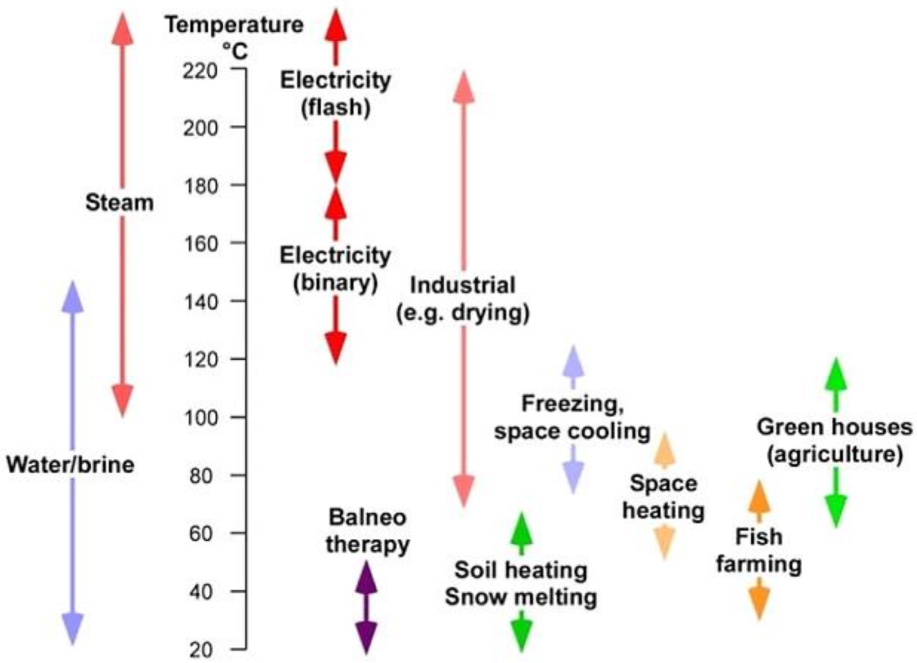

Figure I.4: Geothermal energy applications as per usage [20]

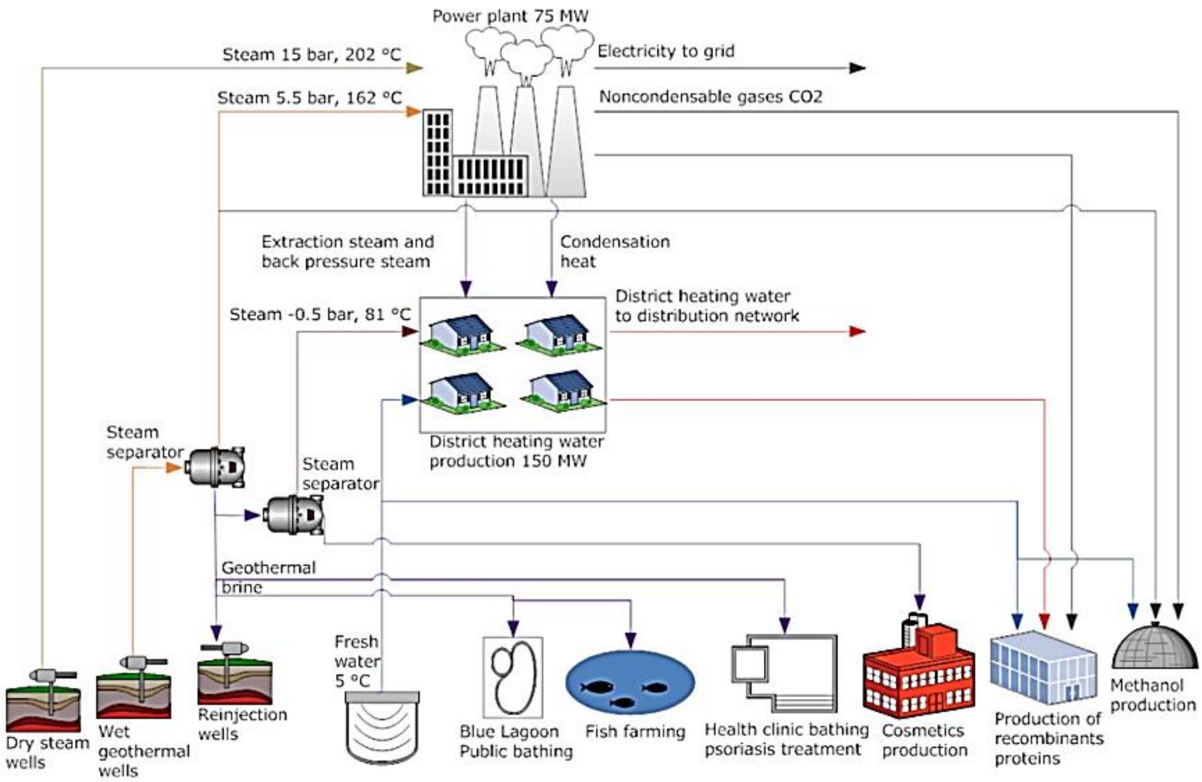

Figure I.5: Example of cascade application of geothermal resources [19]

I.2.2 In Algeria

Algeria has a significant geothermal potential. Although majority of geothermal resources are with relatively low enthalpy, which is not suitable for electricity generation, it is still suitable for direct heating purposes. Algeria is the leading country in the direct utilization of geothermal energy in Africa, as illustrated in Table I.2, with 54.64 MW_t installed thermal power and annual energy use of 1699.65 TJ/year. The distribution of geothermal direct usage by country in Africa is shown in Figure I.6 indicating that more than 39 % of the installed thermal capacity is located in Algeria [11, 24].

The main utilization area of geothermal energy in Algeria is balneology which represents almost 82 % (44.37 MW_t) of the total geothermal power utilization (54.64 MW_t), therefore just 18 % (10.28 MW_t) is utilized for other applications such as space heating, heat pumps and fish farming as indicated in Figure I.7 [11, 25].

Table I.2: The installed direct use geothermal capacity in Africa [11].

Country	MW_t	TJ/year
Algeria	54.64	1699.65
Egypt	6.80	88.00
Ethiopia	2.20	41.60
Kenya	22.40	182.62
Madagascar	2.81	75.59
Morocco	5.00	50.00
South Africa	2.30	37.00
Tunisia	43.80	364.00
Total	140	2,538

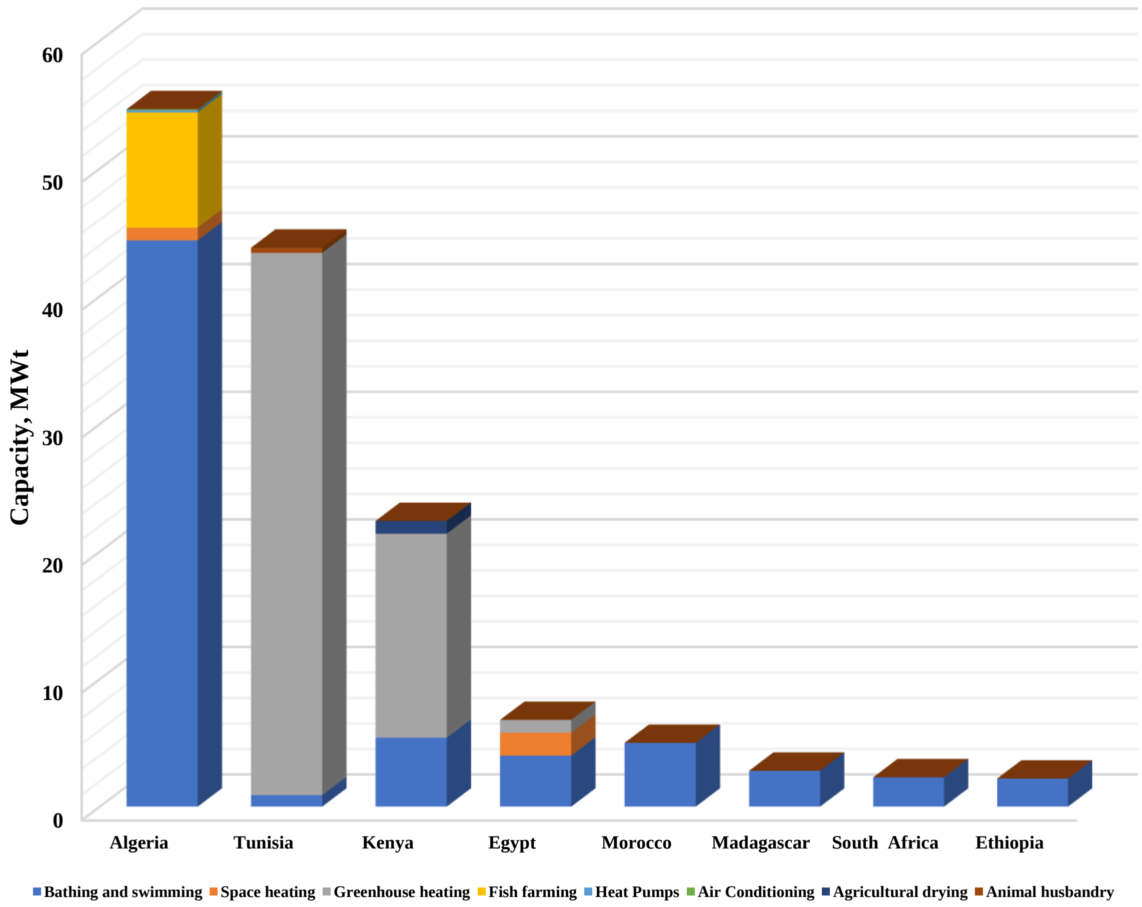

Figure I.6: Distribution of the installed capacity of direct use geothermal energy by country in Africa [11].

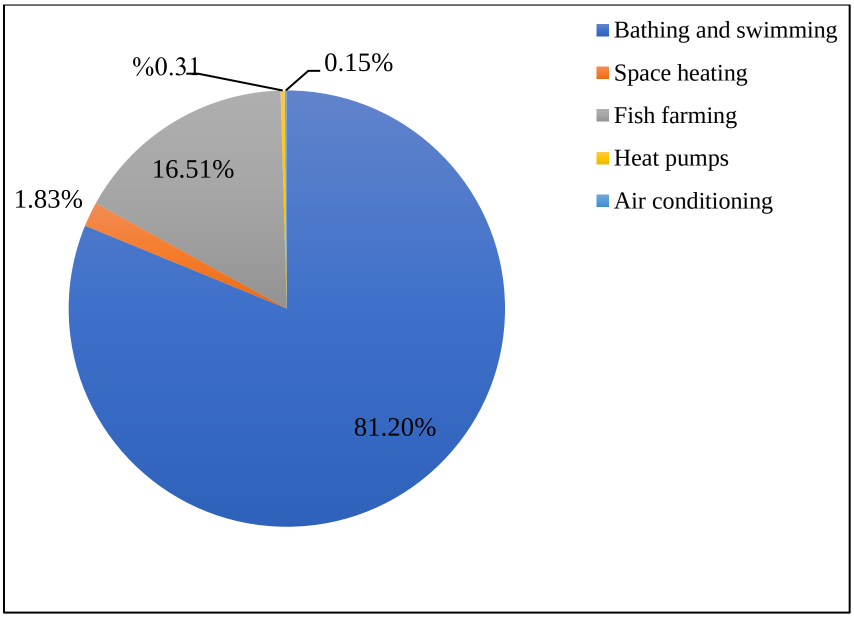

Figure I.7: Distribution of total installed capacity of geothermal energy (MW_t) in Algeria [11].

I.2.3 Utilization opportunities of geothermal energy in Algeria

Taking the increasing energy intensity into consideration, Algeria has put emphasis on the energy efficiency and renewable energy utilization. Authorities has adopted and launched the energy efficiency and renewable energies program in 2011 to create a green momentum. This program is based on a strategy to develop and expand the utilization sustainable resources. As the first stage, the Ministry of Energy has involved the affiliated companies and research centers such as APRUE (Agency for promotion and rationalization of energy use), CDER (Centre of renewable energies development) and CREDEG (Centre for research and power and gas development) to participate in the experimental and technical studies to evaluate the renewable energy potential in the country. Therefore, the establishment has produced many guidelines, procedures, regulations and legislative texts to govern and ensure the best practice of the renewable energies exploitation and development such as the executive decree No. 1-423 dated December 8, 2011 that specifies conditions and terms for the running of earmarked account No. 302-131 entitled National Funds for Renewable Energies and Cogeneration (FNERC), Ministerial order dated October 28, 2012 that defines the bill of expenses and incomes to be debited from FNERC, Ministerial order dated October 28, 2012, which determines conditions and terms for the assessment and follow-up of FNERC. Moreover, the Law No.11-11 dated July 18, 2011 on the complementary finance law for 2011 raises the rate of oil royalty that cashes for the National Funds for Renewable Energy and has extended its application fields to cogeneration facilities [24, 26].

In 2016, Ministry of Energy has launched the updated program of the renewable energies and energy efficiency with the vision of Algeria Energy 2030 where the target was set to install a total power capacity from renewable sources of 22,000 MW. By applying this program, 27 % of the produced electricity is intended to be acquired from renewable energies by the end of 2030. The strategy to implement this program is divided into two phases: the first phase 2015-2020 intended to realize a capacity of 4,500 MW and the second phase 2020-2030 to realize a foreseeable capacity of 17,500 MW. Based on this expectation and by the implementation of the renewable energies and energy efficiency program, the energy saving is evaluated to be more than 60 Million TOE (Ton of Oil Equivalent). In order to assure the execution of the launched program, Ministry of Energy have put in place national and international subcontractors for the purpose of the engineering, procurement and manufacturing of all the equipment required for the planned projects. Algeria also encourages cooperation with research centers in order to develop innovative technologies and processes in regards to the energy efficiency and renewable energies. Universities, research centers, companies and different stakeholders of this program collaborate for its implementation and intervene during the different steps of the innovation chain [27, 28].

To date, several projects have been completed during the first phase, such as the solar-gas hybrid plant based on the integrated solar combined cycle technology, located in Laghouat prefecture with total power capacity of 150 MW, the wind farm of 10 MW power capacity based on Gamesa technology located in Adrar region and the photovoltaic power plants project of 343 MW capacity that have been constructed at multiple locations. However, other projects such as the shrimp farm in Ouargla and the aquaculture farms in the provinces of Biskra, Ghardaia, Adrar, Tindouf and Tamanrasset, are either underway or in the commissioning process [29, 30].

In parallel to the development of the renewable energies utilization, Algeria aims at growing geothermal energy by 15 MW_t in 2030. This intention is planned to be achieved through the implementation of many projects such as some Tilapia fish farming in Ouargla and Ghardaia prefectures, a binary cycle power plant in the north eastern region, and heat pump installation in several locations [26, 27].

From the publications in recent years, it can be observed that there has been a growing interest of several researchers on the possible use of geothermal energy in Algeria. Hydrogen is gaining increasing consideration in the world and appears to be one of the most effective energy. Boudries and Dizene [31] investigated the potential of hydrogen production from renewable energies and concluded that geothermal energy has a good prospect for hydrogen production, especially for high temperature electrolysis systems where the required heat can be supplied from hot thermal water. This conclusion is consistent with the results presented by Ouali, Chader [32] which conducted a study on the exploitation of hydrogen sulfide in geothermal areas for hydrogen production and confirmed that most of thermal waters in Algeria are rich in sulfur and considerably promising for hydrogen production. Nonetheless, the authors did not pay much attention on the risk of the hydrogen sulfide gas where regulations and procedures should be put in place to protect the environment, public health and equipment.

Gouareh et al [33] addressed some technical and economical features through comparing the hydrogen production from geothermal resources for different locations in Algeria to identify the locations where the integrating of the proposed system is suitable. The potential of hydrogen production and power generation from geothermal energy by CO_2 as working fluid coupling electrolysis system was evaluated. Based on the numerical investigation, the results of their comparison revealed that about 3.4 million kg of annual electrolytic hydrogen can be produced in the northeast zone with the geothermal thermal gradient of 60 °C/km and CO_2 mass flow rate of 428 kg/s. The predicted cost of hydrogen in this region was 4.7 \$/kg-H_2. However, the hydrogen production in the southwest zone of the country was estimated to be much less (annually 0.14 million kg) with nearly doubled cost (8.7 \$/kg-H2).

The studies discussed previously in this subsection confirmed that Algeria has a large potential of hydrogen production from geothermal energy. Yet, only a limited number of theoretical studies have been investigated the feasibility of this technic. However, up to date there are no experimental studies have been carried out in this regard. Hence, further research is needed to address existing knowledge gaps such as technical and economical features and possible scenarios taking the required capital and operational cost into account.

Air conditioning system using geothermal energy sources is one of the promising application to decrease the energy consumption in the country. Bendaikha, Larbi [34] experimentally analyzed a hybrid fuel cell and geothermal heat pump employed for air conditioning. Their experimental results indicate that the use of low temperature proton exchange membrane fuel cells (PEMFC) and geothermal sources in northern Algeria is a potential option for air conditioning where the coefficient of performance (COP) was found to be 3.34 for the heating mode. In an extension to their work, Bendaikha and Larbi [35] studied the feasibility of the proposed system including an absorption chiller in the western region of Algeria for the same purpose, i.e. for air-conditioning. They found encouraging results to establish independent energy systems with high efficiency combining low temperature PEMFC with geothermal resources to feed isolated sites from the electrical grid. Detailed studies are needed to analyze the systems level integration of alternative energy technologies to estimate and compare the predicted operational cost.

Salhi, Korichi [36] performed a thermodynamic and thermo-economic analysis on a cascade refrigeration system composed of a compression subsystem using low global warming potential fluids and an absorption system utilizing LiCl-H_2O and LiBr-H_2O as the working fluid and fed by geothermal energy. Results demonstrated that the use of geothermal energy in wells with less than 16 m depth to power the system is more feasible in terms of economic point of view, compared to the utilization of solar energy. Mahmoudi, Spahis [37] conducted a case study in a brackish water greenhouse desalination unit in Algeria where geothermal energy was utilized to supply heating energy and produce fresh water. Their analysis revealed the great potential of the geothermal energy for the considered application, hence, it was concluded that geothermal energy is a viable energy source to power greenhouse desalination units in brackish water that can help developing arid and relatively cold regions.

As noted earlier, despite the promising benefits of geothermal energy applications and the available resources in the country, most of studies have been undertaken regarding the use of this important energy are theoretical and numerical, which provides few broadly applicable observations. Unfortunately, only a limited number of experimental studies have investigated the use of geothermal applications. Thus, further studies on geothermal energy opportunities are needed to highlight key challenges and gaps in the existing knowledge. This will pose several technical challenges concerning the new possible applications such as industrial process and snow melting. Furthermore, this important future research direction will potentially a clearer picture for implementations of large-scale projects.

Based on the above discussion and regarding majority of geothermal resources being low-enthalpy type in Algeria as previously mentioned, the current applications of geothermal energy in practice and further possible utilization of the main geothermal sources in Algeria are presented in Table I.3. From the referred table, it is seen that the temperature of geothermal water ranges from 20 to 98 °C, which represents the potential of geothermal energy for various applications such as space heating, aquaculture pond, raceway and greenhouse heating, agricultural crop drying, space cooling, snow melting, balneology, thermal tourism, generation of electricity and industrial process heat [25, 38-40]. It is clear from the table that further effort should be put to popularize and expand the utilization of geothermal energy throughout the country.

Table I.3: Current applications in practice and potential exploitation opportunities of geothermal energy in Algeria [25, 38-40].

Source	T (°C)	Applications in practice	Potential utilization opportunities
Meskhoutine	98	Balneotherapy, space heating	Balneotherapy, space heating, greenhouse heating, drying, industrial, electricity (binary) and other applications
Bouhanifia	68	Balneotherapy, space heating	Balneotherapy, space and greenhouse heating, drying, industrial, fish farming, snow melting
Righa	68	Balneotherapy	Balneotherapy, space and greenhouse heating, drying, industrial, fish farming, snow melting
Bouhadjar	65	Balneotherapy	Balneotherapy, space and greenhouse heating, drying, industrial, fish farming, snow melting
Guergour	44	Balneotherapy	Balneotherapy space and greenhouse heating, fish farming, snow melting
Elssalhine	43	Balneotherapy	Balneotherapy space and greenhouse heating, fish farming
Boughrara	37	Balneotherapy	Balneotherapy, greenhouse heating, fish farming, snow melting
Chiguer	35	Balneotherapy	Balneotherapy, greenhouse heating, fish farming, snow melting
Ain Skhouna	31	Balneotherapy, fish farming	Balneotherapy, greenhouse heating, fish farming
Albian aquifer (Sahara area)	20–60	Balneotherapy, fish farming, greenhouse heating	Balneotherapy, space and greenhouse heating, drying, industrial, fish farming and other applications

I.2.4 Barriers to the utilization of geothermal energy in Algeria

The potential and advantage of geothermal energy source have not been fully realized in Algeria due to several reasons. This section presents the main reasons hindering the geothermal energy development in Algeria, which are listed as follows:

- Geothermal energy technologies in Algeria are still too far from those in the developed countries in the world. Additionally, there is lack of comprehensive utilization of resource development which leads to low efficiency of resource utilization. However, the geothermal direct use applications are facing big shortage on the adequate equipment, and the equipment available is with low efficiency and poor durability, indicating that the technology development in the country has not reached the international standard.

- Algeria has promoted the use of renewable energy through a series of laws, regulations and decrees but mostly concerning the solar and wind energy. However, there are no nationwide laws, regulations or decrees related to the use and development of geothermal energy such as guidelines and management of geothermal resources. Consequently, there is no uniform process for the exploitation and effective protection of geothermal resources.

- There are no specific strategies, policies, development plans and programs on a regional and sub-regional adequately supporting geothermal energy development and popularization in the country. A renewable energy and energy efficiency program has been launched by the Ministry of Energy in 2016. In this program, the total power capacity from the other renewable energy sources such as solar and wind energy is intended to be 22,000 MW by 2030 whereas the growth of geothermal energy use is planned to be only by 15 MW_t. Additionally, there are no details on the planned geothermal projects and specific method for geothermal development in this program. Moreover, no substantive measures such as economic subsidies and tax reductions have been taken. That is, the investment opportunities and promotion of the industrialization of geothermal energy offered by the government is still far from to be sufficient.

- Despite a number of studies of geothermal energy has been performed in Algeria during recent years, a database of geothermal energy resources has not been yet established since there is no centralized geothermal resources information system and the level of management automation is low. Hence, more detailed studies from aspects of geophysical, hydro-chemical and thermal engineering are required to identify the geothermal reservoirs and assess their potentials for the possible applications. Thus far, due to the lack of knowledge networks and information dissemination, it is relatively difficult to encourage the different stakeholders to invest in geothermal projects.

- In order to develop an energy system respectful to the environment and also ensure the commitment of the country regarding the international agreements, many laws and decrees to protect the environment, natural habitats and public health have been elaborated. Although geothermal energy is an environment friendly renewable energy source, which can limit carbon emissions and air pollution, all stages of geothermal projects can cause environmental impacts, in the context of exploration, commissioning and exploitation resulting in an environmental pollution and damage such as thermal pollution and ground subsidence.

I.2.5 Countermeasures and challenges to ensure geothermal energy development in Algeria

Energy policies for the sustainable development are implemented regarding economic growth and energy security without any detrimental effect on the environment. In this context, green renewable energies such as geothermal plants play a key role as the fossil fuels, which produce emissions, and are responsible for majority of environmental pollutions, are diminishing rapidly. The discussion in the above sections of this study has sufficiently demonstrated that the geographical location of Algeria is perfect to play a leading role in the geothermal energy utilization, therefore it is strongly recommended to emphasize and support the development of this energy, and identify and eliminate the obstacles and challenges given below for a successful integration of geothermal energy source into the national energy inventory.

- A series of laws, regulations and decrees that include financial support, strategies of environmental protection, penalties and awards should be launched to ensure the sustainable development of geothermal energy. Consistent implementation of policy is of crucial importance for the investors in any sector. For that reason, Algeria should formulate energy policies, strategies, development plans and programs, ensure that the decision makers in charge of the energy sector apply them objectively, and pursue the projects through to completion and operation.

- The government has a significant role to play in improving the technical level, particularly the research and development and the implementation of technical system for geothermal energy development of the direct use technology. Hence, the initiatives for manufacturing equipment used for geothermal energy and advancing the manufacturing process should be supported, which will definitely lead to higher device performance and reliability.

- International cooperation is an important key to strengthen the technical communication, support, exchanges, relations and partnership to develop geothermal utilization in the country. Therefore, public and private institutions should be encouraged to collaborate at the international level via bilateral or multilateral arrangements with the countries with relatively more advanced geothermal energy technologies, such as New Zealand, USA, Italy, Turkey and Iceland, to keep up to date with the recent policy, programs and projects, as well as promote the Algerian geothermal energy market at the international level. Within this period, Algeria should benefit from the international expertise, foreign advanced experience and technology transfer. Therefore, as geothermal resources in Algeria are of low-enthalpy type, special focus should be taken on the technologies suitable for the direct use applications.

- A significant number of institutions and organizations, as well as the technical academic universities have been established to carry out educational programs and scientific research. However, the techniques implemented in practice for renewable energy projects including geothermal energy are still far behind the international standards. Authorities should provide financial subsidies and special funds to encourage the institutions, organizations, associations, private organizations and community of industry to support education programs, technology sciences, innovation in applied research and undertake prototype geothermal projects, which could lead to develop appropriate geothermal technologies, future technology ownership and thus to commercial applications.

- It is clear that the lack of scientific, professional and competent technical staff in the country is one of the main reasons of the slow progress in the field of geothermal research. Hence, Algeria should promote the personnel training for geothermal manpower development and reinforce the human abilities required for quality research, development and implementation of geothermal resources. This can be done through the cooperation with the distinguished researchers from institutions and universities all over the world, taking a prominent role in training programs for geothermal technology. The outcome of this cooperation should be that the trained technical and professional staffs are able to perform surface geothermal exploration, drill, monitor geothermal reservoirs and evaluate their possible environmental impacts. Therefore, this would help in further developing the expertise in the country and homegrown solutions to the geothermal development problems.

- The society has a poor knowledge, or even unaware of geothermal energy. Hence, public awareness and acceptance have a significant role in the development of geothermal energy utilization using appropriate technology. This can be carried out through several ways such as organizing popular scientific and awareness conferences, sponsoring round tables and developing an online portal designed on the basis of modern technologies to compile and update data regarding the efforts being carried out in the development of the country's geothermal energy resources.

- Substantive rules, regulations and measures for financial supports specifically for the geothermal energy projects within the sustainable development framework should be established and implemented. Financial incentives including feed-in tariff, financial subsidies and tax breaks will create an environment favorable on investment and ensuring a guarantee on development of geothermal infrastructures, technologies and projects installation.

I.3 Ground air heat exchangers

Ground Air Heat Exchangers (GAHE) is a technique that promotes energy savings. GAHE is an unconventional method of heating and cooling space by harnessing the heat from the earth's subsurface. An understandable overview of the earlier research on GAHE is provided in the following subsections. The review examines the findings from the thermal performance and provides a detailed explanation of the analytical and experimental investigations on the various combinations of GAHE [41].

I.3.1 Working principle of GAHE

The ground-air heat exchanger (GAHE) is a subterranean passive system which is used to provide cooling in the summer and heating in the winter. It transfers heat through the use of air as a medium and soil as a source or sink. The hidden pipes in a typical GAHE system let external air to flow through and exchange heat with the subsurface. A blower is used in the GAHE system to force ambient air to pass through underground pipes. The air that passes through these pipes exchanges heat with the surrounding soil, becoming either hotter or colder depending on the surrounding conditions. The conditioned air from the GAHE system can then be used for heating or cooling in the winter and summer, respectively [42]. The performance of GAHE system is increases with burial depth of pipe but the initial investment also increases with depth of pipe. It is noticed that a horizontal ground heat exchanger's pipe should be positioned 3–4 metres below the surface of the earth [23]. The working principle of GAHE system for summer cooling is illustrated in Figure I.8.

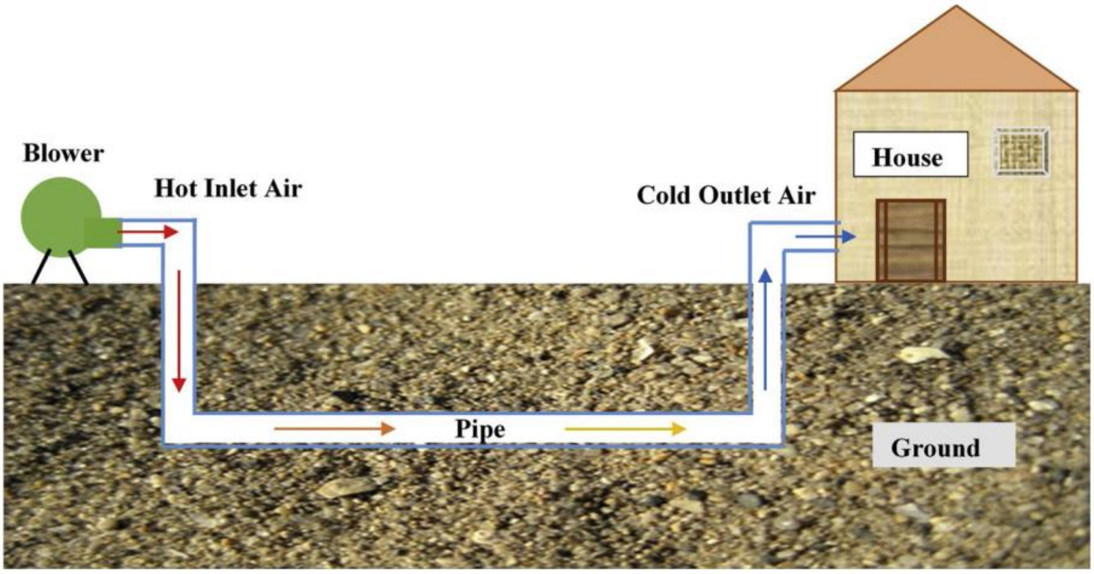

Figure I.8: Working principle of GAHE system for summer cooling [23].

I.3.2 Classification of GAHE

The GAHE systems are primarily divided into two categories: (i) open-loop and (ii) closed-loop, based on the air circulation. Under the open-loop system, ambient fresh air enters the building through the subterranean GAHE pipes, where it is used to provide heating and cooling. Afterward, the air is released into the atmosphere. While in the closed-loop system, air is recirculated through the GAHE pipes. As a result, in the closed loop GAHE system, air needs to transmit significantly less heat to and from the earth [43-45]. However, open-loop systems are preferable than closed-loop systems because the closed system does not offer fresh air [46]. A broad classification of GAHE system is shown in Figure I.9.

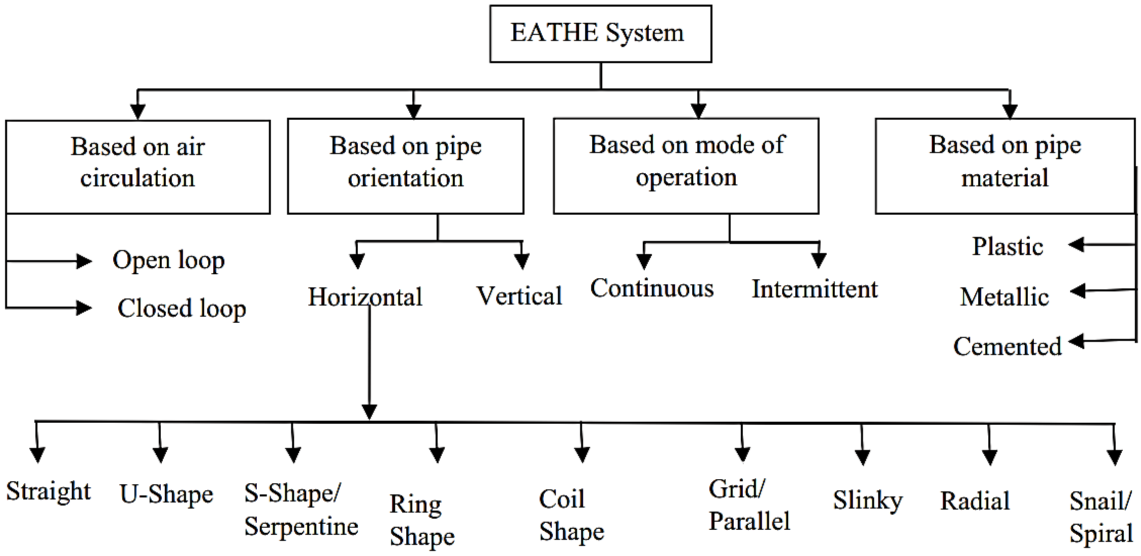

Figure I.9: Classification of GAHE system [47].

I.3.3 GAHE pipe patterns

Pipe layout is an important consideration in the design/disposition of a GAHE system since the land area required for a certain heating/cooling load is exclusively determined by the design and layout of pipes. The heating/cooling potential of a GAHE system is highly dependent on its geometrical arrangement. The GAHE system is divided into two categories based on pipe layout: horizontal and vertical GAHE. The various orientations of the pipe layouts are discussed in the following sub-sections [47].

I.3.3.1 Straight pipe

It is the most popular pipe layout for a GAHE system since straight pipes are simple to install and provide minimal pressure drop. As a result, it is the best pipe configuration for heating and cooling a small building. This pipe configuration can only be used when there is enough land to excavate a lengthy trench. Figure I.10 depicts the GAHE system with a straight pipe architecture [47].

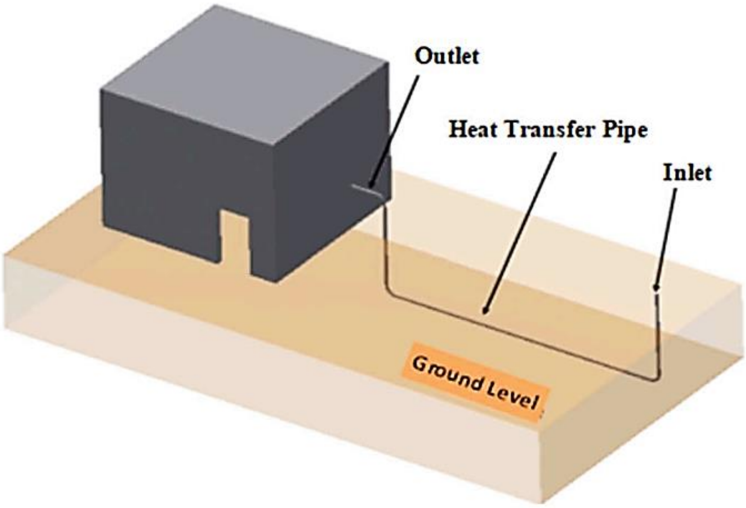

Figure I.10: Straight pipe-layout for GAHE system[47]

I.3.3.2 U-shape pipe

U-shaped pipe GAHE system is similar to the straight pipe GAHE system, but with a U-shaped pipe configuration where the inlet and outlet sections are at the same end of the trench (see Figure I.11). The U-shaped pipe GAHE system is suitable for minimal heating and cooling load needs [47].

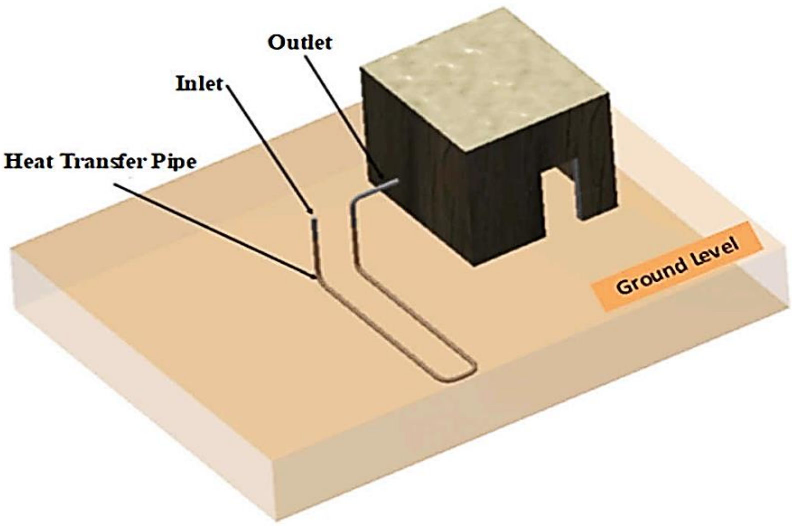

Figure I.11: U-shaped pipe-layout for GAHE system [47]

I.3.3.3 Ring pipe layout

In the ring pipe layout, GAHE pipe is buried in the building's foundations (see Figure I.12). This pipe plan is the most cost-effective option as it eliminates the need for excavation by leveraging the building's existing trench [48].

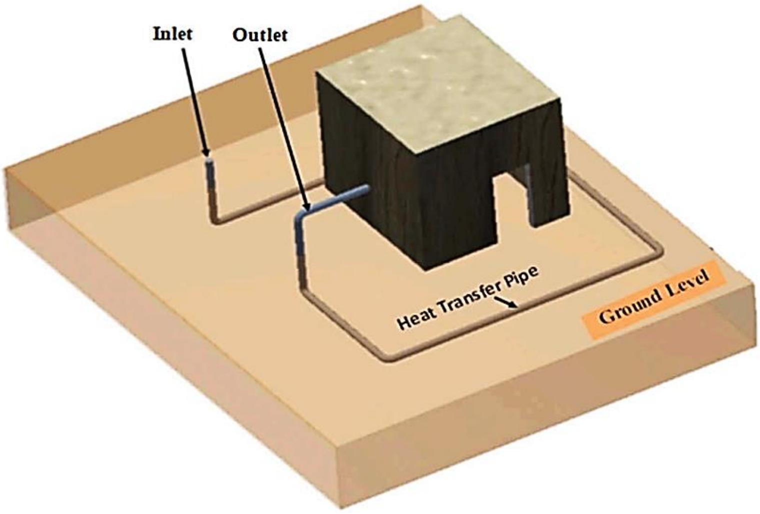

Figure I.12: Ring pipe-layout for GAHE system [48]

I.3.3.4 Serpentine pipe layout

The serpentine pipe arrangement illustrated in Figure I.13, allows for a long pipe to be put in a short trench due to its several turns. Thus, it is an excellent layout for medium-sized GAHE systems [47].

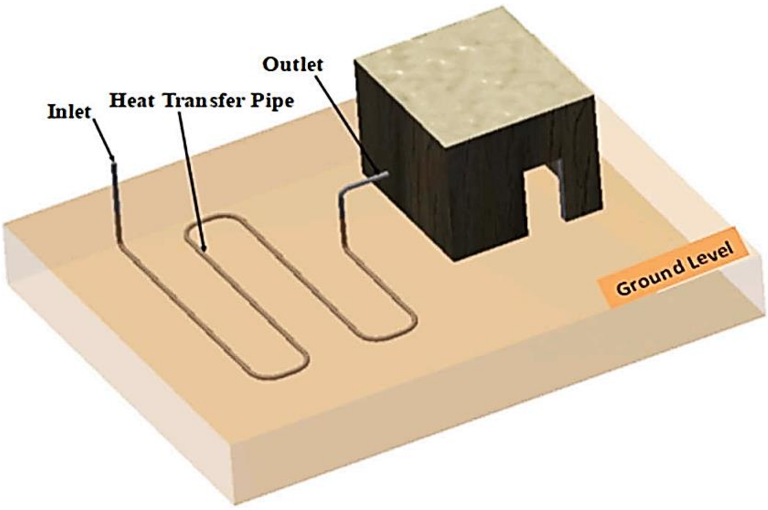

Figure I.13: Serpentine pipe-layout for GAHE system [47].

I.3.3.5 Spiral pipe-layout

Straight and U-shaped GAHE pipes require long trenches with a high aspect ratio (ratio of trench length to trench width). However, in densely populated urban areas, the necessary land area is not available for the excavation of long trenches, limiting the use of straight and U-shape pipe GAHE systems. This paved the way for the utilization of spiral pipe-layout (as shown in Figure I.14), which requires less trench length with a low aspect ratio [48].

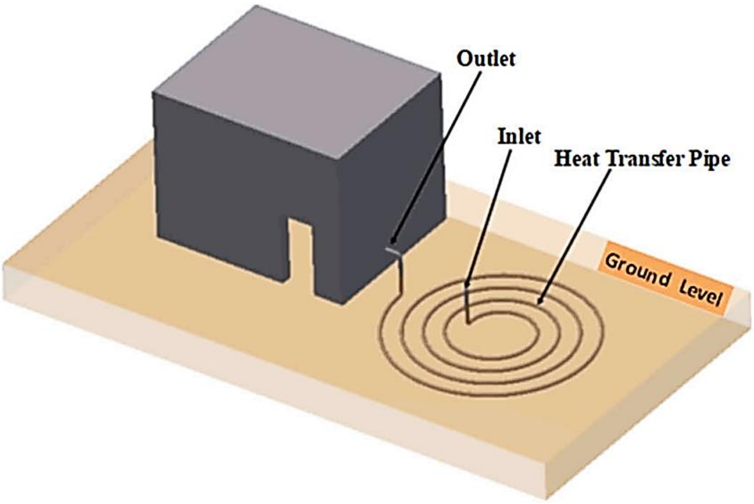

Figure I.14: Spiral pipe-layout for GAHE system [48].

I.3.3.6 Lateral pipe-layout or parallel pipe-layout

When the cooling/heating load is significant and a high airflow rate is necessary, a lateral or parallel pipe architecture is commonly used (as in educational buildings, hotels, and so on). In a lateral or parallel pipe architecture, many heat transfer pipes are linked in parallel to a common header pipe, as illustrated in Figure I.15. However, parallel pipe-layout performance is good, but it requires a big land area and is costly to excavate [48].

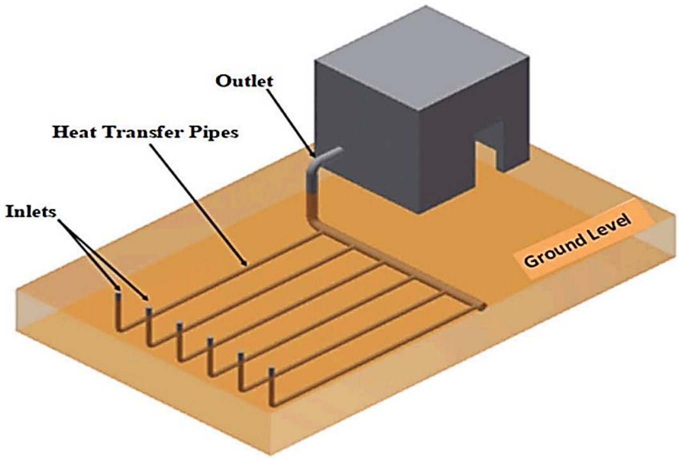

Figure I.15: Lateral pipe-layout for GAHE system [48].

I.3.3.7 Grid pipe-layout

The GAHE system's grid pipe configuration employs a common header pipe at the system's intake and outflow. The ambient air enters the intake header pipe, where it circulates via a series of subterranean pipes before being fed to the room via the exit header pipe, as shown in Figure I.16. Grid pipe layouts are employed in large buildings that require pre-tempered air at a larger flow rate [48].

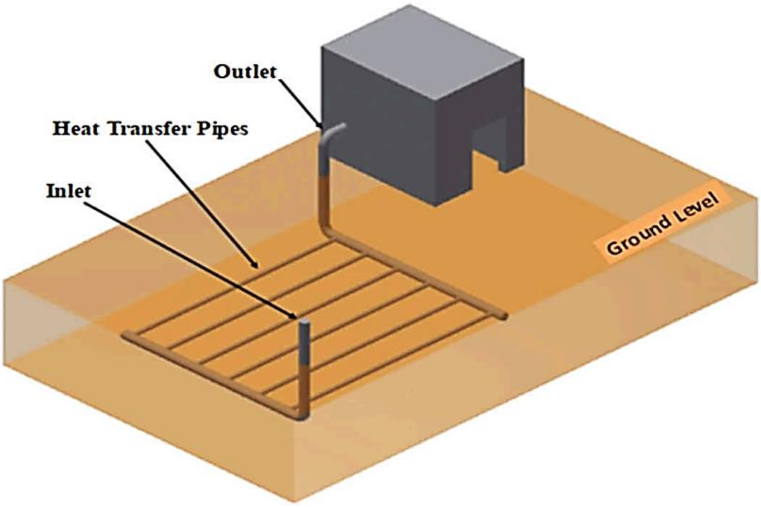

Figure I.16: Grid pipe-layout for GAHE system [48].

I.3.3.8 Radial pipe-layout

Figure I.17 shows a pipe-layout with radial connections to a shared collection tank. This setup does not require manifold pipe, but a huge collection tank is necessary. Radial pipe layouts require less land area than parallel pipe layouts. However, excavation near the collection tank is difficult [48].

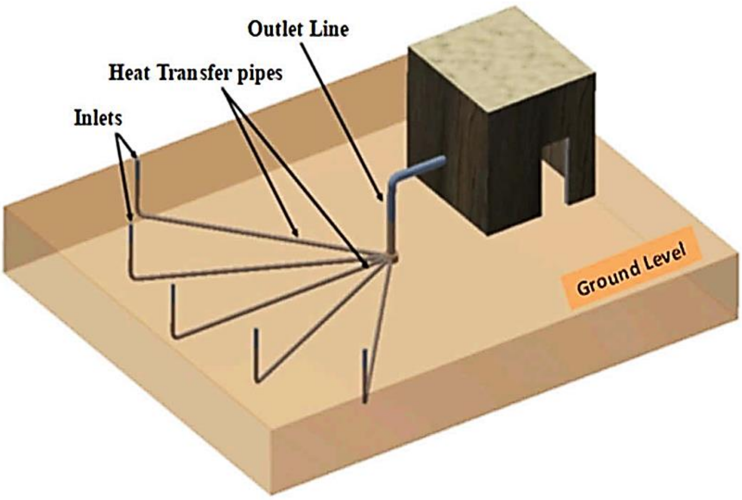

Figure I.17: Radial pipe-layout for GAHE system [48].

I.3.3.9 Slinky-coil pipe layout.

Slinky coil pipe-layout, which requires less land area for lengthy pipe installation, is often utilized in horizontal GSHP systems. This pipe configuration is also suitable for the GAHE system (see Figure I.18) [47].

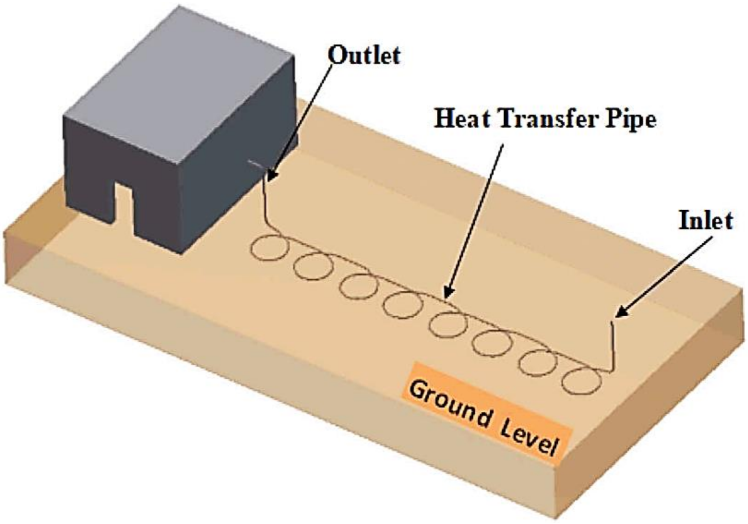

Figure I.18: Slinky pipe-layout for GAHE system [47]

I.3.3.10 Helical coil pipe layout

Helical-coil pipe layout is extensively utilized in GSHP systems since it requires only a minimal amount of land to install a lengthy pipe. Helical pipe-layout can also be employed for the GAHE system (as shown in Figure I.19), although installation with big diameter pipes (0.2-0.3 m) is challenging [47].

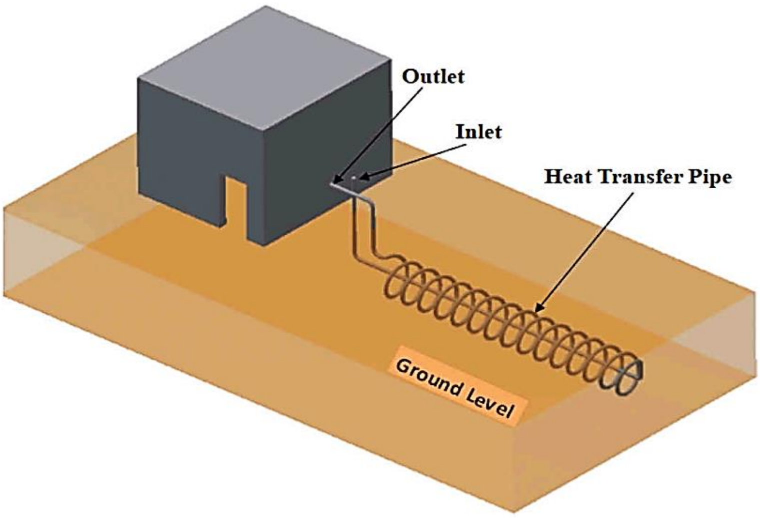

Figure I.19: Helical pipe-layout for GAHE system [47]

I.3.4 Applications of GAHE system

GAHE is a passive technology that requires less energy and decreases CO_2 emissions. As a result, GAHE systems have been effectively employed for cooling, heating, and ventilation in a variety of buildings (residential and commercial), agricultural greenhouses, and animal homes under varying climatic circumstances. GAHE systems are also utilized in hybrid/combined mode with conventional/non-conventional HVAC systems to decrease total electricity consumption for heating, cooling, and ventilation. Following their successful application for heating and cooling in buildings and greenhouses, GAHE systems are now being used for industrial applications. The various applications of a GAHE system are outlined in the following subsections [23].

I.3.4.1 Cooling and heating of the building

The GAHE system has been used to heat and cool buildings all around the world in order to improve energy efficiency and decrease environmental issues. An earth air heat exchanger (EAHE) system was employed to ventilate the residential quarters (south block) at the RETREAT campus in Gurgaon, India [49]. Four tunnels, each 70 m long and 0.7 m in diameter, were buried at 4 m deep to handle an air rate of 169.9 m3/min using four blowers (each having a capacity of 2 HP). A solar chimney was also built to the rooms to promote air flow, as seen in Figure I.20. In the summer, the outside air temperature was decreased from 42-45 °C to 28-30 °C, however in the monsoon season, excess humidity in the air caused a drop in efficiency, which was recovered by incorporating more dehumidifiers and chillers [23].

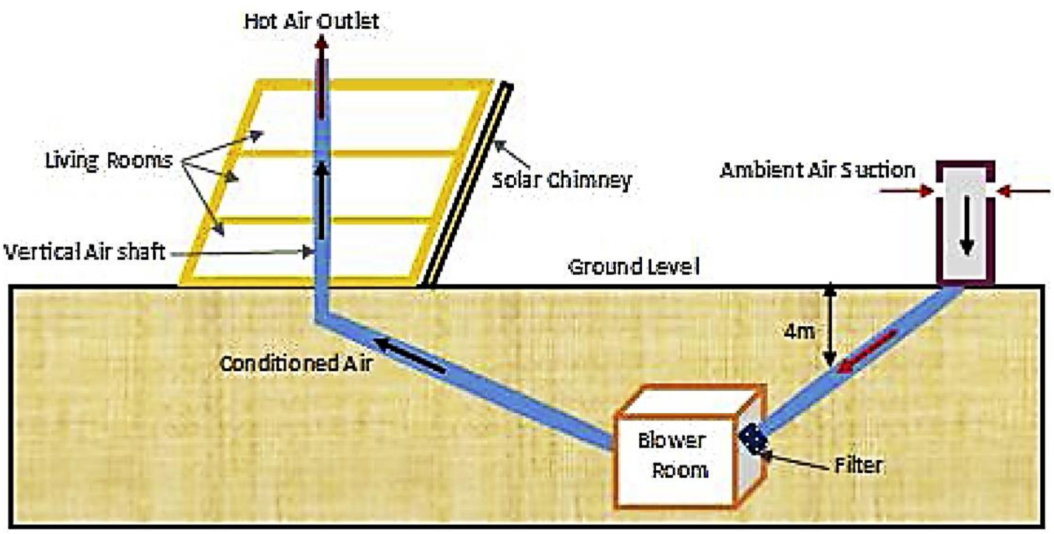

Figure I.20: Schematic diagram of EA GAHE HE applications for ventilations of living quarters [49].

I.3.4.2 Cooling and heating of the greenhouse

Greenhouse is a method of providing a regulated environment for plants by covering the area with a transparent cover. However, the high sun intensity raises the internal temperature of the air not just during the summer, but even on clear days in the winter. As a result, the greenhouse's internal temperature must be kept within the specified range. To regulate the interior atmosphere of a greenhouse space, both a GAHE system and an evaporative cooling system can be used; however, the evaporative cooling system confronts issues when water is scarce. Furthermore, GAHE can efficiently create a controlled environment for plants. As a result, the GAHE system becomes an excellent choice for regulating the interior environment of a greenhouse [23].

Sharan et al [50] employed an earth tube heat exchanger (ETHE) system in a closed-loop configuration for a greenhouse in Kutch (India). The Ethe pipe system was built beneath a greenhouse measuring 20 m × 6 m × 3.5 m. Two layers of four mild steel pipes (each pipe 0.20 m diameter and 23 m length) were laid at a depth of 2 m and 3 m with a common header, as depicted in Figure I.21. A 4.2 kW blower was utilized to deliver air at a rate of 194 m^3/min in the greenhouse, resulting in 20 air changes per hour (ACH), and the greenhouse's air temperature decreased by 7 °C. Thus, crop yields improved by 2.7 times while using 34 % less irrigation water [23].

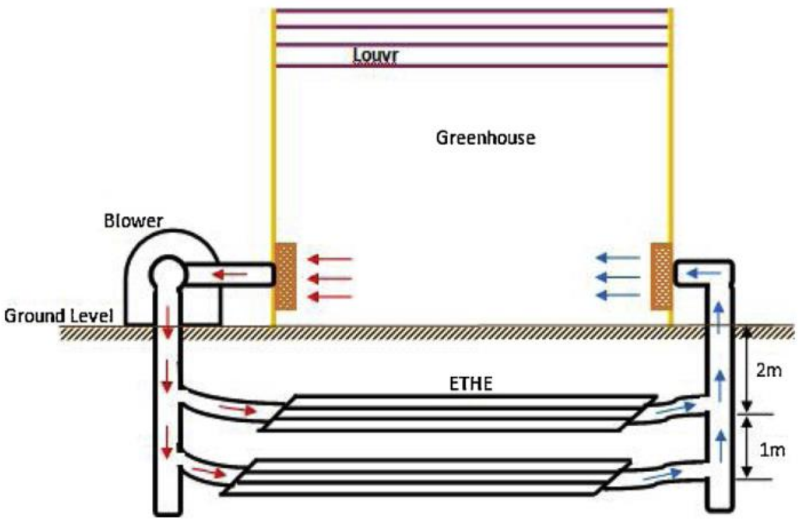

Figure I.21: Schematic diagram of GAHE application for the greenhouse [50].

I.3.4.3 Cooling and heating of livestock

The GAHE was also utilized to heat and cool the air in the tiger enclosure at the Kamala Nehru Zoological Garden in Ahmedabad, India [50]. A GAHE system with two MS pipes (0.2 m diameter and 27 m length each) was constructed at a depth of 2 m in the moat, as shown in Figure I.22. A 1.2 kW blower was utilized to manage the air flow rate at 44.4 m^3/min, and the air temperature was decreased by 8°C in the summer and increased by 10°C in the winter [23].

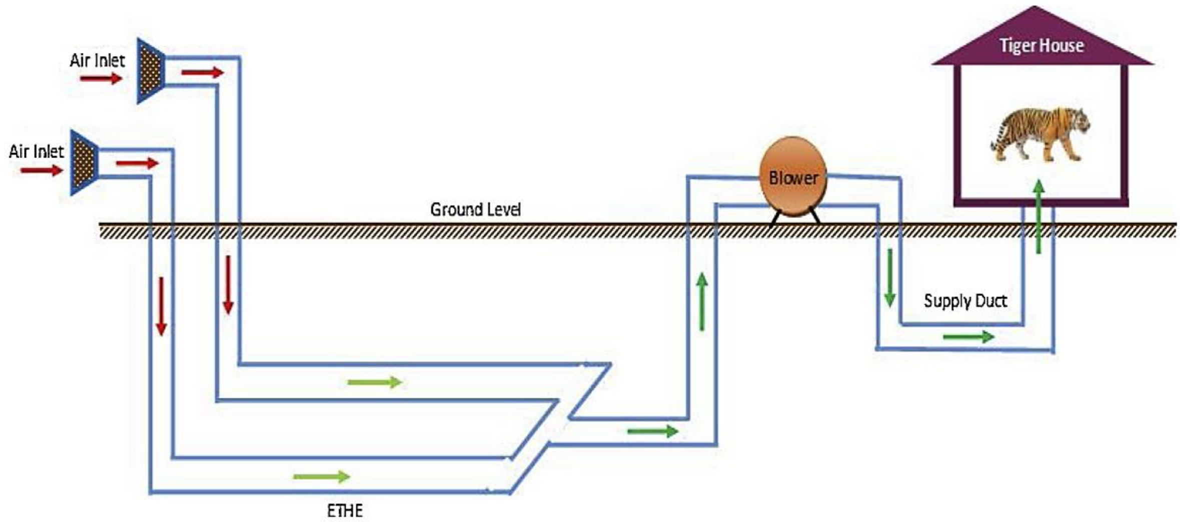

Figure I.22: Schematic diagram of GAHE system application for the dwelling of tigers [50].

I.3.4.4 Cooling of solar PV panels

The effectiveness of solar photovoltaic (PV) panels is highly dependent on their temperature. Maintaining low panel temperatures is crucial for efficient conversion of solar radiation into electrical energy. Increasing panel temperature leads to decreased performance. Elminshawy et al [51] employed the GAHE method to cool solar PV panels in Egypt. In this work, ambient hot air (during the summer) was cooled by passing it via a GAHE pipe before being passed over the back panel surface, as illustrated in Figure I.23. The study found that delivering GAHE cooled air to solar PV decreased the temperature of the solar PV module from an average of 55 °C to 42 °C, while increasing the PV module's electrical conversion efficiency and output power by 22.98 % and 18.90 %, respectively [23].

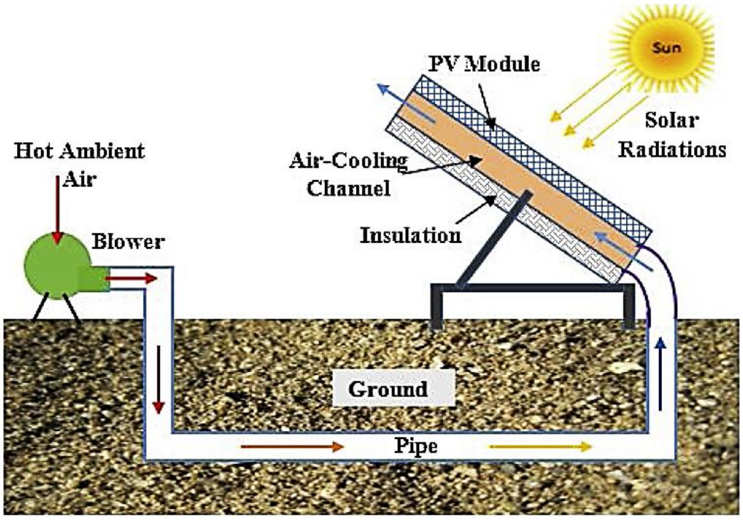

Figure I.23: Schematic diagram of GAHE application for cooling of solar PV panel [51].

I.3.4.5 Industrial applications

Some tests were also undertaken to assess the viability of the GAHE system in industrial substantiating and found that GAHE is a good solution for industrial heating and cooling applications. Vidhi et al [52, 53] used a GAHE system to cool the condenser of a supercritical Rankine cycle (SCR) power generation unit, as shown in Figure I.24. It was discovered that using GAHE for condenser cooling boosted the efficiency of the SCR increased by 1 % while its daily swings is decreased. Barakat et al [54] used a GAHE system in a gas power plant (shown in Figure I.25) to increase the performance of the gas turbine power plant. Findings revealed that, thermal efficiency and power production of the gas power plant employing the GAHE system rose by 4.8 % and 9 %, respectively, while the annual income grew to $1.655*10^6$ $ with a payback period of 1.2 years.

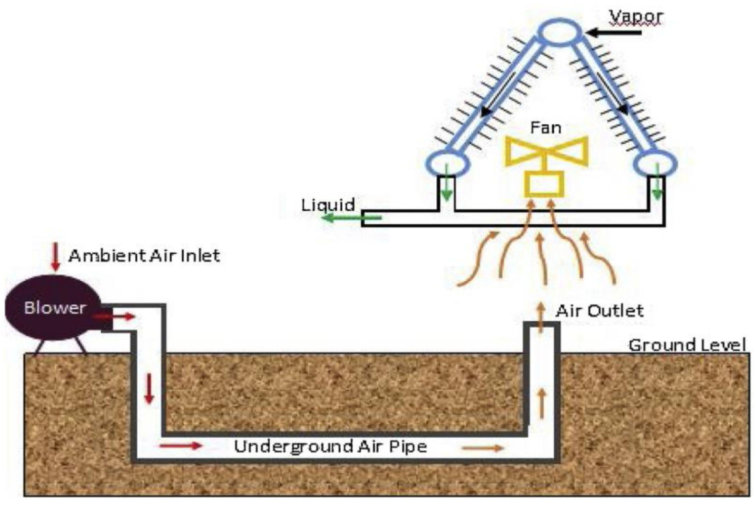

Figure I.24: Schematic diagram of EAHE applications in thermal power plant [52]

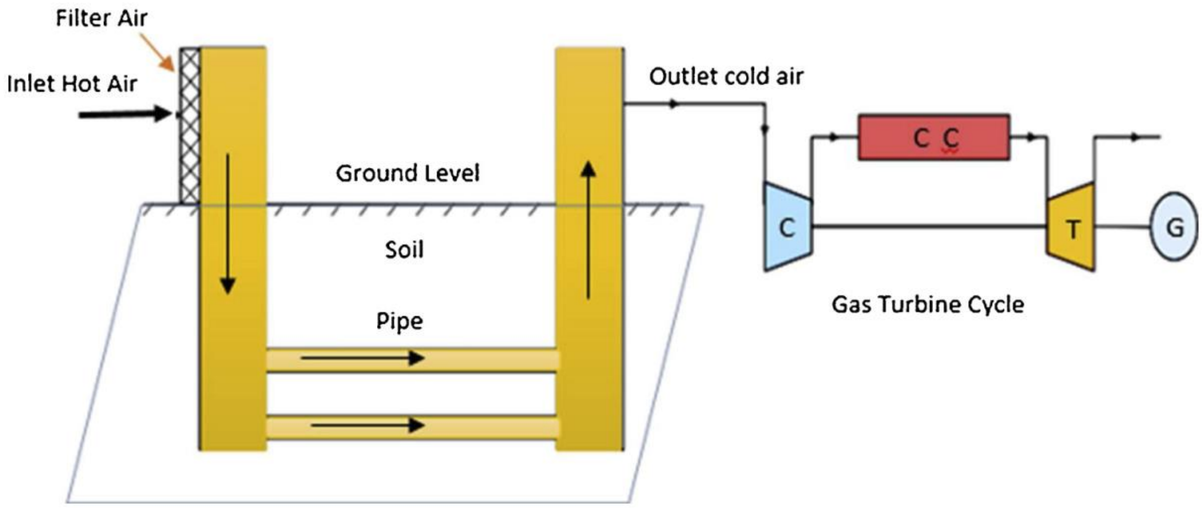

Figure I.25: Schematic diagram of GAHE applications in gas power plant [54]

I.3.5 Recent research trends in GAHE system

Mathur et al [55, 56] carried out numerical simulation to investigate the condition of the ground saturation versus long time operation of GAHE. Results showed that the ground saturation conditions were faster with soil having lower heat conductivity. Kaushal et al [57] presented a GAHE model using the ANSYS Fluent and response surface method to improve the design parameters of the GAHE system. Nazer-Nejad et al [58] numerically assessed the viability of GAHE system with air-conditioner for Tehran’s environment and observed that EAHE provides a comfortable condition except for a short period of time when operating 24 h in a day. Authors also observed that the GAHE system was only suitable for a shorter period of time as soil near vicinity of underground pipe becomes saturated and the performance of GAHE system degrades during longer operation. Ralegaonkar et al [59] compared GAHEs with conventional cooling systems, were concluded that GAHEs save 90 % electricity and 100 % water in comparison with air conditioners and evaporative coolers, respectively. Mathur et al [60, 61] presented different operative strategies for prolonged use of GAHE system under arid condition. Rouag et al [62] established a transient semi-analytical approach to forecast the efficiency degradation of the GAHE during operation period. Agrawal et al [63-65] implemented two of GAHE system to assess the efficiency of the wet and dry GAHE systems. The study showed that the wet GAHE has a lower knee point than the dry GAHE.

Naoufel et al [66] conducted an investigation on thermal performance of GAHE for cooling mode in hot climate of Algerian Sahara. Results showed that, by increasing air speed from 2 to 5 m s^{-1}, the efficiency of the GAHE declines to 33 % from 60 % and the coefficient of performance of the GAHE drops to 0.46 from 2.84. Ramirez et al [67] has compared the thermal performance of the straight tube heat exchanger in three different cities in Mexico. The author has concluded that the thermal performance of the heat exchanger is highly dependent on the climate condition of the installed area. It is more suitable to install the GAHE in the areas with cooler and warmer temperatures and higher soil inertia. Fazlikhani, Goudarzi, and Solgi [68] have investigated the thermal performance of the straight pipe heat exchanger in two cities of Iran in warm, dry and cold weather conditions. The obtained results revealed that the GAHE systems can contribute to the reduction of energy consumption. In hot and cold climates, the heat exchanger was more efficient and could lead to 63.6 % energy savings over the year. The heat exchanger had a maximum storage capacity of 47.9 % in the cold weather for a year. Menhoudj et al [69] investigated the efficiency of GAHE for refreshing buildings under Algerian climate (as depicted in Figure I.26) and found that thermal efficiency of the GAHE is more profound in the southern part of the country compared to the northern part. Results revealed that, in one year, the system could supply 246.815 kWh of energy. Amanowicz [70] conducted CFD simulations to examine the effect of various geometrical parameters on the system efficiency of multi-tube GAHE. Zeng et al [71] implemented GAHE to avoid the infrared exposure of a generator room to decrease the temperature inside the room. Findings revealed that, by using the GAHE system in intermittent mode, the maximum infrared camouflage can be decreased up to 86.96 %.

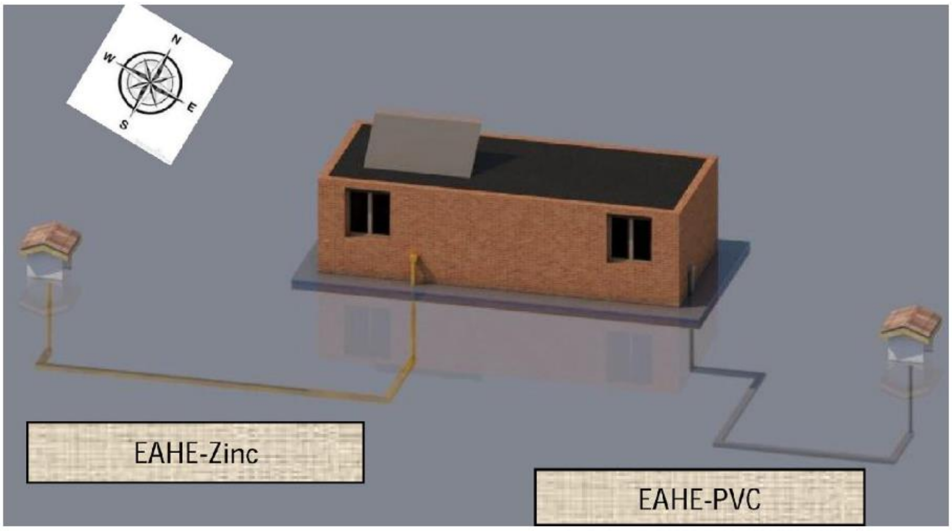

Figure I.26: Schematic diagram of the studies GAHEs [69]

Agrawal et al [72] Investigated thermal performance of a slinky-coil ground-air heat exchanger system with sand-bentonite as backfilling material (see Figure I.27). Finding shows that it can achieve a drop-in air temperature of 18.7 °C at 30 m pipe length (trench length of 10.2 m) with soil at 27 °C and inlet air temperature of 46 °C. Yusof et al [73] developed a mathematical GAHE model to determine the thermal characteristics of EAHE system in a warm climate condition, and showed that GAHE system proves real opportunity for application under such conditions. Mathur et al [74] investigated the heat efficiency of a spiral duct pattern compared to a U-shaped duct pattern of GAHE systems and concluded that thermal efficiency of spiral and U-shaped duct for GAHE are almost the same. Thus, if an enough ground space is not available to install the ducts in U-shaped layout, the spiral configuration could be implemented. Agrawal et al [48] conducted a numerical study to compare the heat efficiency of U-pipe, slinky-pipe, and helical-pipe tube configurations. Findings concluded that, the highest heat efficiency of the GAHE was found with the helical-pipe and slinky-pipe configurations. Ahmed et al [75]examined the impact of different parameters such as pipe lengths, diameters, thicknesses, materials, depths, as well as air velocity on the thermal performance of GAHEs for the humid subtropical climate of Australia. Results showed, pipe with a smaller diameter and thickness leads to higher cooling performance. It is concluded that the GAHE with 60 m pipe length and 1.5 air velocity has maximum performance. Benhammou et al [76] developed a transient model to evaluate the thermal performance of EAHE for summer cooling under the Algerian Sahara. The obtained results revealed that, the thermal performance of GAHE in transient conditions is significantly influenced by the variation of operation period, pipe diameter as well as airflow velocity. The same authors combined GAHEs with windcatchers. Findings showed that, the cooling potential of wind catchers coupled with GAHEs is higher than traditional wind catchers with wet surface [77].

Figure I.27: Arrangement of water trickling systems for the slinky-coil GAHE system [72]

Jamshidi et al [78] studied the thermal performance of spiral coil type GAHE at different climate conditions of Iran as illustrated in Figure I.28. The influence of various factors, such as the depth level of buried pipe in soil, the air velocity and the inlet air temperature on the outlet air temperature have been investigated. The obtained results, showed that, higher buried depth of the pipe increases the transferred heat, while the increase in the inlet air velocity decreases the heat exchange between the soil and the air. Liu et al [79] developed a numerical model of a vertical GAHE system and carried out a parametric study to investigate the effects of pipe parameters, insulation parameters, mass flow rates and soil types. Findings indicated that a system with a smaller pipe diameter provides more thermal capacity at a fixed air mass flow rate, and an increase in pipe depths causes the outlet air temperatures to decrease/increase in summer/winter, with a smaller daily oscillation. Moreover, the study results recommended that, a thickness of 30 mm and a length of from 4 to 5m are the most appropriate insulation parameters for this proposed system. Mathur et al [80] conducted a numerical simulation of helical-coil layout GAHE system compared to conventional U-layout GAHE for heating and cooling purposes. Findings revealed that, the helical-coil layout GAHE system provides the highest effectiveness as well as required lesser land area compared to conventional U-layout GAHE system. Rana et al [81] conducted numerical simulation for optimizing geometric parameters to enhance the thermal performance of the ground to air tunnel heat exchangers. Authors have investigated the impact of introducing multiple fin arrays into the exchanger pipe and findings revealed that, compared to the case without fins introducing 4 fins for temperature variation, the system performance can be incremented by 19.4 %. Furthermore, when the fin spacing is 1 m, the drop in temperature decreases by 5.6 %, while when the fin spacing is 2 m, the drop in temperature increments up to 7 %, with an outlet temperature of 32.95 °C.

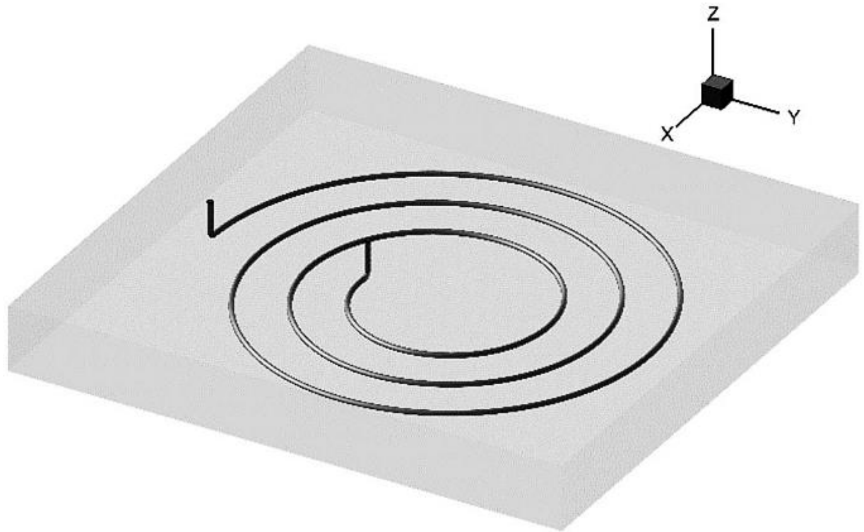

Figure I.28: The spiral coiled tube heat exchanger[78].

I.3.6 Motivation

The above review indicates that, the GAHE systems have several significant advantages, such as the high cooling and pre-heating capacity. However, the existing applications of GAHE systems also show their practical limitations in locations with high building density due to their large installation area during construction as well as the excavation cost needed for long trenches. Such restrictions may severely hinder the successful implementation of GAHE systems in practice. From the literature review, which have been conducted on the helical GHEs efficiency for GSHP, it is inferred that helical GHE needs a minimum piece of land for implementation and assures the maximum heat exchange rate from surrounding soil. However, helical-coil pipe pattern has still not been implemented in field application of GAHE system. Therefore, investigating the thermal behavior of the helical-coil layout GAHE both experimentally and computationally could be a valuable contribution to the field of the GAHEs.

I.4 Conclusion

This chapter reported a literature review of the research which has been conducted within the scope of the current thesis. The review was broadly split into two sections investigating; an overview of geothermal energy and ground air heat exchanger. From the conducted review, it has been revealed that, Algeria has relatively abundant geothermal resources of low-enthalpy type that are feasible for direct use applications, thus provides a clean energy alternative for reducing fossil fuel dependence and its negative impact on the environment. Therefore, government initiatives and efforts are important to emphasize and encourage the exploration, exploitation and development of geothermal resources in the country. In the other hand, based on the conducted review regarding the ground air heat exchanger, it is concluded that the helical-coil pipe pattern has improved the thermal efficiency more significantly than others as well as it requires less area for the installation of longer pipes.

CHAPTER II : EXPERIMENTAL SETUP AND METHODS

II.1 Introduction

The experimental design, installation and site investigation of the in-situ measurement study carried out in this research are presented in this chapter. The instrumentation of the monitoring site has also been selected to facilitate the data collection. The experiment aims to providing a comprehensive data-set which can be used for evaluating the thermal performance of the helical ground air heat exchanger system. The following sections will outline the procedures and methodologies implemented for the experimental study. Following this, details regarding the HGAHE system modeling will be presented, including the heat exchange rate, total thermal resistance, effectiveness, pressure drop and thermal performance derating factor.

II.2 Experimental setup

The experimental setup is mainly composed of a PVC pipe formed in helical-coil pattern and a concrete borehole (see Figure II.1 and Figure II.2). The main reason of constructing the borehole by reinforced concrete is the poor surrounding ground solidity characterizing the installation area. The constructed borehole has an outer diameter of 1.2 m, thickness of 0.1 m and total depth of 5 m. The helical-pipe shaped has a total vertical length of 3 m, diameter of 0.8 m and a pitch length of 0.28 m, and was inserted vertically into the borehole, where the top of the helical-pipe was located 2 m below the ground level. Then, the borehole was filled with water as backfill material and well isolated from the outdoor climatic conditions. It should be pointed out that the backfill material (i.e. water) has been inserted into the borehole several days before the start of the operation. Therefore, the water remained enough time in the borehole to have the same temperature field of the surrounding soil before the beginning of the operation. Properties and working conditions of the application area are depicted in Table II.1.

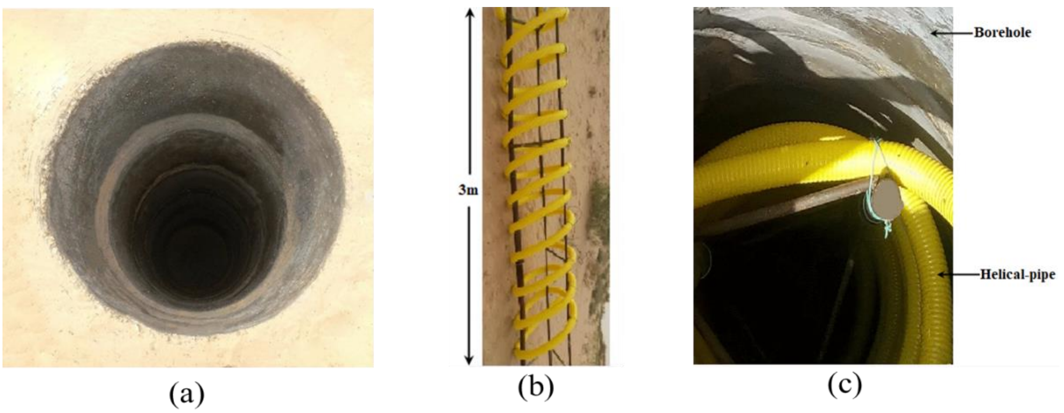

Figure II.1: Pictures of the HGAHE system: (a) borehole, (b) helical-pipe (c) setting up of the helical-pipe into the borehole.

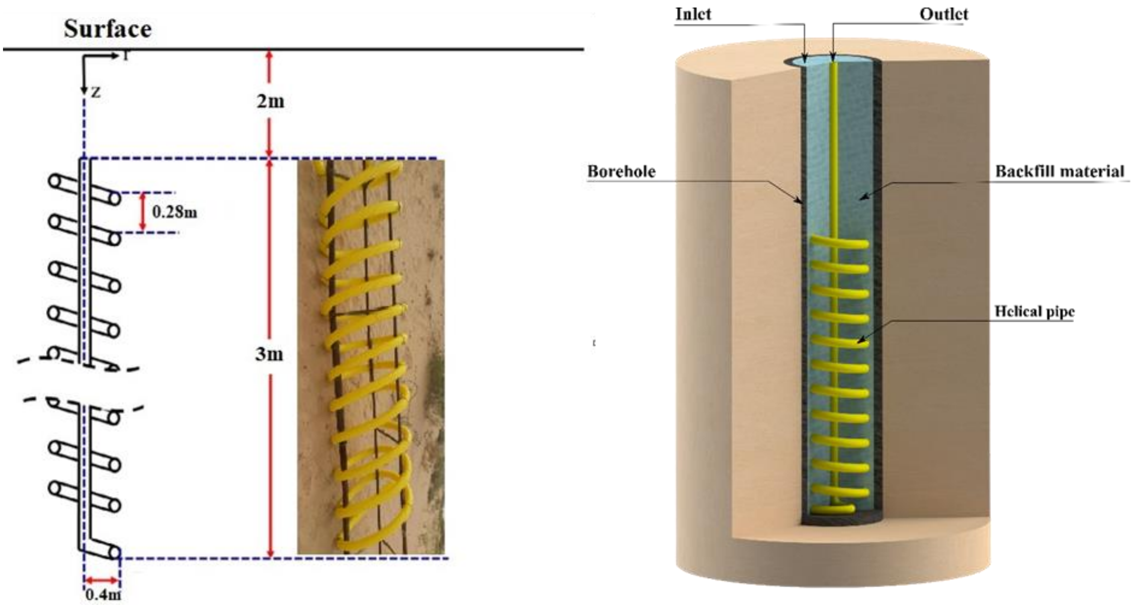

Figure II.2: Schematic diagram of the helical ground air heat exchanger system.

The main reason of studying the helical configuration for GAHE is that, among the configurations for geothermal heat exchanges, it provides the highest response in heat exchange rate per unit of operation area and its shape allows to decrease the surface of installation. A previous study performed by Boughanmi et al [82] showed that the helical layout for GHE occupies less area and has a better performance. Dehghan [83] concluded that it is highly preferable to use helical type due to its low costs in comparison with slinky and U-tube GHEs. In another study conducted by Bezyan et al [84] analyzing the thermal performance of GHE of three different tube types of 1-w-shape, 1-u-shape, and helical type, findings revealed that the helical type tubes are the best choice among others.

This experimental setup was designed and realized in El Oued city (Southeastern Algeria: Latitude 33.36°N, and Longitude 6.85°E), which has a hot and arid climate having the mean maximum ambient air temperature of 44.41 °C during summer season (May to August) [85, 86].

Table II.1: Geometric and material properties of the application area

Parameter	Value
Geometric properties of PVC pipe	
Length of PVC pipe (m)	30
Internal diameter of PVC pipe (m)	0.06
Thickness of PVC pipe (m)	0.0035
Geometric properties of HGAHE	
Vertical length of HGAHE (m)	3
Diameter of HGAHE (m)	0.8
Pitch length of HGAHE (m)	0.28
Geometric properties of Borehole	
Depth of borehole (m)	5
Internal diameter of borehole (m)	1
External diameter of borehole (m)	1.2
Thermal properties of PVC pipe	
Thermal conductivity (W/m.K)	0.16
Specific heat capacity (J/kg.K)	900
Density (kg/m^3)	1380
Thermal properties of borehole (concrete)	
Thermal conductivity (W/m.K)	1.63
Specific heat capacity (J/kg.K)	837
Density (kg/m^3)	2500
Thermal properties of ground	
Thermal conductivity (W/m.K)	0.52
Specific heat capacity (J/kg.K)	1840
Density (kg/m^3)	2050
Thermal properties of air	
Thermal conductivity (W/m.K)	0.0242
Specific heat capacity (J/kg.K)	1006
Density (kg/m^3)	1.225
Viscosity (kg/m.s)	1.7894e-05

II.3 Materials and methods

II.3.1 Instrumentation

Thermocouples (K-type, -200 to 1250 °C range, and 0.4 % accuracy) were utilized to measure the air temperature at the entrance and exit of the HGAHE system, where the temperature sensors were coupled to a digital acquisition BTM-4208SD for collection of data. A centrifugal blower was utilized to pump and maintain the air flow velocity at 10 m/s for all experimental runs, while the A vane anemometer (TESTO 416-type, 0.6 to 40.0 m/s range, and 1.5 % accuracy) was employed to measure the air flow velocity circulated into the helical-pipe. Figure II.3 shows the measurement devices used during the experimentation and Figure II.4 illustrates the schematic of the measurement points.

(a) (b) (c) (d)

Figure II.3: Devices used in experimentation: (a) K-type thermocouple, (b) temperature digital recorder, (c) blower, (d) anemometer.

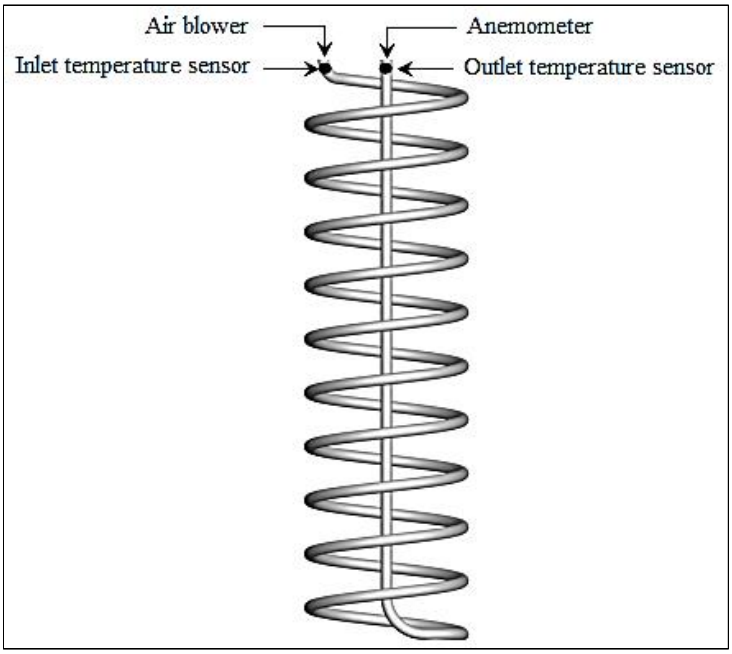

Figure II.4: Schematic of experimental measuring points.

II.3.2 Experimental methodology

II.3.2.1 First experiment

The experimentation was conducted in order to assess the cooling potential of the HGAHE system. Measurements were carried out in summer season 06 May 2017 from 9 am to 6 pm for 09 hours of operation period. In the study, the inlet temperature of air was equal to the ambient temperature of air and the air flow velocity was kept constant at 10 m/s during the experimentation. Ambient air, inlet and outlet temperatures of the system have been recorded throughout the 9 hours continues operation of the HGAHE system with 10 min intervals. It should be pointed out that, prior to the starting of the experiment i.e., the initial state of the application area, measurements of temperature sensors show that, the undisturbed ground mean temperature surrounding the helical-pipe is approximately 24.8 °C.

II.3.2.2 Second experiment

To evaluate thermal response of the HGAHE system, experiments were performed during summer season (May 2017). Since only the cooling operation has been considered for the present study, which is typically required in hot climates like Algeria, the inlet air temperature of 38 °C was maintained for this experimental run. Most of the previous research works have considered velocity of air in the range of 2-10 m s^{-1} [77, 87, 88], and very limited researches have deemed the influence of high velocity of air on the total air temperature drop and cooling capability of GAHE. Thus, high velocities of air (between 10 and 20 m s^{-1}) have been considered in this study. Air temperature across the tube length at multiple sections, as mentioned above, has been recorded. For measuring the temperature at various points in the helical-coil pipe, the time range was originally set at 20 min. However, with a range of 20 min, the variation in the air temperature was insignificant, whilst a remarkable difference in temperature of air can be noticed accurately after a time range of about 1 hour. Thus, the resolution of data for this research work was taken as 1 hour. Temperature measurement has been recorded over an hourly basis, and the HGAHE system has been operated continuously for 3 hours.

II.4 Performance modeling of GHE

The thermal performance of the HGAHE system is mainly analyzed in terms of heat transfer rate, total thermal resistance, effectiveness, pressure drop and thermal performance derating factor, which expressed in the following subsections.

II.4.1 Heat exchange rate

Air temperatures at the inlet and outlet of the pipe are measured to assess the heat exchange rate of the HGAHE system which is determined by Eq. (II.1) [89]:

$$\dot{Q} = \dot{m}C_p(T_{in} - T_{out}) \tag{II.1}$$

where $\dot{m}$ represents the air mass flow rate in kg s^{-1}, C_p denotes the air heat capacity in J kg^{-1} K^{-1}, T_{in} and T_{out} stand for the inlet and outlet air temperatures in °C, respectively.

Heat exchange rate of the HGAHE has been evaluated by hourly basis, taking into account the heat capacity and inlet temperature of air as constant at 1005 J kg^{-1} K^{-1} and 38°C, respectively. However, heat exchange rate per meter of pipe length ($\dot{Q}_L$) can be determined by Eq. (II.2) [89]:

$$\dot{Q}_L = \frac{\dot{Q}}{L} \tag{II.2}$$

where $\dot{Q}$ represents the heat exchange rate in W, and L stands for the pipe length of HGAHE in m.

Moreover, the overall heat transfer coefficient (U) of the system could be calculated using the following Eq. (II.3) [82]:

$$U = \frac{\dot{Q}}{A\Delta TLM} \tag{II.3}$$

where $\dot{Q}$ denotes the heat exchange rate in W, A stands for the heat exchange area in m^2 and ΔTLM represents the log mean temperature drop and defined by Eq. (II.4) [82]:

$$\Delta TLM = \frac{(T_{out} - T_{in})}{\ln \frac{(T_{out} - T_{so})}{(T_{in} - T_{so})}} \tag{II.4}$$

where T_{in}, T_{out} and T_{so} represnt the inlet air, outlet air and mean soil temperatures in °C.

II.4.2 Effectiveness

Thermal exchange rate efficiency of the HGAHE system can be calculated by the efficiency coefficient definition of heat energy (E), which is the fraction of actual heat exchange capability to ideally highest thermal exchange capability and can be determined by Eq. (II.5) [89]:

$$E = \frac{\dot{Q}_{act}}{\dot{Q}_{max}} = \frac{\dot{m}C_p(T_{in} - T_{out})}{\dot{m}C_p(T_{in} - T_{so})} = \frac{(T_{in} - T_{out})}{(T_{in} - T_{so})} \tag{II.5}$$

where $\dot{Q}_{act}$ and $\dot{Q}_{max}$ represent the actual and maximum heat exchange rates in W, and T_{in} , T_{out} and T_{so} denote the inlet air, outlet air and mean soil temperatures in °C.

It should be pointed out that effectiveness of the HGAHE proves its capacity to obtain the lowest outlet temperature (for cooling mode) or the highest outlet temperature (for heating mode).

II.4.3 Total thermal resistance

Heat transfer rate per meter of HGAHE depth ($\dot{Q}_Z$) could be calculated using Eq. (II.6) [90]:

$$\dot{Q}_Z = \frac{\dot{Q}}{Z} \tag{II.6}$$

where $\dot{Q}$ represents the heat transfer rate in W, and Z expresses the HGAHE depth in m.

Total thermal resistance (R) to thermal flow during the operation is given by Eq. (II.7) [90]:

$$R = \frac{T_{so} - T_{avg}}{\dot{Q}_z} \quad \text{(II.7)}$$

In the above equation, T_{so} represents the initial mean soil temperature in °C, which is considered as 24.8°C in this study based on the experimental measurement, and T_{avg} represents the average of inlet and outlet temperatures in °C.

II.4.4 Pressure drop

The pressure drop is an important parameter in the field of the fluid flow and a phenomenon that has to be taken into account while investigating the ground heat exchangers installation. The pressure drop of air flow along the length of pipe can be calculated using Eq. (II.8) [91]:

$$\Delta P = f\left(\frac{L}{d}\right)\left(\frac{\rho V^2}{2}\right) \quad \text{(II.8)}$$

where f is the friction factor, L is the pipe length in m, d is the pipe diameter in m, ρ is the fluid density in kg m^{-3} and V is the fluid velocity in m s^{-1}.

In the present study the range of the applied airflow velocity was from 10 to 20 m s^{-1} which yields to a Renolds number from 41,000 to 82,000, respectively. Thus, a turbulent flow is considered throughout the whole study. For a straight pipe, Blasius correlation for the friction factor f could be used [91].

$$f_s = \frac{0.3164}{Re^{0.25}} \quad \text{(II.9)}$$

where f_s denotes for the friction factor in straight pipe, and Re stand for Reynolds number.

Ju et al [92] proposed a correlation for the friction factor in helical pipes for turbulent flow, the friction factor could be determined using the following correlation [91].

$$f_c/f_s = 1 + 0.11Re^{0.23}(d/D) \quad \text{(II.10)}$$

where f_c denotes for the friction factor in curved pipe, d and D stand for the pipe and the HGAHE diameters respectively.

II.4.5 Derating factor

Thermal performance derating factor is an important performance indicator that allows to assess the decline in thermal efficiency, which is taken place when the helical ground air heat exchanger is placed into service over longer operation time. Thermal efficiency of the HGAHE at the initial time of starting the operation is considered as a reference state to compare the thermal efficiency of the HGAHE in continuous operation. The drop in the air temperature found at the beginning of the operation and after any time of the operation are taken as inputs to calculate the thermal performance derating factor as shown in Eq. (II.11) [65]:

$$TPDF = 1 - \frac{(T_{in} - T_{out})_{at\ time\ t}}{(T_{in} - T_{out})_{initial}} \tag{II.11}$$

where T_{in} and T_{out} stand for the inlet and outlet air temperatures in °C, respectively.

II.5 Multiple linear regression

Multiple-linear regression (MLR) is a commonly used mathematical tool in developing correlations involving the GHEs thermal analysis [90]. Thus; in the parametric study subsection, multiple-linear regression is employed to estimate the correlation between the operating and geometric parameters (inputs) including ventilation velocity, inlet temperature, pipe diameter, pipe thickness, helical pitch and helical diameter with the outlet temperature as an output (i.e. the main performance indicator that allows to assess the HGAHE thermal efficiency).

Mathematical models are often used to describe and explain the behavior of a particular variable of interest. Models usually have coefficients that need to be adjusted to fit data from experiments, and the term regression is the process of determining those coefficients that makes a model best fit data [93], which eventually estimates the correlation level between inputs and outputs. Multiple-linear regression analysis is a statistical process which helps to construct a relation between a set of input variables with an output or a dependent variable. This analysis facilitates in identifying the contribution of each input to produce the output, where each value of the input variables (features) is related to a dependent variable *y* value. In its general form, a multiple-linear equation model may be written in a compact form of equation as follows:

$$\hat{y} = b_0 + \sum_{i=1}^{n} b_i x_i \tag{II.12}$$

In the above equation, $\hat{y}$ is the output (target) of the model, x_i represents the independent inputs (features) of the model, while $b_0, b_1, b_2, \ldots, b_m$ are the regression model coefficients. Eq. (II.12) may be rewritten in a more simple and explicit form for a data available with n measurements of p independent variables in each sample. Equation for variables x_1, x_2,. . ., x_p is defined as:

$$y = b_0 + b_1 x_1 + b_2 x_2 + \cdots + b_p x_p + \epsilon \tag{II.13}$$

where ε is the error term which represents the deviation between the actual and predicted values.

For evaluation of the prediction accuracy and performance assessment of the regression models, in addition to the simple Mean Absolute Error (MAE), a number of statistical indicators were used. These metrics include the MSE (Mean Squared Error), RMSE (Root Mean Squared Error), and coefficient of determination (R^2), while R^2 is used to assess variability of data that is being accounted or explained by the model [94]. Other indicators are used to quantify predictions errors, e.g., MAE expresses quantitative errors in predictions, but since all values having the same importance [95], this may not be desired. Hence, MSE and RMSE are employed to overcome this drawback. MSE measures how far the estimation is from the true values since it is an expectation of the Euclidean distance between predicted and true values [96]. RMSE is also a frequently-used metric to evaluate mean square differences (deviations) between predicted and actually observed values from a variable being estimated [97]. Additionally, the adjusted R^2 as well as the predicted R^2 are used in this study. The statistical indicators used can be expressed mathematically as follows:

$$MAE = \frac{1}{n}\sum_{i=1}^{n}\left|T^{*}outlet_{i,numerical} - T^{*}outlet_{i,predicted}\right| \tag{II.14}$$

$$MSE = \frac{1}{n}\sum_{i=1}^{n}\left(T^{*}outlet_{i,numerical} - T^{*}outlet_{i,predicted}\right)^2 \tag{II.15}$$

$$RMSE = \sqrt{\frac{1}{n}\sum_{i=1}^{n}\left(T^{*}outlet_{i,numerical} - T^{*}outlet_{i,predicted}\right)^{2}} \tag{II.16}$$

$$R^{2} = 1 - \frac{\sum_{i=1}^{n}\left(T^{*}outlet_{i,numerical} - T^{*}outlet_{i,predicted}\right)}{\sum_{i=1}^{n}\left(T^{*}outlet_{i,numerical} - \overline{T^{*}outlet_{i,predicted}}\right)} \tag{II.17}$$

where $T^{*}outlet_{\mathrm{i},numerical}$ and $T^{*}outlet_{\mathrm{i,predicted}}$ are the i^{th} numerical and predicted dimensionless outlet temperatures, while n is the number of observations.

A final step before modeling and implementing the MLR, the numerical dataset should be normalized to an interval of [0, 1] to eliminate the influence of each attribute dimension. The normalization is achieved using Eq. (II.18):

$$\bar{x} = \frac{x - x_{min}}{x_{max} - x_{min}} \tag{II.18}$$

where $\bar{x}$ is the normalized variable, x is the original variable from dataset, while x_{max} and x_{min} are the maximum and minimum values of the corresponding variable in the dataset, hence $\bar{x}$ is 0 when x is minimum and 1 when it is maximum.

II.6 Uncertainty analysis

In order to demonstrate the accuracy of the experiments, error analysis is required since uncertainties and errors may cause from the device choice, condition, calibration, and environment. Uncertainties can be determined by the fraction of the measurement device lowest count and minimal parameter reported rate [98]. In this study, least count of measurement devices of air temperature and velocity are respectively 0.1 °C and 0.1 m/s. Whereas, the lowest recorded values for air temperature and velocity are 22°C and 10 m/s, respectively. Hence, the maximum error in the air temperature and flow velocity measurement is estimated as ± 0.45 % and ±1.0 %, respectively.

II.7 Conclusion

This chapter has presented the design and implementation of the experimental set up installed to investigate the helical ground air heat exchanger behavior. The site design and implementation are described, including; the instrumentation selection, experiment methodology as well as the uncertainty analysis. Experiments have been conducted under the regulated conditions of the operational criteria. Hence, the in-situ measurement data will be used to assess the thermal performance of the HGAHE system in terms of air temperature drop, heat transfer rate, total thermal resistance, effectiveness, pressure drop as well as thermal performance derating factor.

CHAPTER III : NUMERICAL MODELLING

III.1 Introduction

In this chapter, the theoretical and numerical formulations of the model have been presented. Within the context of this study, the formulated three-dimensional transient model has been applied to the investigate the heat efficiency of helical ground air heat exchanger as well as the heat penetration into the borehole using CFD software package, ANSYS Fluent. The finite volume method is used in the Fluent software which transforms the governing equations in numerical solvable algebraic equations. The details of CFD model, boundary conditions and solution method of the numerical model have been communicated in the next sub-sections.

III.2 Physical model

The developed HGAHE system material properties and physical geometry including the PVC pipe, backfill material, borehole and soil domain were created by the ANSYS DESIGN MODELER as shown in Figure III.1. The HGAHE system consists of 30 m long pipe with 3.5 mm thickness and 0.06 m inner diameter. The total vertical length of the designed helical-coil layout is 3 m, the diameter is 0.8 m, and the pitch size is 0.28 m as presented in Figure III.1b. The backfill material, borehole and surrounding soil were defined through creating cylinders volume. The backfill material diameter, borehole diameter and soil domain diameter are 1, 1.2, and 3 m respectively, and total length of soil domain is 5 m, as shown in Figure III.1a. It should be pointed out that, the geometry and properties of material are maintained the same as available in the studied application area, which is depicted in Table II.1.

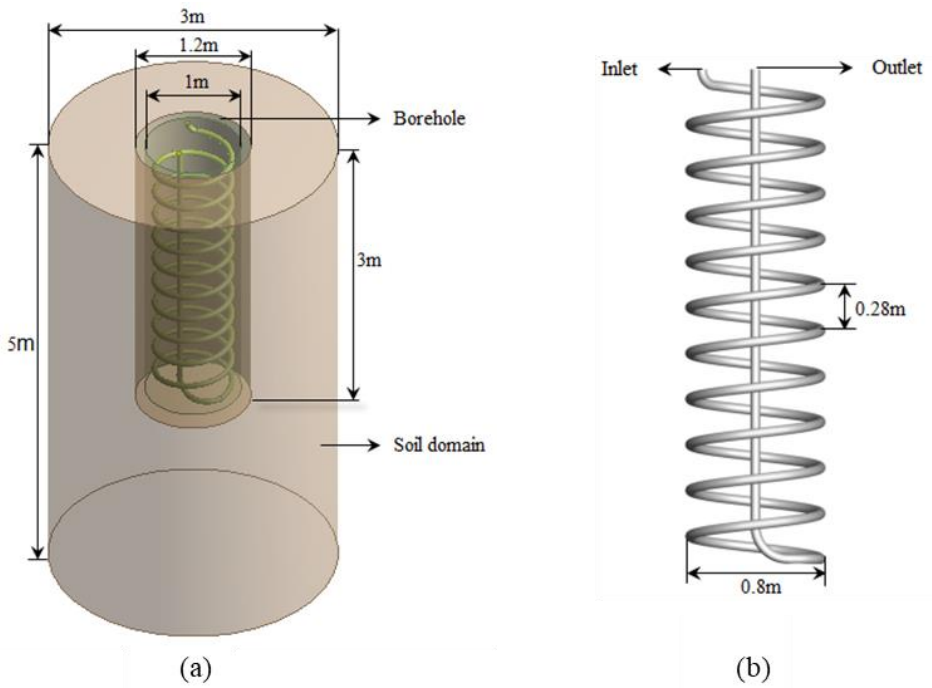

Figure III.1: Physical model geometry: (a) HGAHE system, (b) helical pipe.

III.3 Assumptions

The following assumptions have been considered in the CFD program Fluent used in this work to analyze the air flow and heat exchange processes in a GAHE system.

- The thermophysical properties of all parts are homogenous, isotropic, and temperature-independent.
- Thermal contact between all components is perfect.
- Initial temperature of all components is considered equal to the undisturbed ground temperature.

III.4 Mathematical formulation

III.4.1 Governing equations

For the HGAHE under investigation in present work, the working fluid was considered to be air, a Newtonian, incompressible fluid with constant thermophysical properties (since the highest airflow velocity used in the present study is 20 m/s provides a Mach number of 0.058 which is less than 0.3. Therefore, the flow can be treated as incompressible). While the fluid flow was considered to be turbulent, the viscus dissipation rate was negligible, under the considered assumptions, the governing Reynolds Averaged Navier-Stokes (RANS) and energy equations for the problem under investigation are as stated below [99]:

$$\frac{\partial \rho}{\partial t} + \frac{\partial (\rho u_i)}{\partial x_i} = 0 \tag{III.1}$$

$$\frac{\partial (\rho u_i)}{\partial t} + \frac{\partial (\rho u_i u_j)}{\partial x_j} = -\frac{\partial p}{\partial x_i} + \frac{\partial}{\partial x_i}\left[\mu\left(\frac{\partial u_i}{\partial x_j} + \frac{\partial u_j}{\partial x_i} - \frac{3}{2}\delta_{ij}\frac{\partial u_j}{\partial x_j}\right)\right] + \frac{\partial}{\partial x_j}\left(-\rho\overline{u_i' u_j'}\right) \tag{III.2}$$

$$\frac{\partial (\rho c_p T)}{\partial t} + \nabla.\left(\rho u_i c_p T\right) = \nabla. q + S_e \tag{III.3}$$

where the term $-\rho\overline{u_i' u_j'}$ is known as the Reynolds stresses, it must be modeled in order to close the system of governing equations, one of the widely used approaches to model it is the Boussinesq hypothesis, which is employed in several eddy viscosity turbulence models, in this work, the $k - \epsilon$ turbulence model is used and it is presented in the numerical procedure section.

The finite volume method transforms the set of governing partial differential equations to a system of linear algebraic equations. The conservation equations mentioned in the preceding equations (Eqs. (III.1), (III.2), (III.3)) can be written in the form of a single equation over a given control volume known as the transport equation which provides the ability to discretize the governing equations. This method consists of integrating the transport equation of each control volume, yielding a discrete equation that expresses the conservation law on a control volume basis. The transport equation can be written in integral form by the following equation [100].

$$\int_V \frac{\partial \rho\varphi}{\partial t} dV + \oint \rho\varphi\vec{u} \, . \, d\vec{A} = \oint \Gamma_\varphi \nabla\varphi \, . \, d\vec{A} + \int_V S_\varphi dV \tag{III.4}$$

where φ denotes the transported quantity such as velocity, mass or temperature. V and $\vec{A}$ refer the arbitrary control volume and the surface area vector. Γ_φ, $\nabla\varphi$ and S_φ respectively stand for diffusion coefficient, gradient and source term of the transported quantity φ.

Discretization of Eq. (III.4) on a given cell yields in nonlinear equation. A linearized form of Eq. (III.4) can be written as follows [99].

$$a_p\varphi = \sum_{nb} a_{nb}\varphi_{nb} + b \tag{III.5}$$

where the subscript nb stands for the neighbor cells, b refer the source term vector. a_p and a_{nb} denote the linearized coefficients for φ and φ_{nb}.

Similar equations can be applied for each control volume in the domain. This yields in a set of algebraic equations. A CFD code (ANSYS Fluent) using an appropriate algorithm solves this linear system by the point implicit linear equation solver in conjunction with an algebraic multigrid method [99].

III.4.2 Pressure drop calculation

Another important parameter in this study, is the pressure drop of air flow along the length of heat exchanger, ΔP is defined as the difference in pressure between the inlet and outlet of the heat exchanger, and is given by the following formula [90]:

$$\Delta P = P_{in} - P_{out} \tag{III.6}$$

where ΔP, P_1, and P_2 are pressure drop, inlet and outlet pressure respectively, the pressure drop along the pipe, can be calculated using Eq. (II.8):

In order to verify the accuracy of the model, numerical pressure drop along the heat exchanger obtained from the simulations, is compared to the results of correlations for the calculation of pressure drop (friction factor) in straight pipe (with the same dimensions as the original helical pipe), as well as correlations for helical pipes, for a turbulent flow in straight pipe, Blasius proposed a simple correlation for the friction factor f [101, 102], where it is given by Eq. (II.9):

Ju et al [103] presented a correlation for the friction factor in helical pipes for turbulent flow, according to their experimental results, the friction factor is calculated using Eq. (II.10):

In addition, Schmidt [102, 104] also proposed a correlation for the pressure drop in helical pipes, where the friction factor f is given by Eq. (III.7) [102, 104]:

$$f = \frac{0.3164}{Re^{0.25}}\left[1 + 0.0823\left(1 + \frac{D}{d}\right)\left(\frac{D}{d}\right)^{0.53} Re^{0.25}\right] \tag{III.7}$$

In this equation d and D are pipe and heat exchanger diameters respectively, it is worth mentioning that Eq. (III.7) is valid for flows where $Re > 22000$.

III.5 Numerical procedure

ANSYS Fluent CFD code was used to investigate the transient fluid flow and heat transfer phenomena in the HGAHE, the Fluent solver, based on the finite volume method, was implemented to solve the set of governing equations of continuity, momentum and energy, for which the $k - \epsilon$ turbulence model in its realizable version was used to model turbulent flow and solve the RANS equations numerically. Transport equations for the turbulent kinetic energy k and the dissipation rate ϵ of the turbulence model are given as follows [105]:

$$\frac{\partial(\rho k)}{\partial t} + \frac{\partial(\rho k u_j)}{\partial x_j} = \frac{\partial}{\partial x_j}\left[\left(\mu \frac{\mu_t}{\delta_k}\right)\frac{\partial k}{\partial x_j}\right] + G_k + G_b - \rho\epsilon - Y_M + S_k \tag{III.8}$$

$$\frac{\partial(\rho\epsilon)}{\partial t}+\frac{\partial(\rho\epsilon u_j)}{\partial x_j}=\frac{\partial}{\partial x_j}\left[\left(\mu\frac{\mu_t}{\delta_\epsilon}\right)\frac{\partial\epsilon}{\partial x_j}\right]+\rho C_1 S\epsilon-\rho C_2\frac{\epsilon^2}{k+\sqrt{\nu\epsilon}}+C_{1\epsilon}\frac{\epsilon}{k}C_{3\epsilon}G_b+S_\epsilon \quad \text{(III.9)}$$

The eddy viscosity μ_t is calculated using the following expression:

$$\mu_t=\rho C_\mu\frac{k^2}{\epsilon}$$

It should be noted that C_μ for this version of the $k-\epsilon$ model is not constant, and the model constants are: $C_{1\epsilon}=1.44, C_2=1.9, \delta_k=1.0$ and $\delta_\epsilon=1.2$, further details about the model's equations can be found in reference [105].

III.5.1 Boundary condition

The main parts of the considered model are the air, backfill material, borehole, and surrounding ground. Far-field boundaries in the ground domain have been treated as constant temperature surfaces, similar to the soil average temperature (24.8 °C). Beyond this, the ground conditions are considered as a constant. Researchers in numerous simulations works [106, 107] noted that, temperature of the ground does not vary considerably beyond the distance of more than 10 times the tube diameter and therefore, temperature variation may be ignored. In present work, the pipe diameter is 0.06 m and the helical-pipe diameter is 0.8 m, therefore, the cylinder diameter of the soil domain has been taken as 3 m. It should be noted that, mutual interfaces between all parts were considered as a temperature-coupled wall. Also, a velocity-inlet boundary at 10 m/s of a constant flow velocity is considered for the inlet. However, the air temperature at the inlet boundary is adjusted to the range of 10 min based on the measured ambient air temperature through a transient table function. For the outlet, an outflow boundary is applied.

III.5.2 Solution approaches

Three-dimensional unsteady numerical simulation of the HGAHE system was performed using a CFD software. 10 m/s as a constant inlet airflow velocity has been considered during the whole operation period, resulting in turbulent fluid flow occurred in the helical pipe. The SIMPLE scheme was implemented for pressure-velocity coupling and the second-order upwind was adopted in the spatial discretization of the governing equations. Furthermore, under-relaxation factors of 1 and 0.7 were adopted for energy and momentum, respectively. In addition, the convergence criteria were set to 10^{-3} for continuity, momentum, k, and ε equations, and 10^{-6} for energy equation.

III.6 Conclusion

This chapter has presented the mathematical formulation and numerical procedure of the established transient numerical model which has been validated against the experimental data. The validated model will be employed to understand the borehole temperature distribution and analyze the heat penetration into the axial and radial directions. Furthermore, the numerical model will be used to investigate the influence of different important operating and geometric parameters. The overall thermal performance of the HGAHE system will be mainly evaluated in terms of the outlet temperature, heat exchange rate, effectiveness and pressure drop. The main findings and outcomes will be described in the following chapter.

CHAPTER IV : RESULTS AND DISCUSSION

IV.1 Introduction

The investigations presented within the scope of this chapter can be divided into three sections. Section IV.2 contains experimental analyzes of the thermal performance of the proposed helical ground air heat exchanger for cooling purposes under Saharan climate. Thermal performance of the HGAHE system is mainly analyzed in terms of air temperature drop, heat transfer rate, total thermal resistance, effectiveness, pressure drop as well as thermal performance derating factor. Section IV.3 contains numerical simulation results conducted using ANSYS Fluent for cooling purposes in 24 hours continuous operation using the ambient air temperature to assess the thermal performance of the HGAHE system under unsteady conditions as well as to understand the borehole temperature distribution and analyze the heat penetration into the axial and radial directions. Section IV.4 presents the parametric study results as well as the multiple regression model which predicts the thermal performance of the HGAHE system.

IV.2 Experimental

IV.2.1 First experiment

The HGAHE system has been evaluated in terms of cooling thermal potential by operating the system at a constant air flow velocity of 10 m/s. Experiments were performed on 06 May 2017 from 09 am to 06 pm for 09 hours of operation period.

Figure IV.1 illustrates the inlet temperature (i.e. ambient air temperature) and outlet temperature and the heat exchange rate of the HGAHE system versus operation time. It is observed that, for higher inlet temperature better thermal performance is attained at 12:40 pm when the inlet temperature was 41.0 °C, resulting in an air temperature drop of 13.3 °C. It is also observed from the figure that, the outlet temperature of the HGAHE system significantly depends on the inlet temperature, even though the variation in the outlet temperature is much lower due to the large borehole and surrounding soil thermal mass. When the inlet air temperature fluctuated from 41.0 °C to 32.5 °C (averaged at 36.7 °C) the outlet temperature attained ranged from 27.4 °C to 25.1 °C (averaged at 26.2 °C).

Temperature of air at the inlet and exit of the pipe was recorded using the temperature sensors to calculate the heat exchange rate (HER, $\dot{Q}$) between the pipe surface and borehole. From Figure IV.1, it can be seen that the HER varied according to the inlet air temperature. As evident in the figure, the HER was in the range of 463.4 W to 228.2 W when inlet air temperature fluctuated from 41.0 °C to 26.6 °C. It is observed that, the maximum HER (463.4

W) was attained at the highest inlet temperature (41.0 °C) at 12:40 pm. The variation of the HER is dependent to the inlet temperature, which could be attributed to the fact that, the heat exchange is dependent to the air temperature drop, as indicated in Eq. (II.1). Definitely, when the inlet temperature augments or decreases, the air temperature drop increments or decrements respectively, resulting in the trend of heat exchange rate to be similar to the inlet temperature variation.

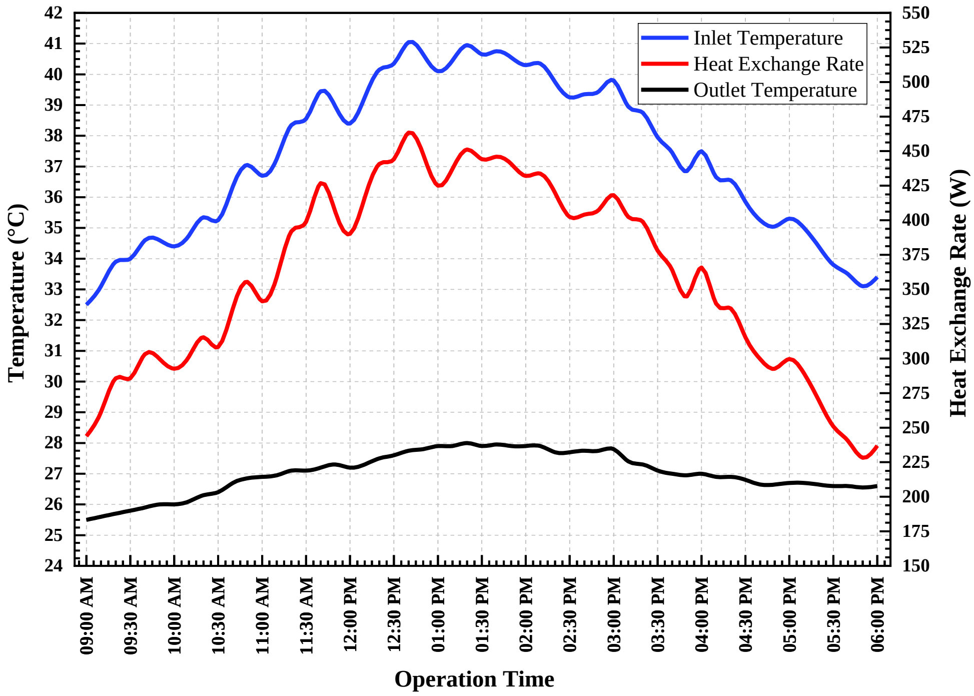

Figure IV.1: Inlet and outlet air temperature and heat exchange rate versus operation time.

IV.2.2 Second experiment

For evaluating thermal performance of the HGAHE, the system was continuously run for 3 hours. The performance of the system is mainly analyzed in terms of air temperature drop obtained, heat transfer rate, total thermal resistance, effectiveness, pressure drop and thermal performance derating factor, which will be discussed in the following subsections.

IV.2.2.1 Air temperature drop

Air temperature drop after a period of 1, 2 and 3 hours versus airflow velocity is presented in Figure IV.2. It is noticed that after a period of 1-hour, the overall air temperature drop is 11.0, 10.4, and 9.6 °C for the flow velocity of air at 10, 15 and 20 m s^{-1}, respectively, at the pipe exit. But, after a period of 3 hours, the air temperature drop is 10.5, 9.4, and 8.3 °C for the flow velocity of air respectively at 10, 15 and 20 m s^{-1}. This finding proves that, in a period of 3 hours, total reached temperature drop is decreased by 4.5, 9.6, and 13.5 %, respectively, for the air flow velocity of 10, 15, and 20 m s^{-1}. Furthermore, the highest temperature drops after a period of 1, 2 and 3 hours were 11.0, 10.7, and 10.5°C respectively, which were registered for V=10 m s^{-1}. Since air retention time inside the pipe is incremented at lower speed, it induces further heat exchange and therefore raises the drop in air temperature.

The findings of the above paragraphs show that, by the passage of time, further thermal flow is performed, which contributes on incrementing the outlet air temperature, and thus decreasing the air temperature drop. Moreover, with higher velocity of air (20 m s^{-1}), the pipe of the heat exchanger is warmed up at much quicker rate, resulting in less drop in air temperature record at the exit of HGAHE system.

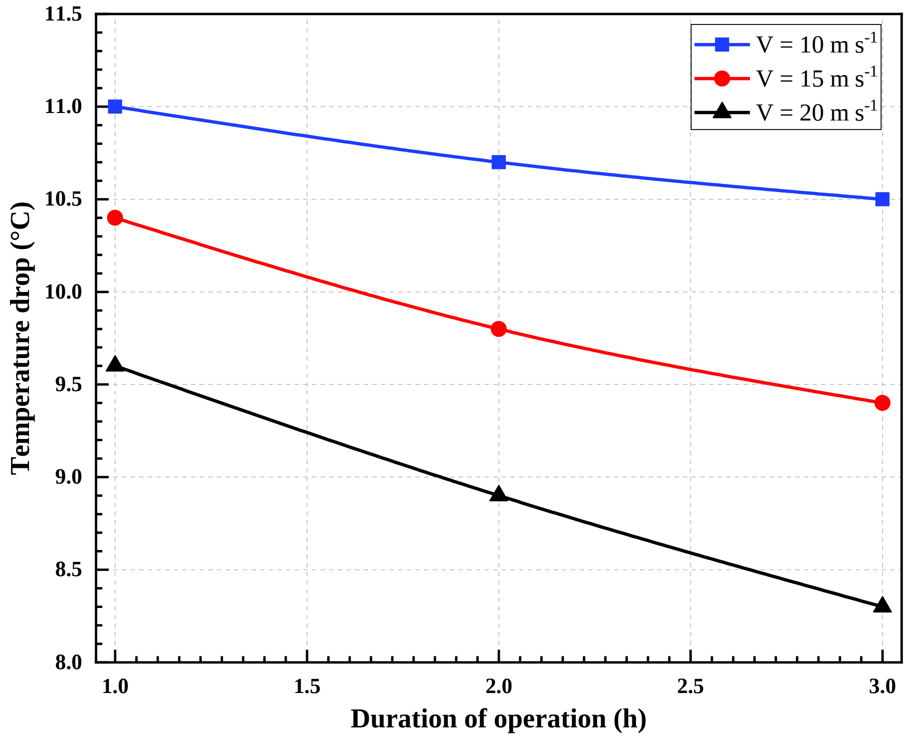

Figure IV.2: Drop in air temperature versus operation time for different airflow velocities.

IV.2.2.2 Temperature of air across the pipe

Figure IV.3 illustrates the air temperature variation across the pipe length of the heat exchanger after a period of 1 and 3 hours for V=10 m s^{-1} and T_{in}=38 °C. It can be seen that after 1 hour of time duration of operation, outlet temperature of air was 27 °C at the pipe outlet. Whereas, after 3 hours of time duration of operation, the outlet temperature of air at the pipe exit was 27.5 °C. Therefore, an increment of 0.5 °C is obtained at the outlet air temperature between 1 and 3 hours of operation time. Similarly, after a period of 1 and 3 hours, a drop in the air temperature of 11.0 and 10.5 °C is noticed at the pipe outlet, respectively.

Moreover, drop in temperature of air in HGAHE system is observed to be significantly higher in the first section of the pipe and smaller in the last section (i.e. third section). After a period of 1 hour, the reported air temperature drop is 6.5, 2.9, and 1.6 °C at the first section (from 0 to 10 m), second section (from 10 to 20 m), and third section (from 20 to 30 m), respectively.

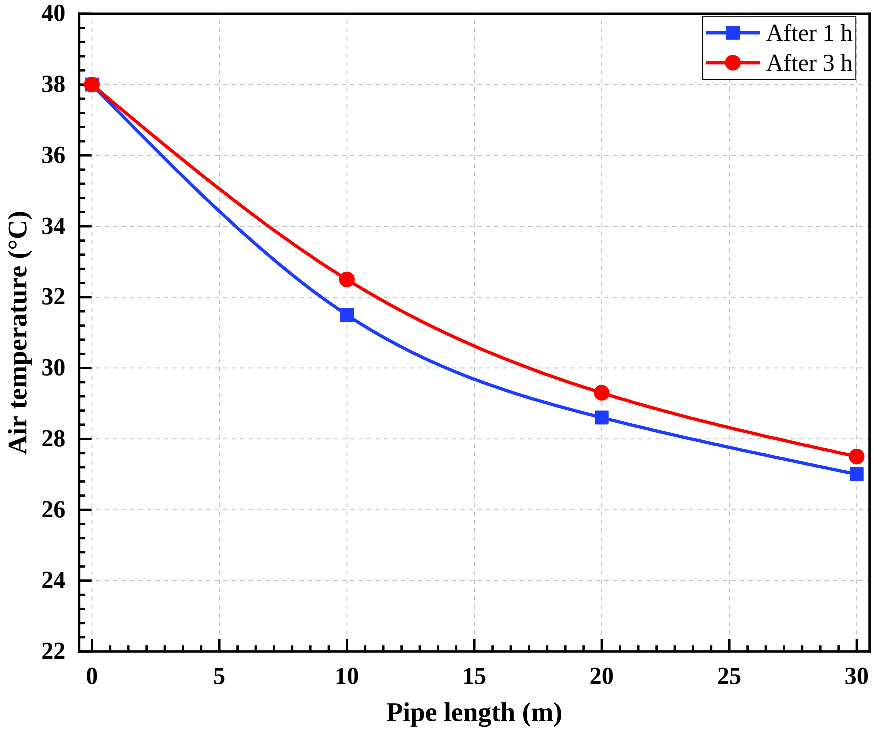

Figure IV.3: Air temperature across the length of pipe after a period of 1 and 3 hours.

IV.2.2.3 Heat exchange rate

Heat exchange rate of HGAHE system determined on hourly basis at various velocities is illustrated in Figure IV.4. It can be seen that, after a period of 1 hour, heat exchange rate was 383.2, 543.5 and 668.9 W corresponding to flow velocities of 10, 15 and 20 m s^{-1}, respectively. Besides, after 3 hours of operation time, the heat exchange rate is obtained to be 365.8, 491.2 and 578.3 W, respectively, for V=10, 15 and 20 m s^{-1}. This outcome indicates that, in a period of 3 hours, the heat exchange rate of the HGAHE system decreases by 4.5, 9.6, and 13.5 %, respectively, for the corresponding air flow velocities, in comparison with its heat exchange rate after 1 hour.

It is further noticed from Figure IV.4 that, by raising the velocity of air from 10 to 20 m s^{-1}, the heat exchange rate of the HGAHE system increases from 383.2 W and 365.8 W to 668.9 W and 578.3 W, after a period of 1 and 3 hours, respectively. Due to the same reason, i.e. raising the air velocity, the mass flow rate through the pipe also increments, which rises the total heat exchange rate of the system.

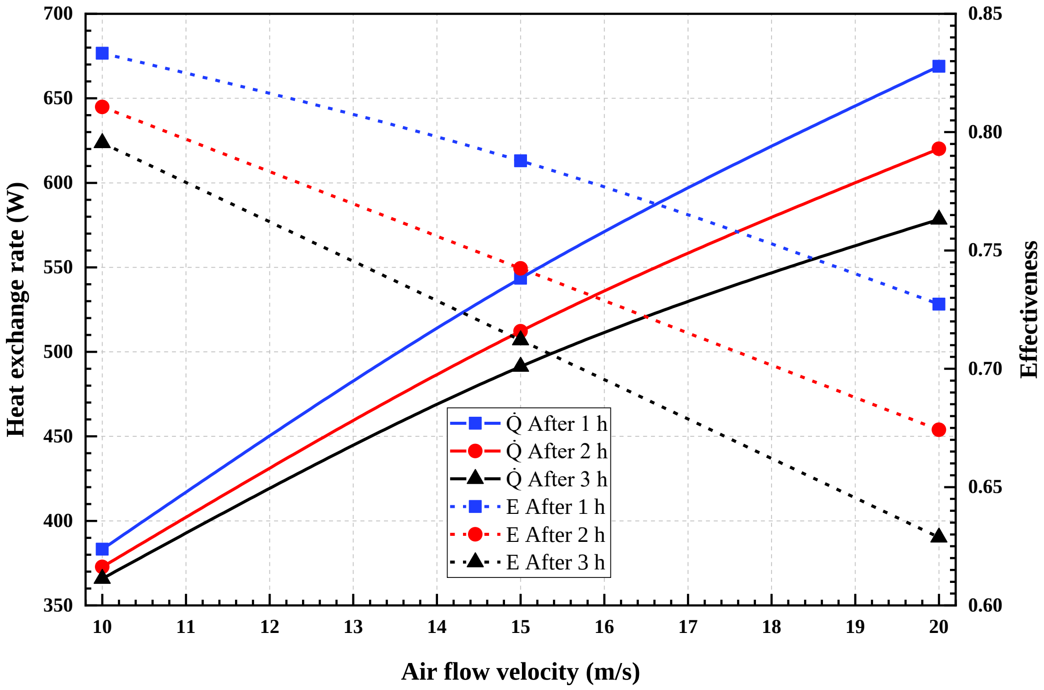

Figure IV.4: Heat exchange rate and effectiveness versus airflow velocity after a period of 1, 2 and 3 hours.

A similar trend of the decline in the heat transfer rate per meter of pipe length with the time duration of operation is also noticed for 10, 15 and 20 m s^{-1} air velocities, which is calculated by Eq. (II.2) and presented in Figure IV.5. As evident in the figure, the maximum heat transfer rate per meter of pipe length was attained at the highest airflow velocity of 20 m s^{-1}. It is 22.2 W m^{-1} after 1 hour of operation and decreased by 3.0 W m^{-1} after 3 hours of operation time.

The overall heat transfer coefficient of the HGAHE system versus the operation time has been determined by Eq. (II.3) and depicted in Figure IV.5. As per Eq. (II.3) the overall heat transfer coefficient is a function of the heat exchange rate. Obviously, as the heat exchange rate increases, the overall heat transfer coefficient also increases, therefore similar to the heat exchange rate behavior the overall heat transfer coefficient has a decline trend with the operation time and an increase tend with the air flow velocity. It can be seen from Figure IV.5 that, the maximum overall heat transfer coefficient was obtained at the highest airflow velocity of 20 m s^{-1} which is 6.9 W m^{-2} °C^{-1} after 1 hour of operation, whereas it is dropped to 5.3 W m^{-2} °C^{-1} after 3 hours of operation time.

These results reveal that the heat transfer rate of HGAHE diminishes with operation time due to the fact that, at the beginning of the operation, the borehole and surrounding ground has a steady temperature which generates high heat exchange rates. Borehole and surrounding soil temperature incremented after certain period of time by transmitting heat from air to borehole and surroundings, consequently, the heat exchange rate gradually decreases. Furthermore, by increasing the air velocity, the heat exchange rate of the HGAHE system increment, however, the progressive improvement rate decreases. This can be due to the fact that as the air velocity increments, the total mass flow rate augments and the quantity of heat transferred by air to the surrounding ground also increments in a particular time frame. But the heat cannot get transmitted to the corresponding earth layers instantly, hence, the ground temperature around the HGAHE system increases. It is similarly justified for the overall heat transfer coefficient as mentioned in Eq. (II.3) that with an increase in the heat exchange rate the overall heat transfer coefficient also increments.

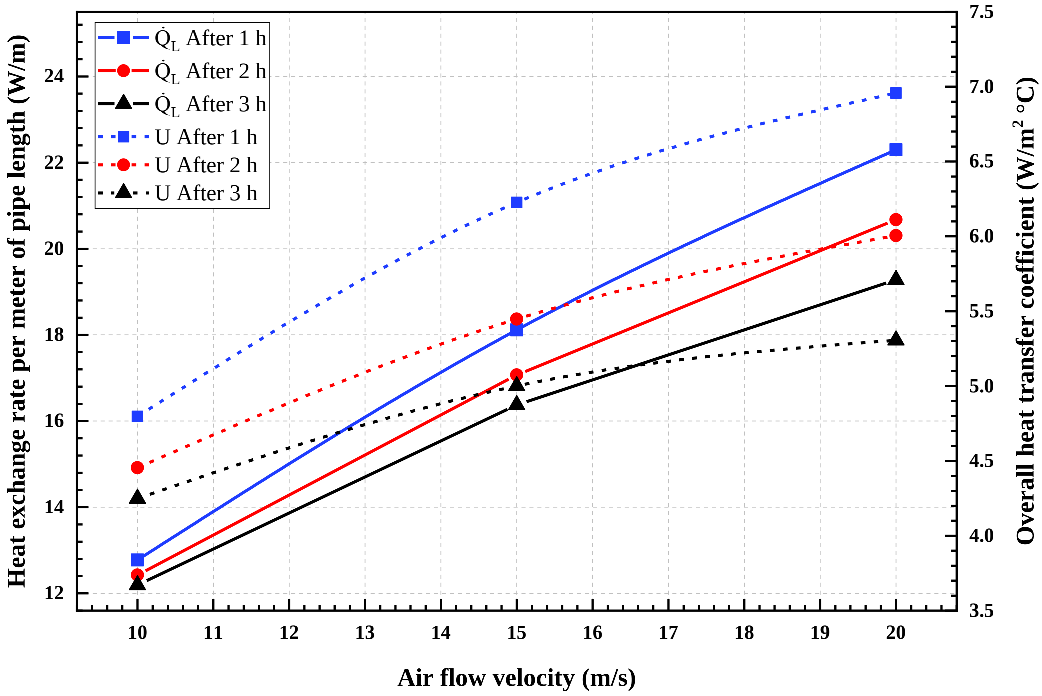

Figure IV.5: Heat exchange rate per meter of pipe length and overall heat transfer coefficient versus airflow velocity after a period of 1, 2 and 3 hours.

IV.2.2.4 Effectiveness

The effectiveness of the HGAHE system at different airflow velocities is presented in Figure IV.4. It is noticed from the figure that, after a period of 1 hour, effectiveness of the HGAHE was 0.83, 0.78 and 0.72 for 10, 15 and 20 m s^{-1} air velocities, respectively. Whereas, after 3 hours of time duration, the effectiveness of the HGAHE decreases to 0.79, 0.71 and 0.62, respectively, for V = 10, 15 and 20 m s^{-1}. Thus, the effectiveness of HGAHE drops with the operation period. Furthermore, by incrementing velocity of air from 10 to 20 m s^{-1}, effectiveness of the HGAHE diminishes by 13.25 and 21.51 %, after a period of 1 and 3 hours, respectively. In addition, at the air velocity of 10 m s^{-1}, the highest effectiveness (0.83), which is obtained after 1 hour of operation, is decreased by 4.9 % after 3 hours of operation time.

The above findings indicate that the effectiveness of the HGAHE decrements with the operation time. That is, with the operation time increasing, more heat is transferred in the ground from the HGAHE system, which results in a significant increase in the ground temperature compared to its initial undisturbed value, which decreases the total drop of air temperature inside the pipe, hence, diminishes effectiveness of HGAHE. Furthermore, at higher velocity of air, the decline in the effectiveness of the HGAHE system is much faster and marked. Because, with the increment in air velocity, the amount of the air rate across the pipe raises and the residence period inside the pipe also decrements, which decreases the total drop in temperature of air, hence, drops effectiveness of the HGAHE system.

Nevertheless, upon raising velocity of air from 10 to 20 m s^{-1}, the heat exchange rate of the HGAHE increased by 174 and 158 % after 1 and 3 hours of the time duration operation, respectively. Whereas, the effectiveness decreased by 13.25 and 21.51 %, after 1 and 3 hours of operation time, respectively. The behavior of augmentation in the heat exchange rate and decline in the effectiveness of the HGAHE system could be clarified due to the fact that the rate of the heat transfer is dependent to the volume rate and air temperature drop obtained, as shown in Eq. (II.1). Definitely, with raising the air velocity, the mass flow rate also raises, whilst the air temperature drop achieved diminishes owing to the decreased air residence period into the pipe. After a period of 3 hours, by incrementing velocity from 10 to 20 m s^{-1}, the mass flow rate of air raises from 0.035 to 0.07 kg s^{-1}, but the air temperature drop declines from 10.5 to 8.3 °C. Hence, upon raising the velocity of air from 10 to 20 m s^{-1}, the air mass flow rate enhanced up to 100 % and the drop in the air temperature decreased by just 20.9 %. Therefore, the overall augmentation in the air mass flow rate is more profound than the reduction in the air temperature, i.e., the raise in the air mass flow rate is greater compared to the decline in the air temperature drop. Consequently, the absolute influence of incrementing velocity of air is to enhance heat exchange rate of the HGAHE. For effectiveness, it is identically explained as referred in Eq. (II.5), by an increment in air flow velocity, the decline in temperature of air decrements, which in return drops the effectiveness value.

It should be highlighted that; a moderate airflow velocity should be considered to prevent a shorter decline in the performance of the HGAHE. Therefore, the intersection between the heat exchange rate and effectiveness plots might can present an optimal performance for the HGAHE system.

IV.2.2.5 Total thermal resistance

Figure IV.6 shows the total thermal resistance versus airflow velocity after a period of 1, 2 and 3 hours of continuous operation that is calculated by Eq. (II.7). It is found that, after a time period of 1 hour, the total thermal resistance was 0.100, 0.073, and 0.062 °C m W^{-1} at 10, 15 and 20 m s^{-1} air velocities, respectively. Whereas, after 3 hours of operation time, total thermal resistance was found to be 0.108, 0.086, and 0.078 °C m W^{-1} for the air velocities of 10, 15 and 20 m s^{-1}, respectively. Moreover, upon raising velocity of air from 10 to 20 m s^{-1}, the total thermal resistance decreases from 0.100 and 0.108 °C m W^{-1} to 0.062 and 0.078 °C m W^{-1}, after 1 and 3 hours of operation time, respectively. These findings indicate that the total thermal resistance increases with the operation time and decreases with the increment in the velocity of air, because the heat transfer rate of the HGAHE system drops with operation time, and increases with the increment in velocity of air as presented in Figure IV.4.

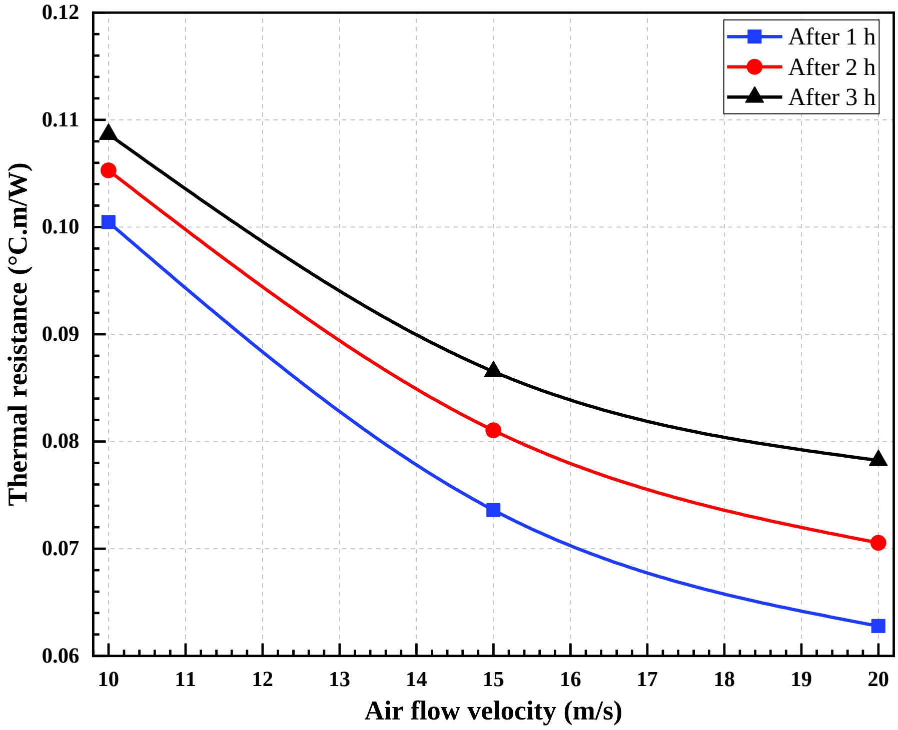

Figure IV.6: Total thermal resistance versus airflow velocity after a period of 1, 2 and 3 hours.

IV.2.2.6 Pressure drop

The calculated pressure drop of air flow along the length of pipe versus airflow velocity is shown in Figure IV.7. It is observed from the figure that; the pressure drop is raising with the increase of the flow velocity. By raising the airflow velocity from 10 to 20 m s^{-1} the pressure drop increases significantly from 1278.7 Pa to 4649.5 Pa which is about 363.6 % incremental. From these findings, it can be concluded that the flow velocity has a remarkable impact on the pressure drop of air flow along the length of pipe, this is due to the fact that, the flow velocity has a direct relation to the pressure drop as indicated in Eq. (II.8).

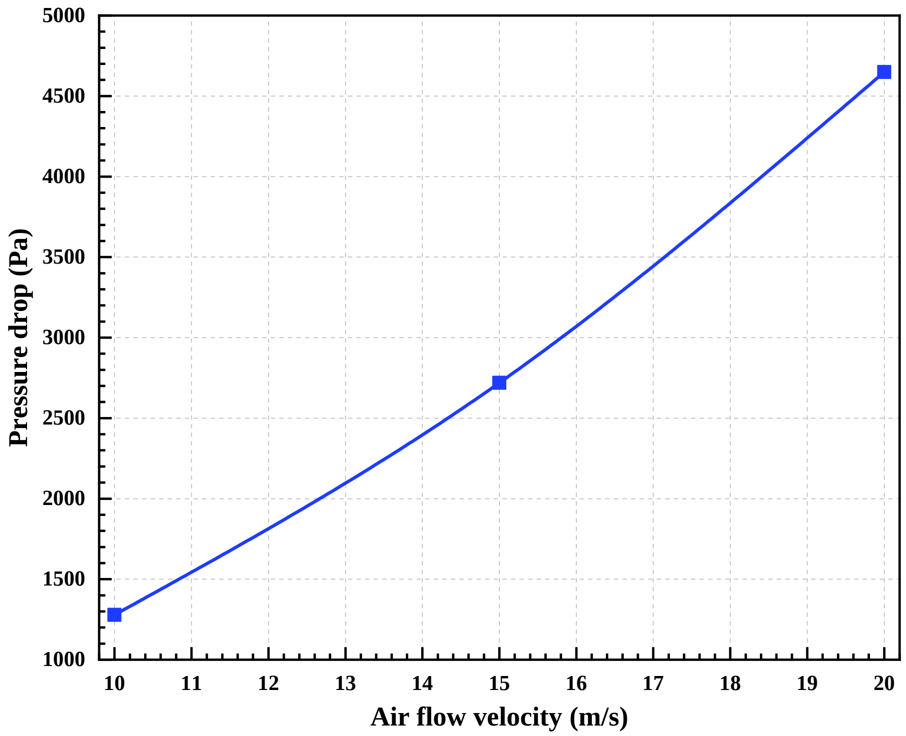

Figure IV.7: Pressure drop of air flow along the length of pipe versus airflow velocity.

IV.2.2.7 Derating factor

Thermal performance derating factor (TPDF) obtained for the HGAHE system versus operation time for different airflow velocities is plotted in Figure IV.8. It is evident from the figure that the TPDF increments with the operation time. After a period of 3 hours, TPDF is 0.14, 0.20 and 0.27 for air velocity of 10, 15 and 20 m s^{-1}, respectively. This reveals that, within a period of 3 hours, the performance of the HGAHE decreases by 27 % at velocity of 20 m s^{-1}, while, it drops only by 14 % at velocity of 10 m s^{-1}. Furthermore, the TPDF slope decreases with the operation time. Thus, the TPDF line slope for velocity of air at 10 m s^{-1} is lesser than that obtained for the velocity of air at 20 m s^{-1}. It obviously shows that the performance decline rate is significantly smaller at air velocity of 10 m s^{-1}, compared to 20 m s^{-1}. The reason can be explained as follows: By raising the velocity of air, the heat exchange rate of the HGAHE system is enhanced as presented in Figure IV.4, and more heat is transferred into the borehole and surrounding ground. This results in higher ground temperature, which increment the air outlet temperature and consequently raises the performance deterioration rate of the HGAHE system.

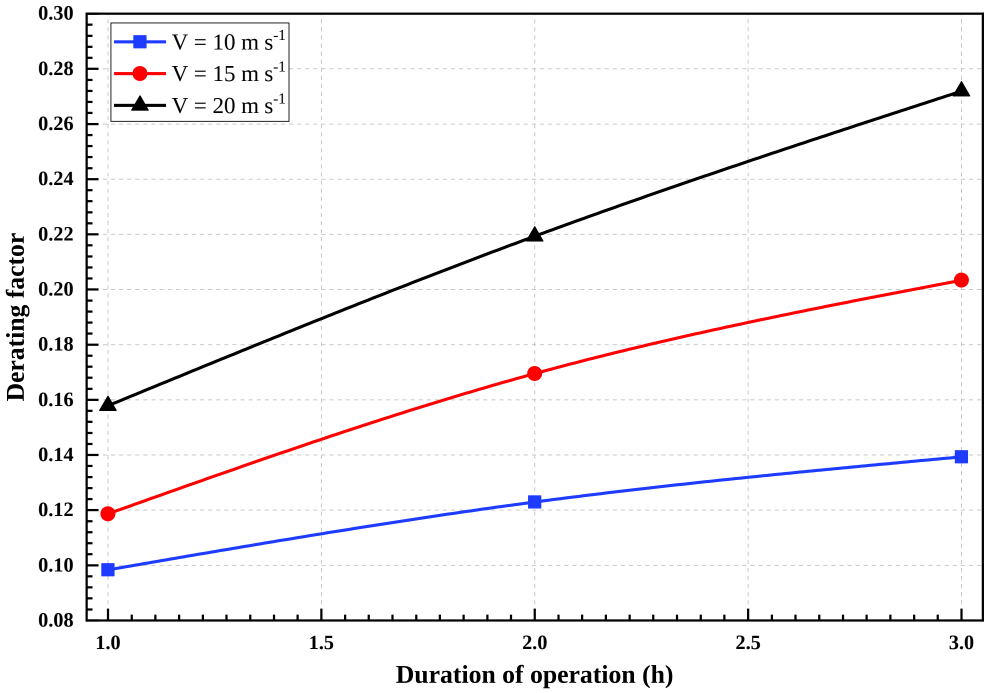

Figure IV.8: Thermal performance derating factor versus operation time for different airflow velocities.

IV.2.2.8 Comparison of the results

A comparative study has been performed to highlight the efficacy of the designed HGAHE. The comparison results of the present study with the available studies from the literature are illustrated in Table IV.1. Agrawal et al [65] investigated experimentally, thermal performance of ground air heat exchanger system using different backfilling material. They found that by using dry soil as backfilling material and with inlet air temperature of 48 °C and flow velocity of 5 m s^{-1}, after a period of 3 hours the heat exchange rate, effectiveness and TPDF was 26.6 W, 0.60 and 0.18, respectively. In another study of the same research group [108], experimental parametric study on the thermal performance of ground air heat exchanger system was conducted. Results showed that, with using dry soil as backfilling material, 42 °C of inlet air temperature and 5 m s^{-1} of airflow velocity, after a period of 3 hours operation time the heat exchange rate, effectiveness and TPDF was 530.4 W, 0.58 and 0.18, respectively. In the study performed by Benhammou et al [77] to investigate the cooling performance of EAHE during summer under Algerian Sahara climate, authors showed that, after a period of 3 hours with ambient air temperature as inlet temperature and 2 m s^{-1} as flow velocity, the heat exchange rate, effectiveness and TPDF was 836.5 W, 0.74 and 0.12, respectively. Misra et al [109] carried out a CFD simulation to analyze the thermal performance of earth air tunnel heat exchanger for summer cooling. Findings showed that, after operation period of 3 hours, the heat exchange rate, effectiveness and TPDF was 880.3 W, 0.96 and 0.01, respectively.

Table IV.1: Performance comparison of studies

Study	System technical specification	HER (W)	E	TPDF
Present	pipe length: 30 m;material: PVC; pipe diameter: 0.06 m	365.8	0.79	0.14
Agrawal et al **[65]**	pipe length: 10 m;material: PVC;pipe diameter: 0.025 m	26.6	0.6	0.18
Agrawal et al **[108]**	pipe length: 30 m;material: PVC;pipe diameter: 0.1 m	530.4	0.58	0.18
Benhammou et al **[77]**	pipe length: 50 m;material: PVC; pipe diameter: 0.3 m	836.5	0.74	0.12
Misra et al **[109]**	pipe length: 60 m;material: PVC;pipe diameter: 0.1 m	880.3	0.96	0.01

IV.3 Numerical

IV.3.1 Mesh independence and time step test

In order to achieve mesh independent results, successive refinements by incrementing the elements number from coarse mesh (1,502,920) to fine mesh (3,940,387) were tested. All the computational grids of the numerical model were formed by tetrahedral elements and were refined close to the pipe. Table IV.2 reports test results based on the outlet air temperature (main operating parameter). According to the present sensitivity analysis, the medium mesh with 2,977,894 elements was employed for the calculations, since the difference in the percentage between the obtained findings by employing the medium mesh and the fine mesh was less than 1 %. Therefore, the medium mesh has been used in the numerical simulation investigation. Figure IV.9 illustrates the mesh of the HGAHE system used in the simulations.

In this simulation, various time steps were used to examine the effect of time steps on the outlet temperature using the medium mesh. According to Figure IV.10, the outlet temperature decreases obviously when going forward to time steps higher than 600 s whilst below this value, the outlet temperature changes are beyond recognition. As a result, the time step of 600 s time was employed for the analyses in this work.

Table IV.2: Independency test of the grid system.

Parameters	Coarse mesh	Medium mesh	Fine mesh
Number of elements	1,502,920	2,977,894	3,940,387
Outlet temperature (°C)	29.13	29.46	29.51

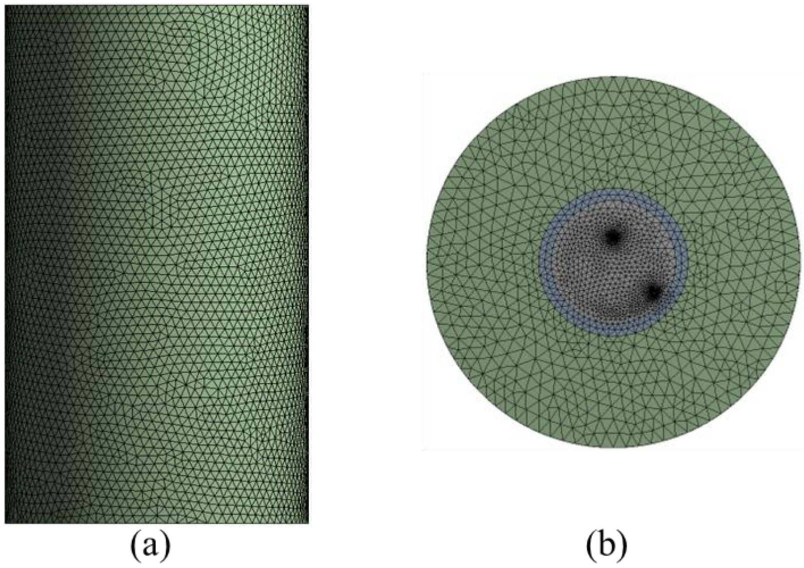

Figure IV.9: Mesh schematic of the HGAHE system: (a) side view, (b) top view.

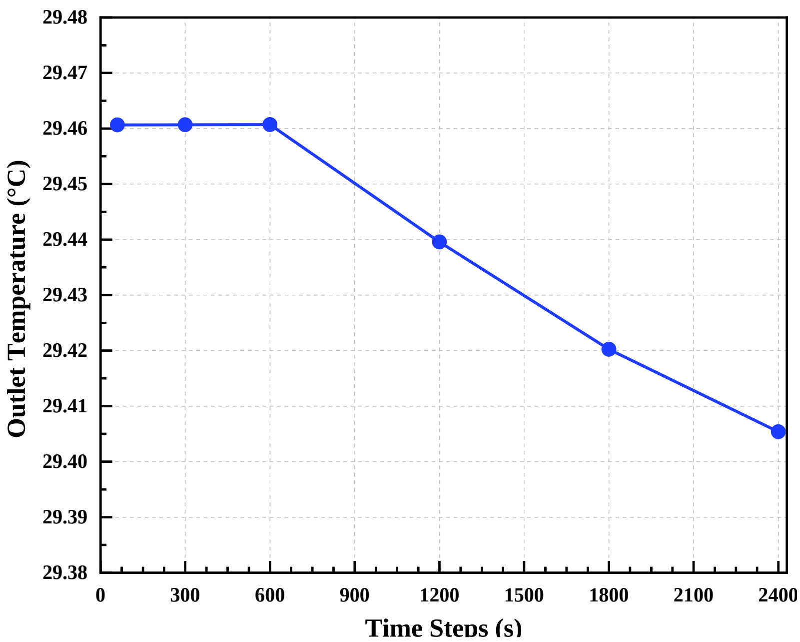

Figure IV.10: Variation of outlet temperature with time step.

IV.3.2 Validation

The established numerical model was validated with the obtained experimental data for summer weather conditions. Inlet flow velocity of 10 m/s was kept constant over the whole operation period, also the inlet temperature was changed each 10 min interval based on the measured ambient temperature using the transient table function. The difference between experimental and simulated outlet temperature results (main operating parameter) is depicted in Figure IV.11. As evident in the figure, the maximum outlet temperature difference between the experimental and simulated values is 3.2 %, which is quite small and can be used to carry out further simulation and analysis.

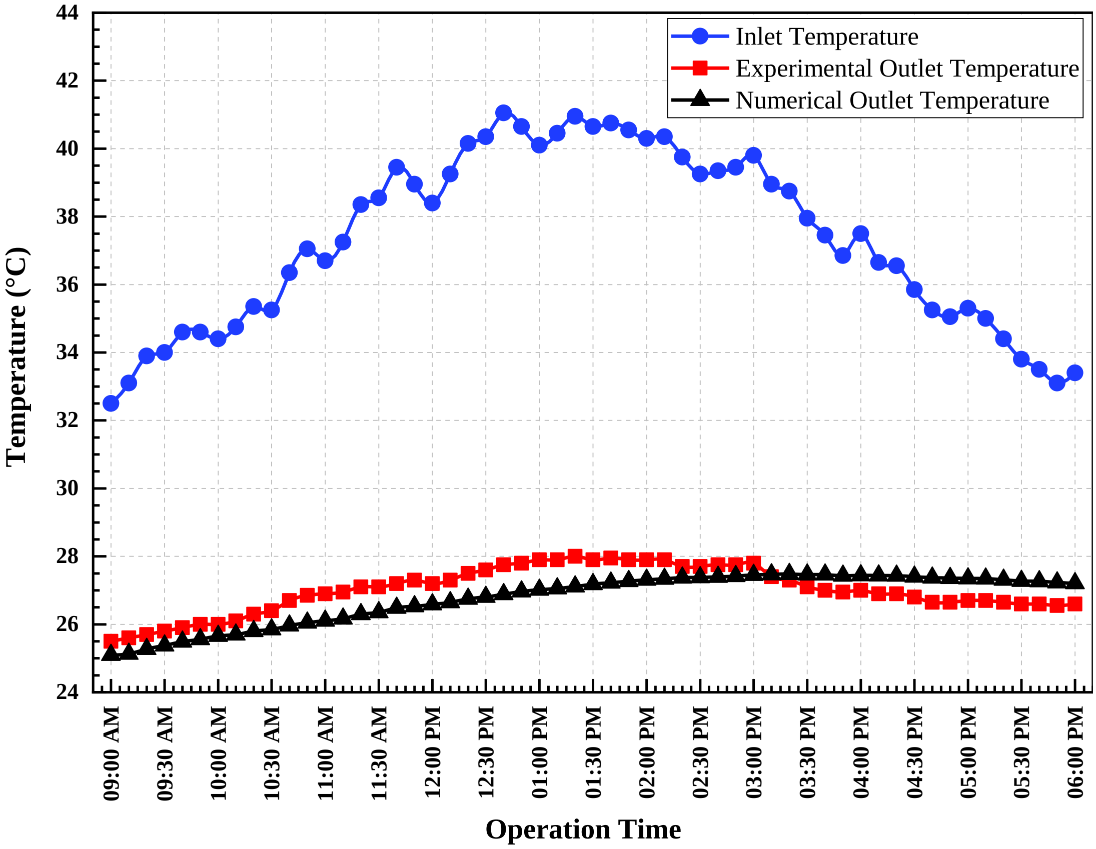

Figure IV.11: Validation of simulation results with experimental results.

IV.3.3 Results

To assess the heat performance of the HGAHE system under unsteady conditions, numerical simulations were conducted using ANSYS Fluent for cooling purposes in 24 hours continuous operation using the ambient air temperature data from 06 May 2017 at 09 am to 07 May 2017 at 09 am.

Figure IV.12 presents the inlet and outlet air temperatures for the 24 hours operation time of the HGAHE system. It can be seen that, the HGAHE outlet air temperature is significantly dependent on the inlet air temperature, even though the variation in HGAHE outlet temperature is much lower due to the large borehole and surrounding soil thermal mass. It is observed that, during the first cooling period from the start of operation (i.e. 09 am) to 00:30 am (after 15.5 hours operation period), the outlet temperature was found in the interval of 27.4 °C to 25.1 °C (averaging at 26.8 °C) when inlet temperature fluctuated from 41.0 °C to 26.6 °C (averaging at 34.4 °C). Furthermore, it is also noticed that, a maximum temperature drop of 14.1 °C was achieved at 12:40 pm when the ambient air was at the maximum temperature (41.0 °C).

From Figure IV.12, it is interesting to observe that from 00:30 am to 07:40 am, the inlet temperature is below the outlet temperature, implying that inlet air is being heated instead of cooled and the HGAHE system start operating in heating mode (recovery). During this period, the obtained outlet temperature was in the range of 26.4 °C to 25.5 °C (averaging at 25.7 °C) when inlet temperature changed from 26.6 °C to 22.5 °C (averaging at 23.8 °C). Additionally, it can be seen that, a maximum air temperature drop of 3.1 °C was found at 04:00 am when the inlet air was at the minimum temperature, i.e. 22.5 °C.

When ambient air temperature during the summer nights is lower than the borehole temperature, which known as night purging by forced convection is very useful to allow the borehole and surrounding soil to restore its initial bulk temperature, therefore recovering the cooling ability. It can be pointed out that the forced air convection occurred during the night is more efficient than the natural heat conduction in such cases. Moreover, it can be seen that after 07:40 am, the inlet (ambient) temperature rises above the outlet temperature, meaning that the air flowing in the system is being cooling down and the system gets back to operating in cooling mode during the second cooling period.

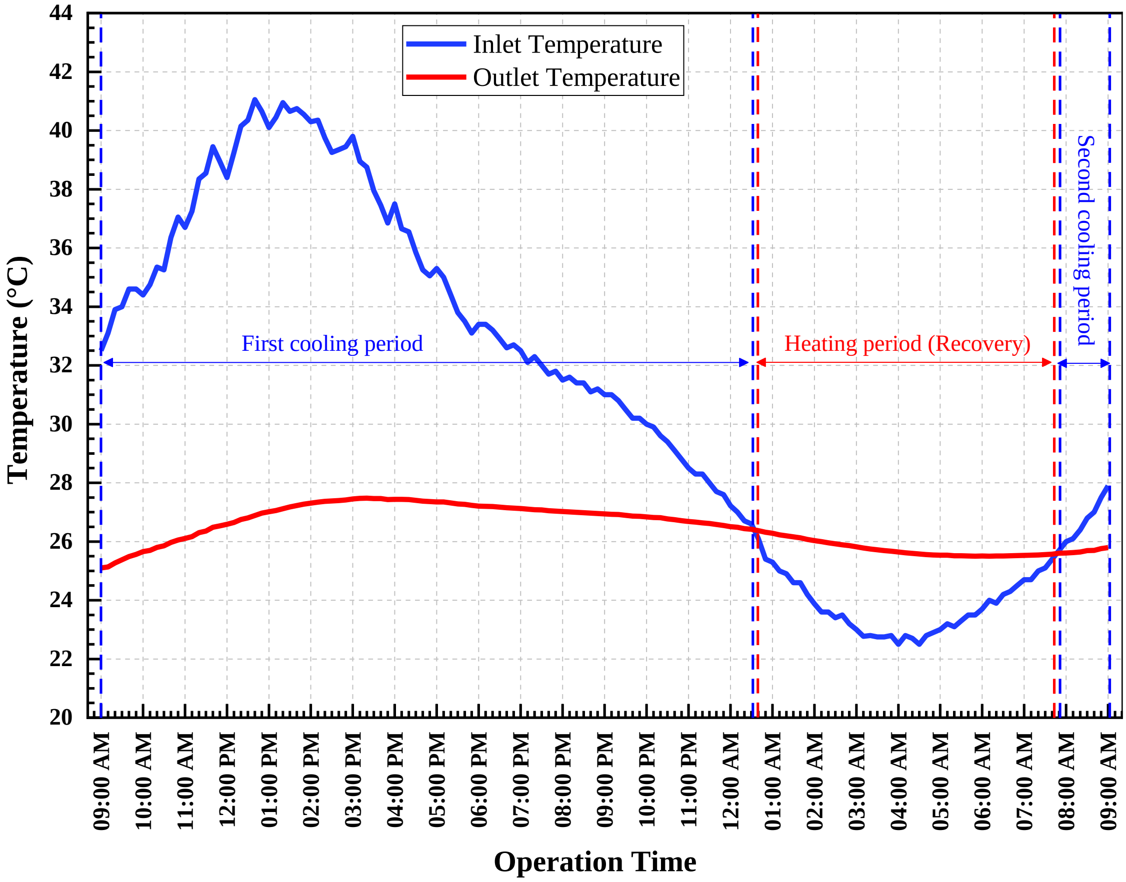

Figure IV.12: Inlet and outlet air temperature variation versus operation time.

Figure IV.13 shows temperature contours of the helical pipe wall at 02:00 pm, 00:30 am, 04:00 am and 07:40 am. From this figure, it is evident the highest temperature drops are at 02:00 pm and 04:00 am, which can be explained due to the high (40.3 °C) and low (22.5 °C) inlet air temperatures, respectively, indicating that at 02:00 pm and 04:00 am, the HGAHE system is operating in cooling and heating mode, respectively. Nevertheless, the temperature drop at 02:00 pm is higher than at 04:00 am due to the fact that the gap between inlet and soil mean temperatures is higher at 02:00 pm than at 04:00 am. Furthermore, it is noticed that, at 00:30 am and 07:40 am, i.e. the end of the cooling and heating mode, respectively, there are no temperature drops due to the reason that the inlet air temperatures are equal to the mean ground temperatures, resulting in the outlet air temperatures to be equal to the inlet air temperatures.

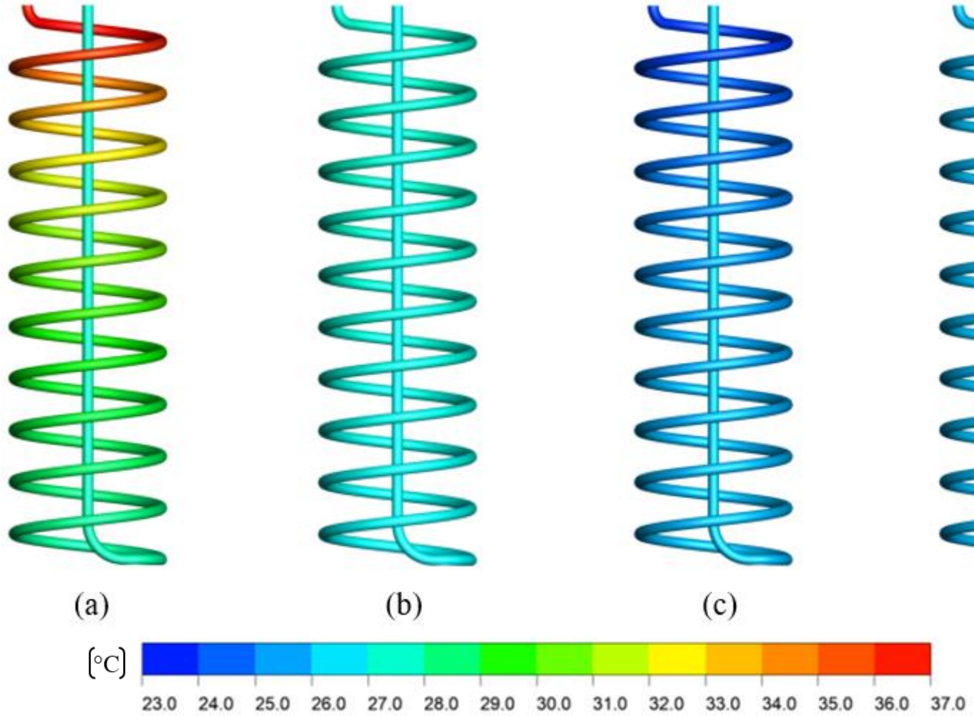

Figure IV.13: Pipe wall temperature contours for different operation time: (a) at 02:00 pm, (b) at 00:30 am, (c) at 04:00 am, (d) at 07:40 am.

The HER of the HGAHE system for the 24 hours operation time has been determined based on the simulation results. Figure IV.14 illustrates the ambient air temperature (i.e. inlet temperature) and the HER versus operation time. From the figure, it can be seen that, during the cooling period the highest heat exchange rate of 493.9 W was obtained at 12:40 pm for the highest inlet temperature of 41.0 °C. Whereas the maximum HER during the heating period was observed as -109.4 W at 04:00 am for the lowest inlet temperature of 22.7 °C. It should be highlighted that, the negative value of the heat exchange rate means the heat is transmitted from the borehole to the air, thus the system is operating in heating mode. Moreover, it is revealed that, the HER is fluctuated similar to the inlet temperature due to the same reason explained in subsection IV.2.1.

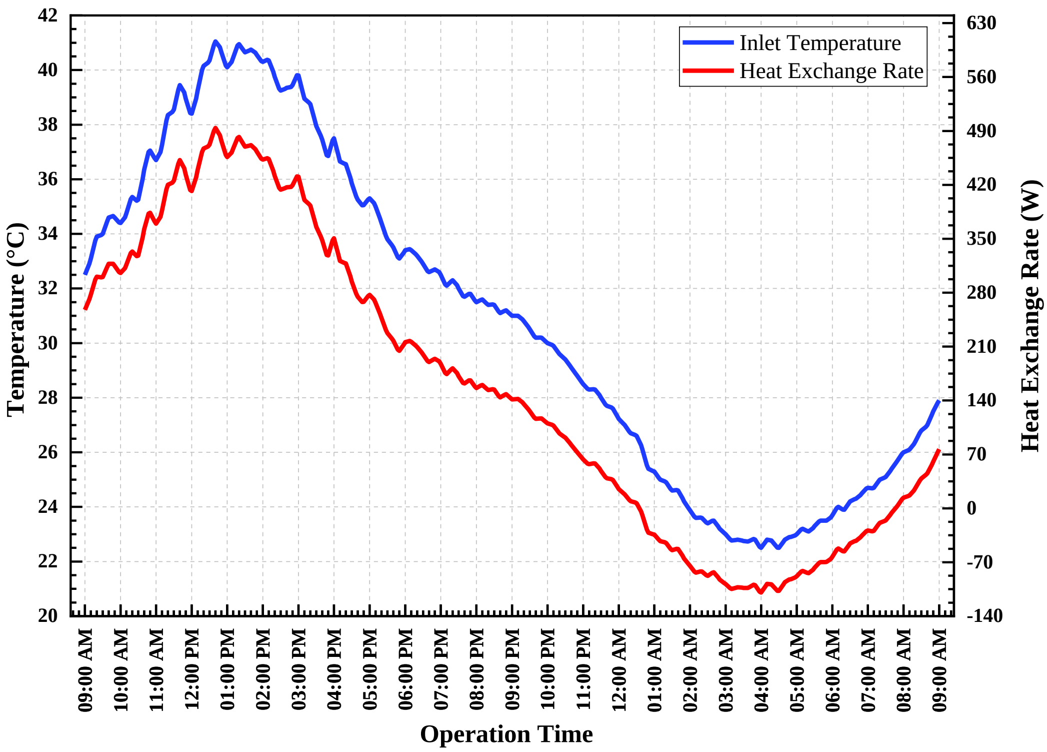

Figure IV.14: Inlet air temperature and heat exchange rate variation versus operation time.

Based on the obtained results from the validated simulation model, more comprehensive borehole temperature distribution analyzes in axial and radial directions were performed in order to evaluate the influence of the borehole on the thermal performance of the HGAHE system. Investigations of the borehole and surrounding ground temperature distribution near to the embedded helical pipe should be relevant on the HGAHE system design and its real operation conditions.

Borehole temperature distribution in the axial direction at a distance of 0.1, 0.2 and 0.3 m away from the helical-pipe wall (towards to the center of the borehole) along the length of the HGAHE at the end of the first cooling period i.e. 00:30 am is depicted in Figure IV.15. It is noticed that, after 15.5 hours operation time (i.e. in the end of the first cooling period), the borehole temperature at the upper surface of the HGAHE is 26.926, 25.622 and 25.007 °C at 0.1, 0.2 and 0.3 m away from the helical pipe surface, respectively. Whereas, the borehole temperature at the bottom surface of the HGAHE is 25.330, 24.975 and 24.869 °C at 0.1, 0.2 and 0.3 m away from the helical pipe surface, respectively. This finding proves that, in a period of 15.5 hours, the borehole temperature at the upper surface of the HGAHE is increased by 2.1, 0.8, and 0.2 °C at 0.1, 0.2 and 0.3 m away from the helical pipe surface, respectively. However, the borehole temperature at the bottom surface of the HGAHE is increased by 0.5, 0.1, and 0.06 °C, respectively, at 0.1, 0.2 and 0.3 m from the helical-pipe wall.

Furthermore, it can be seen that, the borehole temperature distribution along the length of the HGAHE oscillated similarly to a sinusoidal curve with a decreasing trend. The borehole temperature is maximal next to each spire and minimal between two consecutive spires. In addition, the highest borehole temperature was found near the top spire, whereas the lowest borehole temperature was obtained between the two bottom spires.

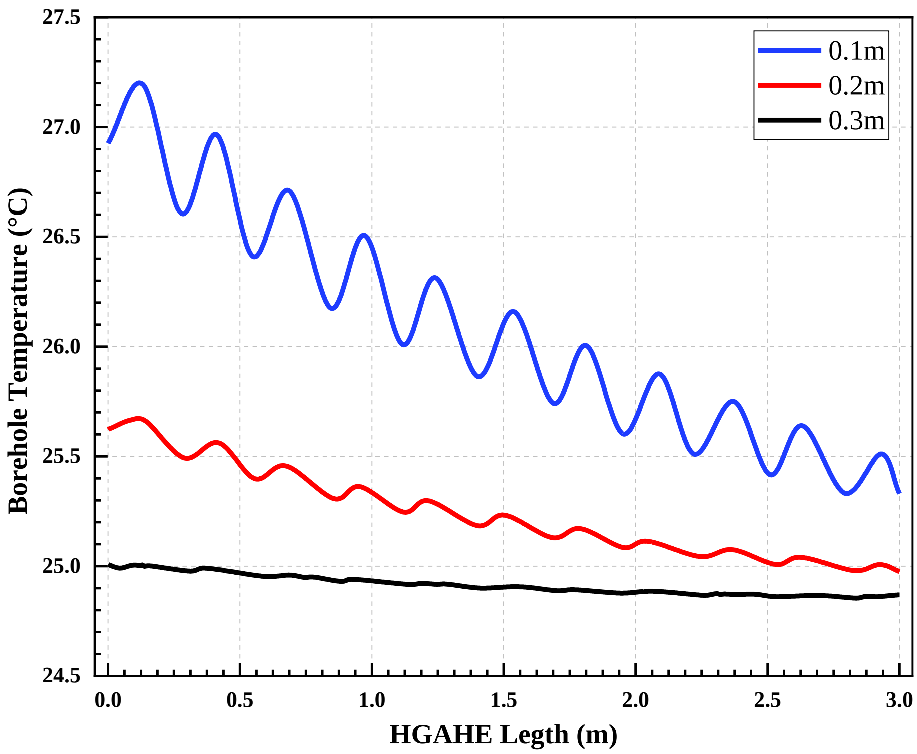

Figure IV.15: Borehole temperature distribution in axial direction at various distance from the pipe wall versus the length of the HGAHE.

Figure IV.16 illustrates the temperature distribution contours in horizontal plane for upper and bottom surfaces of the borehole at various operation times. It is clearly shown that, the effect of the temperature is significantly greater in the upper surface in comparison with the bottom surface during different operation times. These results exhibit that, the borehole temperature decreases according to the HGAHE length. Moreover, the HER is significantly higher in the top section of the HGAHE compared to the bottom section, because the temperature gap between the air and borehole on the top section is higher than that at the bottom section.

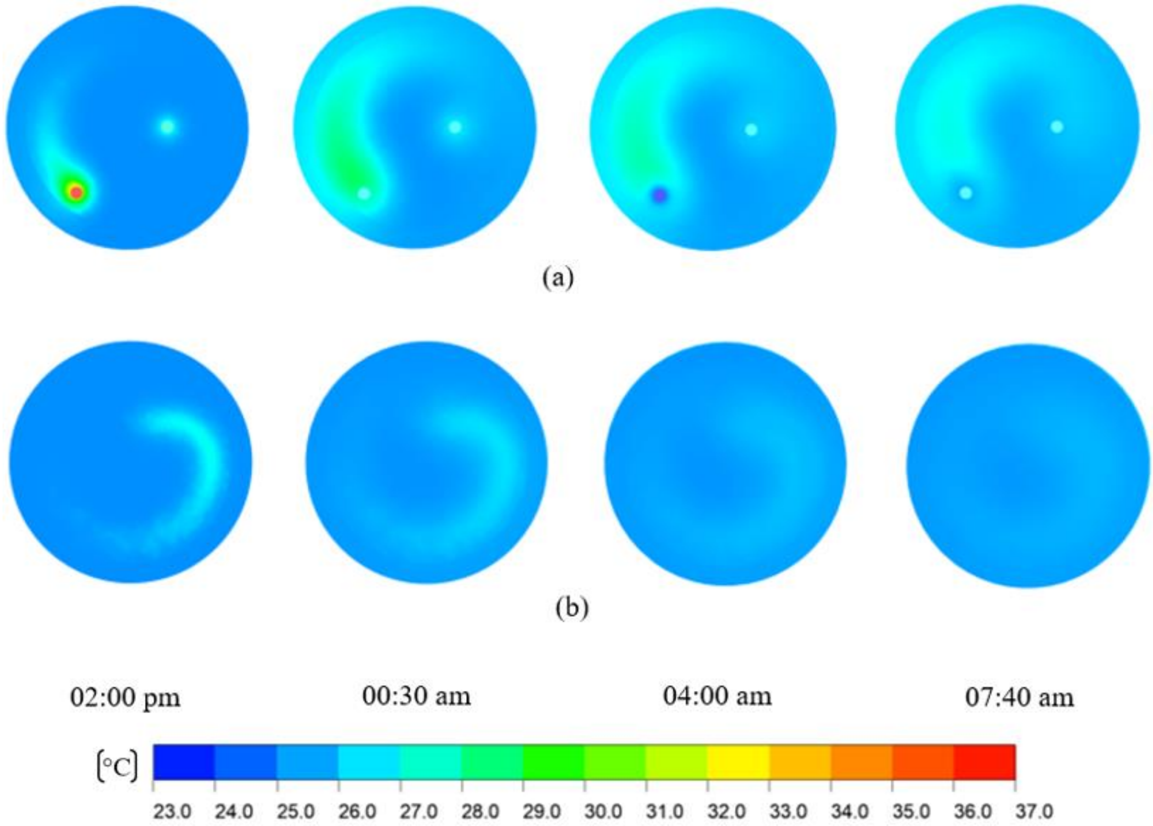

Figure IV.16: Contours of the borehole temperature distribution: (a) upper surface, (b) bottom surface, at different operation time.

For analyzing the heat penetration into the borehole, temperature distribution in radial direction was simulated and determined at a regular range of 0.1 m up to 0.3 m away from the pipe surface towards to the center of the borehole at 1.5 m below the upper surface of the HGAHE (i.e. middle of the HGAHE). The simulated results of the first cooling period have been depicted in Figure IV.17, which shows that the borehole temperature diminishes faster according to the distance from the helical pipe wall. When the distance from the pipe wall is far enough, the increase in the borehole temperature is not much pronounced. Furthermore, the affected borehole thickness by operation time in hours can be analyzed. After a period of 5 hours, i.e. at 02:00 pm, the borehole temperature at a distance from the helical pipe surface of 0.27 m starts to increment. Therefore, the circulated air has impacted 0.27 m thickness of borehole in 5 hours. Afterward, the thickness of the affected area grows to 0.3 m after 10 hours. These results reveal that the thickness of the affected area and temperature keeps incrementing with the duration of operation. However, the thickness of the affected area changes depending on the inlet temperature.

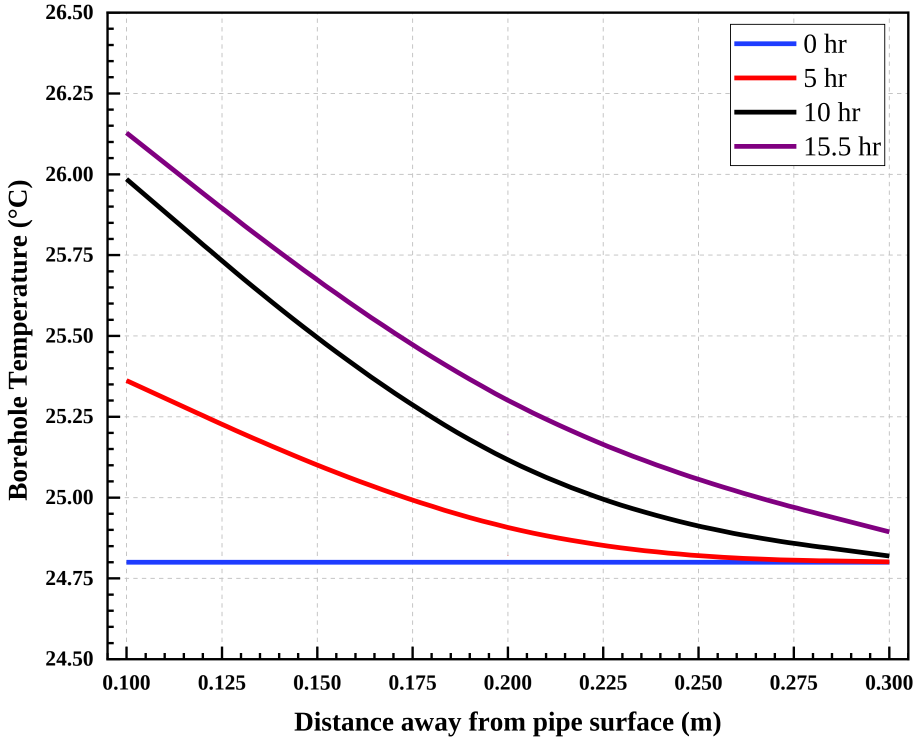

Figure IV.17: Borehole temperature distribution in radial direction at different operation time versus distance from the pipe wall.

Figure IV.18 presents the borehole temperature at 0.1, 0.2, and 0.3 m away from the pipe wall in radial direction versus the operation time. As illustrated in this figure, the borehole temperature rises rapidly close to the pipe wall and then gradually drops down. As evident in the figure, the borehole temperature increments, at 0.1 m from the helical pipe wall by the incremental of the inlet temperature and reaches the maximum temperature of 26.128 °C after 15 hours of operation time. It is also noticed that when the ambient temperature of air goes down during the night, the borehole temperature decreases to 25.773 °C, taking advantage of night purging to start cooling the warmed backfill material and aids the borehole and surrounding ground to restore its cooling load. However, the borehole temperature increases just to 25.455 and 25.137 °C at 0.2 and 0.3 m away from the helical pipe surface, respectively. It is also seen that, when the ambient air temperature goes down during the night, the borehole temperature slope at 0.2 and 0.3 m away from the helical pipe surface decreases with the operation time.

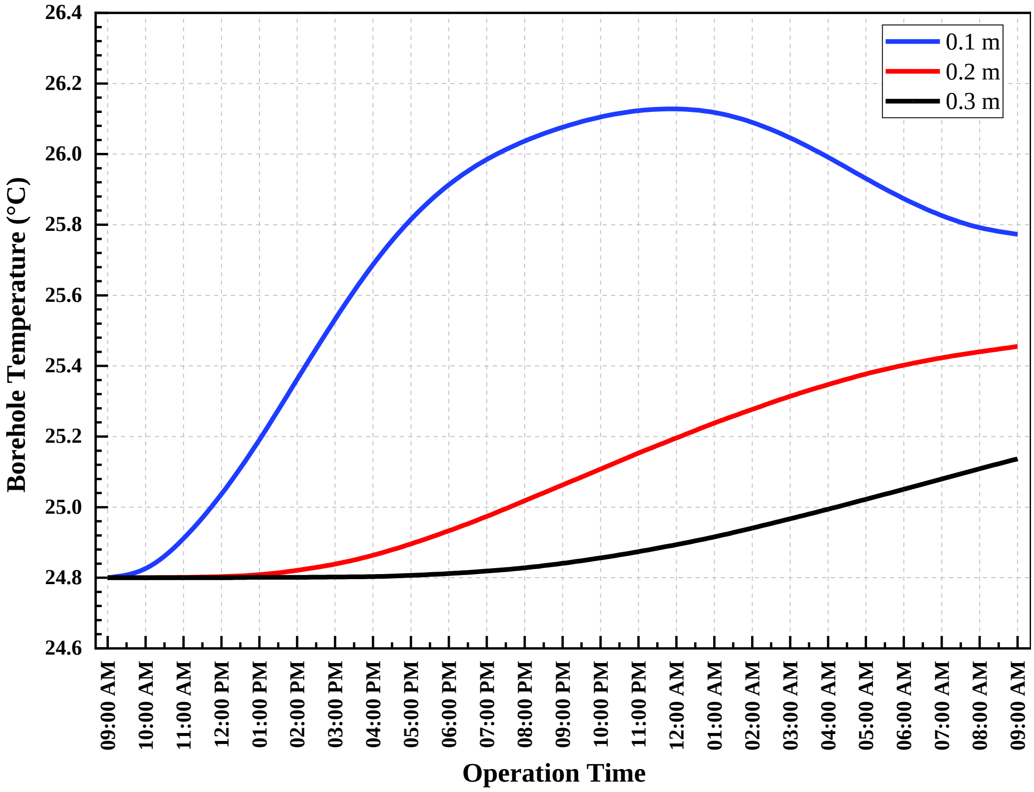

Figure IV.18: Borehole temperature distribution in radial direction at various distance away from the pipe wall versus operation time.

Figure IV.19 shows the temperature distribution contours of the HGAHE system at different operation times in 3D view. Similar to the observation made above, from this figure it is seen that at 02:00 pm high heat exchange rate and high temperature around the pipe vicinity are observed due to the high inlet temperature of 40.3 °C. However, the heat penetration into the borehole is not so profound because the system was operated only for 5 hours. At 00:30 am, i.e. in the end of the cooling period, there is no temperature drop since the inlet temperature equals to the outlet temperature, whereas a high penetration of heat into the borehole is noticed due to the long operation period of 15.5 hours in cooling mode. Moreover, at 04:00 am, the system was operating in heating mode because the inlet air temperature (22.5 °C) was lower than the ground mean temperature, hence, the borehole was being cooling down by the ambient temperature of air through the forced convection between the borehole and air. Furthermore, it is worth mentioning that at 07:40 am, there was no temperature drop due to inlet air temperature being equal to the outlet air temperature, while the borehole was influenced by the night purging period and cooled down thoroughly. It is also revealed that, at the end of the first cooling period and the heating period, the inlet air temperature was equal to the outlet air temperature as of 26.5 °C and 25.5 °C respectively, indicating that during the night purging period the borehole recovered its cooling ability by 1.0 °C.

The above findings indicate that, the borehole temperature rise decrements with the distance away from the helical-pipe surface. Thus, borehole temperature at the helical pipe surface vicinity has more intensity than the ground far from the helical-pipe wall. Moreover, while the inlet temperature is higher, the borehole temperature increments continuously supplying cooling effect. On the other hand, the borehole temperature can restore the cooling ability in the night period when the ambient air temperature drops considerably lower than the borehole temperature through the forced convection between the borehole and air. This recovery rate varies depending on the nighttime ambient temperature.

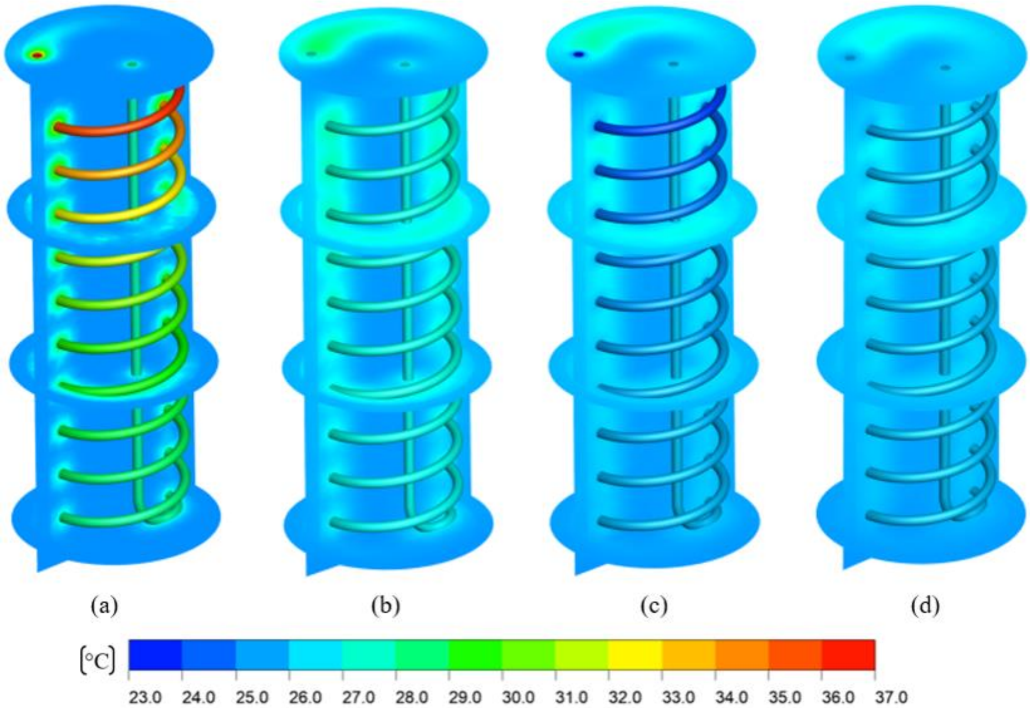

Figure IV.19: HGAHE system temperature distribution contours for different operation time in 3D view: (a) at 02:00 pm, (b) at 00:30 am, (c) at 04:00 am, (d) at 07:40 am.

IV.3.4 Comparison of the results with other studies

In this section, a comparison is made between the performance results of the realized helical ground air heat exchanger in this study with the results of other research studies. The results of this comparison are summarized in Table IV.3. In the study conducted by Misra et al [110], a transient CFD simulation were performed to evaluate the thermal performance of earth air tunnel heat exchanger with a length of 60 m and diameter of 0.1 m. Results revealed that, after operation period of 12 hours at 5 m/s of airflow velocity, the air temperature drop and the heat exchange rate was 17.0 °C and 818 W, respectively. While, at a pipe length of 10 m from inlet, soil temperature rise situated at 0.1 m away from pipe surface was 2.0 °C. Another study conducted by Mathur et al [56] aimed to analyze the effect of soil thermal diffusivity on performance of earth air tunnel heat exchanger system (40 m length and 0.1 m diameter) using transient simulation. They found that, after operation time of 12 hours at 5 m/s of air velocity, the air temperature drop and the heat exchange rate was 15.8 °C and 767 W, respectively. Whereas, the soil temperature rise at 10 m section of pipe length from inlet at radial distance of 0.05 m from the pipe surface was 5.6 °C. The same authors [74] carried out an experimental comparative study of straight and spiral earth air tunnel heat exchanger system. Findings showed that, for the spiral EAHE of 60 m length and 0.1 m diameter, after 5 hours of operation duration at air velocity of 6 m/s, the air temperature drop and the heat exchange rate was 11.0 °C and 638 W, respectively. They also found that, the soil temperature rise at 10 m length from inlet at 0.1 m radial distance from the pipe surface was 3.3 °C. Agrawal et al

[48] conducted numerical simulation to compare various pipe layouts in EAHE system for cooling purposes. For the EAHE with helical layout constituted by PVC pipe of 31.1 m length and 0.1 m diameter, the obtained results revealed that, after operation time of 12 hours at 5 m/s of airflow velocity, the air temperature drop and the heat exchange rate was 14.9 °C and 721 W, respectively. Whereas, the soil temperature rise at a distance of 0.1 m from the pipe surface at a trench length of 5 m was 1.15 °C.

Table IV.3: Performance comparison of the present study with other studies.

Study	System technical specification	Air temperature drop (°C)	Heat exchange rate (W)	Soil temperature rise (°C)
Misra et al **[110]**	Horizontal layout; Material: PVC; Pipe length: 60 m; Pipe diameter: 0.1 m; Pipe surface: 18.84 m^2	17.0	818	2.0
Mathur et al **[56]**	Horizontal layout; Material: PVC; Pipe length: 40 m; Pipe diameter: 0.1 m, Pipe surface: 12.56 m^2	15.8	767	5.6
Mathur et al **[74]**	Spiral layout; Material: PVC; Pipe length: 60 m; Pipe diameter: 0.1 m; Pipe surface: 18.84 m^2	11.0	638	3.3
Agrawal et al **[48]**	Helical layout; Material: PVC; Pipe length: 31.1 m; Pipe diameter: 0.1 m; Pipe surface: 9.76 m^2	14.9	721	1.15
Present	Helical layout; Material: PVC; Pipe length: 30 m; Pipe diameter: 0.06 m; Pipe surface: 5.65 m^2	14.1	494	0.3

IV.4 Parametric study

In the present parametric study, a slight change has been applied to the physical model and boundary conditions compared to the first numerical study presented in subsection IV.3. The main objective of the minor change was to accurately simulate the real applications of the GAHE. It should be highlighted that the main changes in the reference case are as follows; sandy soil for the borehole and concrete for the backfill material were considered, non-dimensionlization of parameters were applied as well as soil far field temperature equation was modelled based on heat conduction theory in a semi-infinite homogenous solid. Further details are addressed in the following bullet points.

- A schematic view of the studied helical earth to air heat exchanger is presented in Figure IV.20, dimensions and different geometric parameters of the model are nondimensionalized with respect to H the heat exchanger height, and they are D, its diameter, P the distance between two spires (known as pitch), pipe diameter, thickness d and t respectively, for the borehole, the depth was kept 0.2 below the bottom, and 0.32 on both sides of the heat exchanger, backfill material used for the reference case is concrete, while the soil surrounding the borehole was considered to be at 0.6 in diameter, for the standard case, the ground was considered to be sandy soil, the working fluid is air for all cases, and its thermophysical properties are listed in Table IV.4.

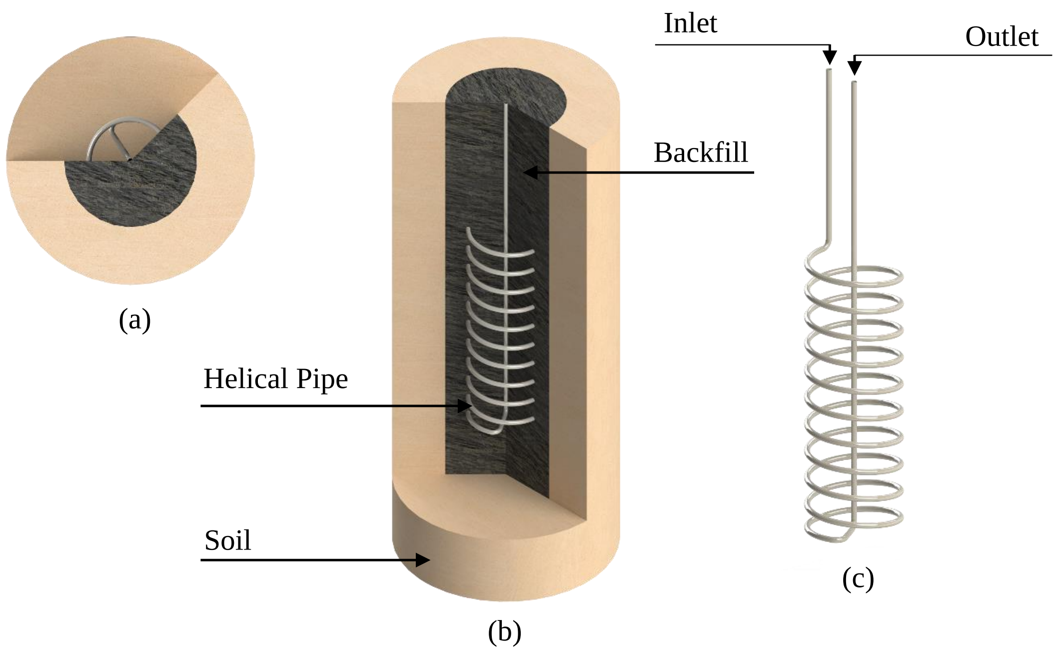

Figure IV.20: 3D schematic view of the studied helical earth to air heat exchanger, (a) top view, (b) slice, and (c) heat exchanger.

Table IV.4: Thermophysical specifications of working fluid ground, backfill, pipe material.

Parameter	Value	Definitions
ρ_g	2050	Ground density $[kg/m^{-3}]$
Cp_g	1840	Ground specific heat capacity $[J/kg.K]$
k_g	0.52	Ground thermal conductivity $[W/m.K]$
ρ_b	2500	Backfill material density $[kg/m^{-3}]$
Cp_b	837	Backfill material specific heat capacity $[J/kg.K]$
k_b	1.63	Backfill material thermal conductivity $[W/m.K]$
ρ_a	1.225	Air density $[kg/m^{-3}]$
Cp_a	1006.43	Air specific heat capacity $[J/kg.K]$
k_a	0.0242	Air thermal conductivity $[W/m.K]$
μ_a	$1.7894.10^{-5}$	Air viscosity $[Pa.s]$
ρ_{pipe}	958	Pipe density $[kg/m^{-3}]$
C_{pipe}	2093	Pipe specific heat capacity $[J/kg.K]$
k_{pipe}	0.476	Pipe thermal conductivity $[W/m.K]$

- It is worth noting that the non-dimensionlization process of the governing equations was accomplished using the following quantities:

$$x^* = \frac{x}{H} \;, y^* = \frac{y}{H} \,, z^* = \frac{z}{H}, d^* = \frac{d}{H} \,, P^* = \frac{P}{H} \,, t^* = \frac{t}{H}, D^* = \frac{D}{H} \,, u^* = \frac{u}{u_\infty}$$

$$v^* = \frac{v}{u_\infty} \,, w^* = \frac{w}{u_\infty}, T^* = \frac{T - T_{min}}{\Delta T}, P^* = \frac{P - P_\infty}{\rho u_\infty^2}$$

where x^*, y^*, z^* are coordinates, u^*, v^*, w^* are the velocity components in x, y, z directions respectively, T^* is dimensionless temperature, P^* is the dimensionless pressure and ΔT is the maximum temperature difference.

- For the boundary conditions, at the inlet of the computational domain, a set of different Reynolds numbers (ventilation velocity) dimensionless inlet temperature were applied depending on the studied parameter and case of study, while at the outlet, a pressure outlet boundary condition was selected, soil far field temperature was modelled by Eq. (IV.1) at a time t and depth z based on heat conduction theory in a semi-infinite homogenous solid, soil temperature prediction takes a sinusoidal form due to the annual fluctuations of ambient temperature, for present study soil temperature for the day of 18 June 2021 was set according to the model equation as follows [66]:

$$T(z,t) = T_m - T_s e^{\left(-z\left(\frac{\pi}{8760\alpha}\right)^{1/2}\right)} . \cos\left[\frac{2\pi}{8760}\left(t - t_0 - \frac{z}{2}\left(\frac{8760}{\pi\alpha}\right)^{1/2}\right)\right] \quad \text{(IV.1)}$$

where the variables mentioned in the equation above are the annual mean ground temperature T_m, annual surface temperature amplitude T_s, soil thermal diffusivity α, phase constant t_0 (i.e. coldest time of the year) and time in hours t, while values of these constants are, $24.37\ °C$, $22.775\ °C$, $0.000406\ m^2/h$, $8448\ hr$, and $4218\ hr$ respectively [66, 111].

The time in hours t is $4218\ hr$ which corresponds to the chosen day of the test i.e. 18 June 2021. It should be pointed out that the phase constant t_0 is $8448\ hr$ which is the coldest time of the year and corresponds the day number 352 of the year based on the Algerian National Weather Office [66].

Initially the temperature, velocity and pressure fields of the computational domain was initialized with a constant value (domain averaged) by solving an appropriate Laplace equation for each variable.

IV.4.1 Mesh sensitivity test

A mesh independency test was performed to ensure the accuracy of the solution, for all simulations, numerical results were obtained using the $k-\epsilon$ turbulence model, in conjunction with the Enhanced wall treatment wall functions, values of Y^+ of the order of 1 were desired for the numerical resolution of the near wall region to assure accurate values of the wall shear stress and wall heat transfer. Results and details of the mesh refinement study are shown in Table IV.5 below, considering mesh elements number, simulation time and the rate of change in the dimensionless temperature at the outlet, we can take mesh 04 as an optimum mesh for the subsequence simulations, as it provides accurate results for both T^* and Y^+, and further refinement in the mesh beyond that is just more computation cost.

Table IV.5: Mesh test details and results.

Mesh #	Mesh elements	Y^+	Simulation time	Final Outlet T^*(After 24 h)
01	1856871	1.3825	47 min	0.665
02	2111317	1.2735	57 min	0.666
03	2347182	1.1181	62 min	0.668
04	2716469	1.0657	66 min	0.669
05	3175693	1.0017	114 min	0.669

IV.4.2 Model validation

In order to validate the CFD model in hand, a case of the numerical study performed by Javadi et al [89] was considered, where the performance of different configurations of helical ground to air heat exchangers was analyzed, the considered case for this validation is a helical heat exchanger with inner outlet, water was considered to be the working fluid and Silica Sand as backfill material, while Clay and Sandy Clay as soil, the inlet temperature at the beginning of the operation was set to 289 K as well as the initial backfill and soil temperature, a comparison between water outlet temperature for that study and present model is presented in Figure IV.21 a good agreement in results is shown, and hence the accuracy and reliability of present model.

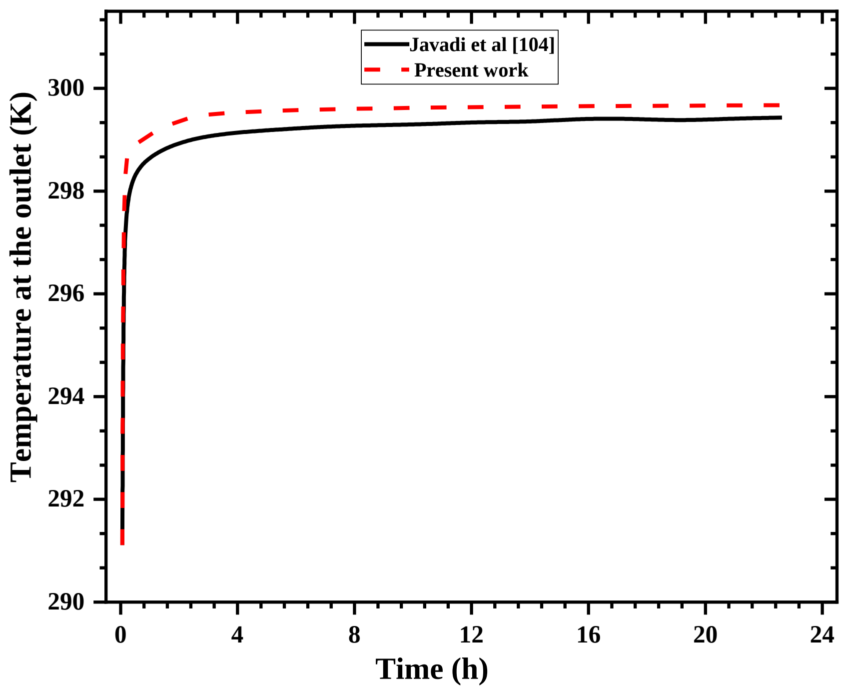

Figure IV.21: Validation of the numerical CFD code from present study with study performed by Javadi et al [89].

IV.4.3 Results

After verification and validation, the CFD model has been used to carry out a parametric study in order to evaluate the various operating and geometric parameters on the thermal performance of the HGAHE system, namely, ventilation velocity, inlet temperature, pipe diameter, pipe thickness, helical pitch, helical diameter as well as the thermal effusivity of the backfill material. Thermal performance of HGAHE system has been evaluated in terms of the outlet temperature, heat exchange rate, effectiveness and pressure drop. It should be pointed out that, the parametric analysis has been carried out by varying one parameter per time, on the basis of the corresponding values depicted in Table IV.6, while keeping all other parameters constant and equal to the reference values illustrated in Table IV.7.

Table IV.6: Operating and geometric parameters considered for the parametric study.

Reynolds number	Inlet temperature	Pipe diameter	Helical pitch	Pipe thickness	Helical diameter	Backfill material
80,000	0.617	0.008	0.02	0.0002	0.04	Silt loam
110,000	0.701	0.01	0.04	0.0004	0.06	Sandy
140,000	0.784	0.012	0.06	0.0006	0.08	Silica sand
170,000	0.868	0.014	0.08	0.0008	0.1	Concrete
200,000	0.952	0.016	0.1	0.001	0.12	Sandy loam

Table IV.7: Reference case of the parametric study

Parameter	Value
Reynolds number	140,000
Inlet temperature	0.952
Pipe diameter	0.012
Helical pitch	0.06
Pipe thickness	0.0006
Helical diameter	0.08
Backfill material	Concrete

IV.4.3.1 Effects of Reynolds number

Selecting inlet fluid velocity is a significant and influential factor in the efficiency of GAHE. In this study, the impact of the change in ventilation velocity has been evaluated by considering five different Reynolds numbers i.e. 80,000, 110,000, 140,000, 170,000 and 200,000, while other parameters were kept constant. Figure IV.22 shows the variation of T^* outlet with operation time at different Reynolds numbers. It is evident from the figure that the T^* outlet increments with the operation time. It is also observed that, after 24 h operation, T^* outlet was 0.543, 0.616, 0.669, 0.708 and 0.738 for Reynolds numbers of 80,000, 110,000, 140,000, 170,000 and 200,000, respectively. This result shows that, the T^* outlet is incremented by increasing Reynolds number. It is due to the fact that by incrementing the ventilation velocity, the quantity of heat transmitted by air to the borehole in a given time period also increments, which resulting in raising T^* outlet. Furthermore, Figure IV.23 shows the temperature distribution contours of the HGAHE system after 24 h of operation time at different Reynolds numbers in 3D view. For a better understanding of changes, only three contours of each view are shown. It is evident for this figure that, incrementing Reynolds number from of 80,000 to 200,000 has a significant influence on the temperature distribution into the backfill material and surrounding soil which result in raising the T^* outlet.

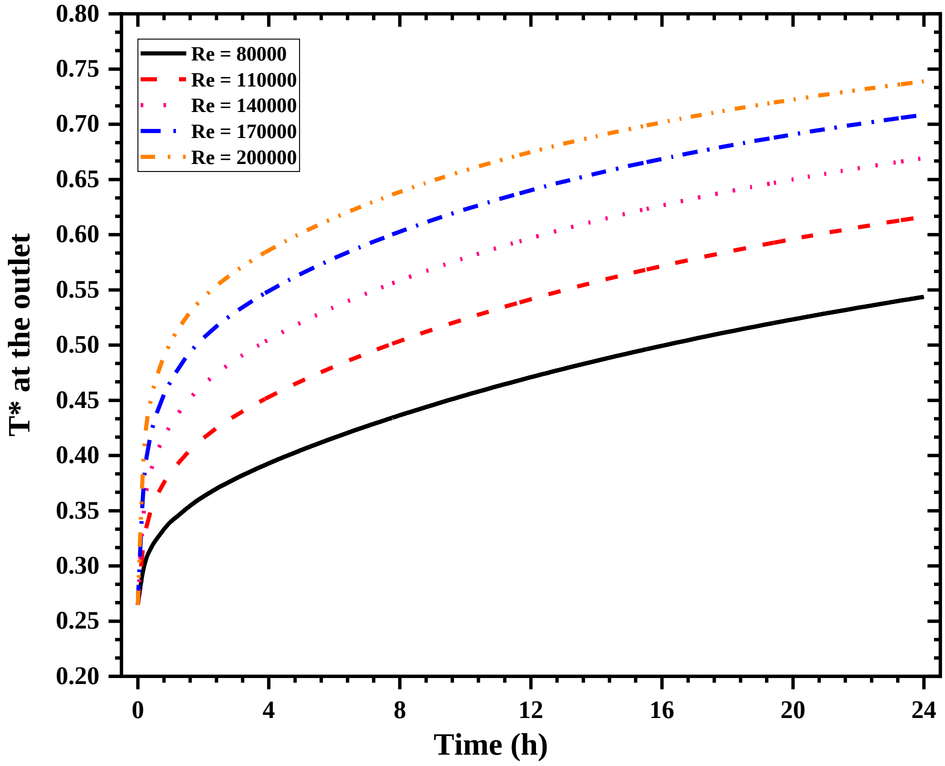

Figure IV.22: Variation of T^* outlet with operation time at different Reynolds numbers.

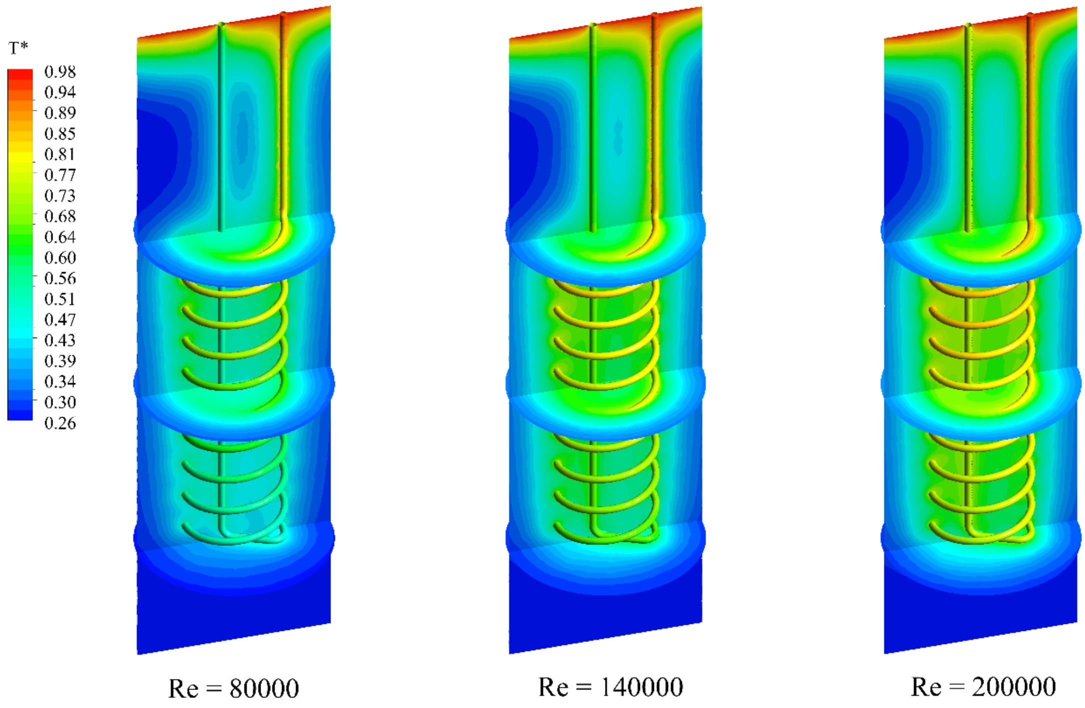

Figure IV.23: Temperature distribution contours of the HGAHE system after 24 h of operation time at different Reynolds numbers in 3D view.

The Influence of Reynolds number on the heat exchange rate and effectiveness has also been analyzed. From Figure IV.24, it can be seen that after 24 h of operation time, by raising Reynolds number from 80,000 to 200,000 the heat exchange rate increases from 662.4 W to 865.1 W, because by increasing ventilation velocity, the mass flow rate increases and thus, the heat exchange rate increments. However, upon raising Reynolds number from 80,000 to 200,000 the effectiveness decrements significantly from 0.51 to 0.26, because at higher ventilation velocity, air temperature drop decreases, and hence, the effectiveness decreases. Therefore, by raising Reynolds number from 80,000 to 200,000, the heat exchange rate improved by 30.6 %, but its effectiveness dropped by 49.0 %.

Reason for raising the heat exchange rate with the increase of ventilation velocity can be attributed to the fact that, as expressed in Eq. (II.1), the heat exchange rate is related to the mass flow rate and obtained temperature drop. As evident, by raising the ventilation velocity, air mass flow rate also increments, however the temperature drop decreases due to the shorter residence time of air into the helical pipe. Upon incrementing Reynolds number from 80,000 to 200,000, the mass flow rate increases from 0.067 kg/s to 0.168 kg/s, whereas the drop in air temperature decreases from 9.7 °C to 5.1 °C. Hence, by incrementing Reynolds number from 80,000 to 200,000, the mass flow rate is incremented by 150.7 %, while the temperature drop decremented by 47.4 % only. Therefore, the relative increment in mass flow rate is greater than decrease in air temperature drop and consequently raises the heat exchange rate of the GAHE system. Similarly, as per Eq. (II.5) that by raising ventilation velocity, temperature drop decreased, which resulting in reduction of the effectiveness.

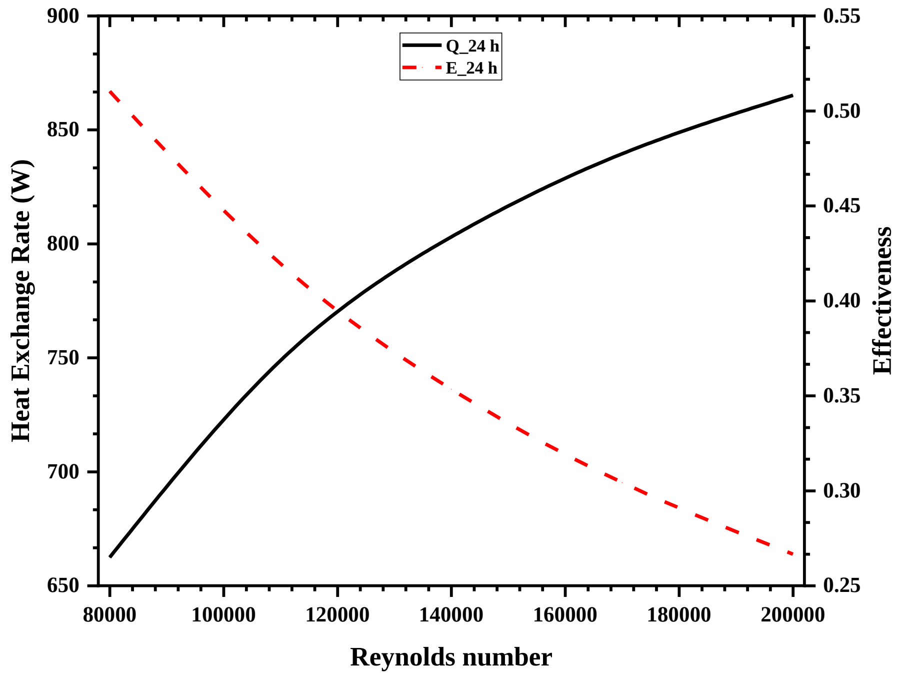

Figure IV.24: Variation of heat exchange rate and effectiveness with operation time at different Reynolds numbers.

Figure IV.25 illustrates the pressure drop for different Reynolds numbers after 24 hours of operation time. Form the figure it can be seen that, the pressure drop is increasing with the increase of Reynolds number. Based on the numerical results, by raising Reynolds number from 80,000 to 200,000 the pressure drop increases strongly from 4564.4 Pa to 25810.6 Pa which is about 465.4 % incremental. From these findings, it can be concluded that the ventilation velocity has a notable impact on the flow pressure drop of the GAHE system, because the flow velocity has a direct relation to the pressure drop as indicating in Eq. (II.8). Furthermore, the numerical results have been compared with the results of some correlations which shows a reasonable agreement as presented in Figure IV.25, where the maximum difference between the numerical results and Ju et al correlation is 11.6 %, while the maximum difference between the numerical results and Schmidt correlation is 20.1 %. In addition, the pressure drop of the helical pipe was compared to the pressure drop of a straight pipe (with same dimensions as the helical pipe). From Figure IV.25, it is noticed that the pressure drop of the helical pipe is higher than that of the straight pipe, as an example, at Reynolds number of 200,000 the pressure drop of straight pipe and helical pipe is 11898.2 Pa and 25810.6 Pa respectively, indicating 116.9 % of pressure drop increase in the helical pipe.

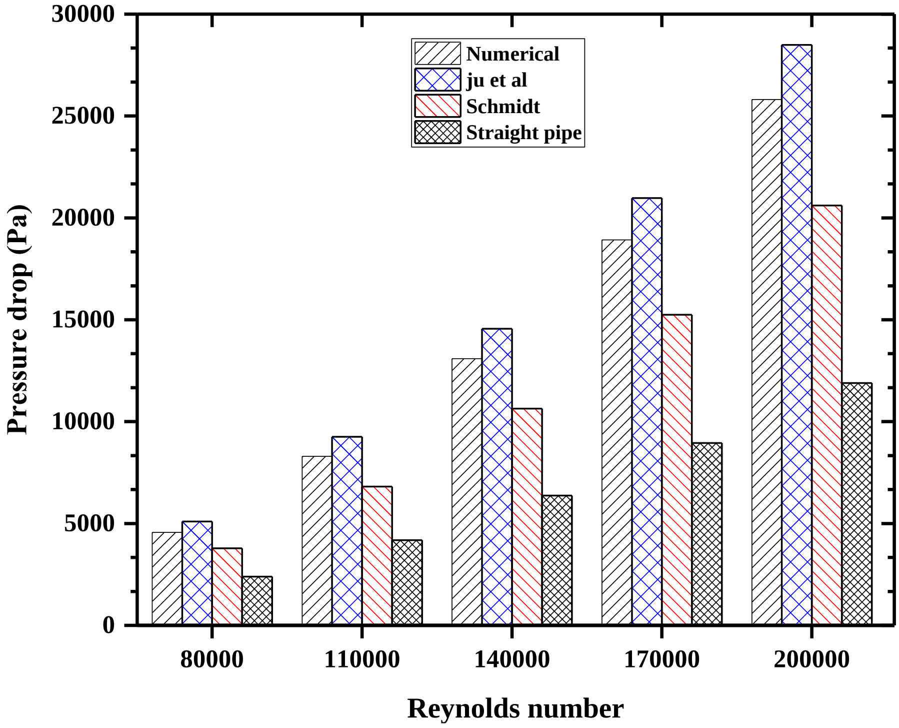

Figure IV.25: Pressure drop for different Reynold numbers after 24 h of operation time.

IV.4.3.2 Effects of inlet temperature

The GAHE system in real field setup uses air with different temperatures at the pipe inlet due to the variation of the ambient air temperature with the time. Ambient air temperature depends on the season as well as the climate condition of the application area. Hence, it is essential to consider the impact of inlet air temperature in the designing of GAHE system.

In order to investigate the effects of different inlet air temperature on the performance of the GAHE system, dimensionless inlet temperatures (i.e. T^* inlet) of 0.617, 0.701, 0.784, 0.868 and 0.952, are selected in this study and the performance of GAHE system has been examined, while other parameters were kept constant. Figure IV.26 shows the variation of T^* outlet with operation time for various T^* inlet. From this figure, it can be seen that all curves of the dimensionless outlet temperature are increasing with the operation time. It is also noticed that, after 24 h of continuous operation, T^* outlet at T^* inlet of 0.617, 0.701, 0.784, 0.868 and 0.952 was 0.479, 0.526, 0.574, 0.621 and 0.669, respectively. This result shows that the T^* outlet increases with incrementing T^* inlet and the highest dimensionless outlet temperature was obtained at the highest dimensionless inlet temperature i.e. 0.952. In addition, Figure IV.27 illustrates the temperature distribution contours of the HGAHE system after 24 h of operation time at different T^* inlet in 3D view. As explained above, it can be seen in this figure that, by increasing T^* inlet the areas affected by HGAHE system operation have increased so that at T^*

inlet of 0.617 and 0.952, the temperature of backfill material and surrounding soil significantly increases.

Furthermore, it is reveals that the minimum and maximum dimensionless temperature drop of 0.138 and 0.283 were obtained at the minimum and maximum T^* inlet of 0.617 and 0.952, respectively. Therefore, the drop in dimensionless temperature is incremented by increasing the dimensionless inlet temperature. Based on these findings, it can be concluded that the T^* inlet significantly affects the heat exchange rate between air and borehole and reason can be attributed to the fact that, at higher T^* inlet, the difference between the borehole temperature and air increments, which resulting in more heat exchange rate and greater drop in dimensionless temperature.

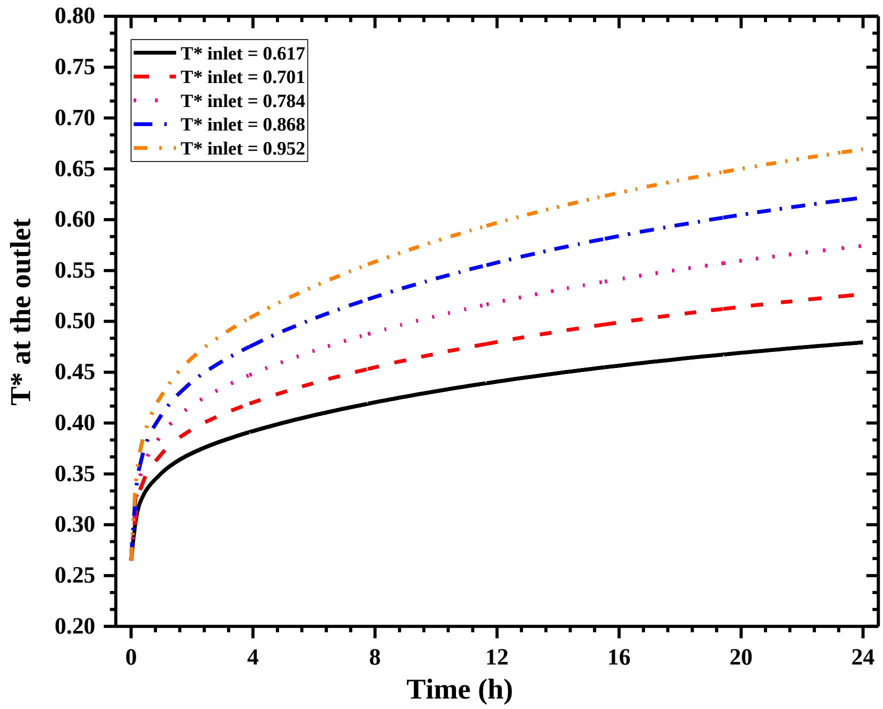

Figure IV.26: Variation of T^* outlet with operation time at different inlet temperatures.

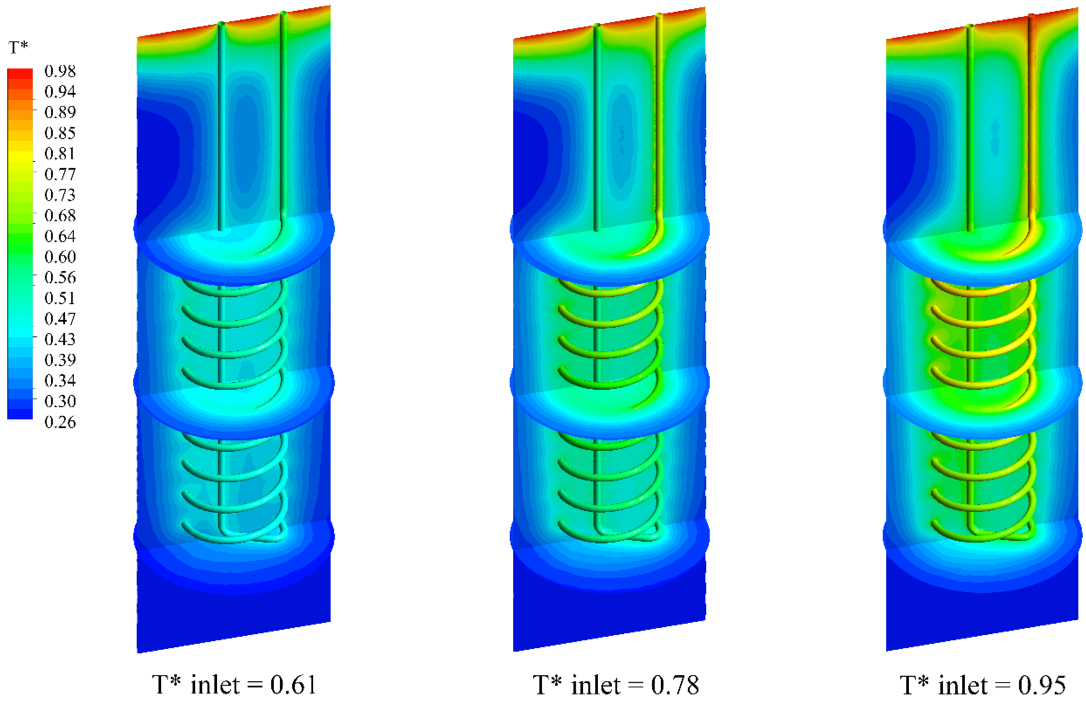

Figure IV.27: Temperature distribution contours of the HGAHE system after 24 h of operation time at different T^* inlets in 3D view

The effect of T^* inlet on the heat exchange rate and effectiveness of the system also examined. From Figure IV.28, it is observed that after 24 h of operation time, by incrementing T^* inlet from 0.617 to 0.952 the heat exchange rate increases considerably from 392.0 W to 803.1 W. However, the effectiveness increments from 0.30 to 0.35. It can be concluded that as the T^* inlet is incremented from 0.617 to 0.952 the heat exchange rate improved by 104.8 %, whereas the effectiveness increments only by 16.6 %. These findings reveal that with the increment in T^* inlet, the drop in dimensionless temperature increments, which resulting in greater heat exchange rate and effectiveness.

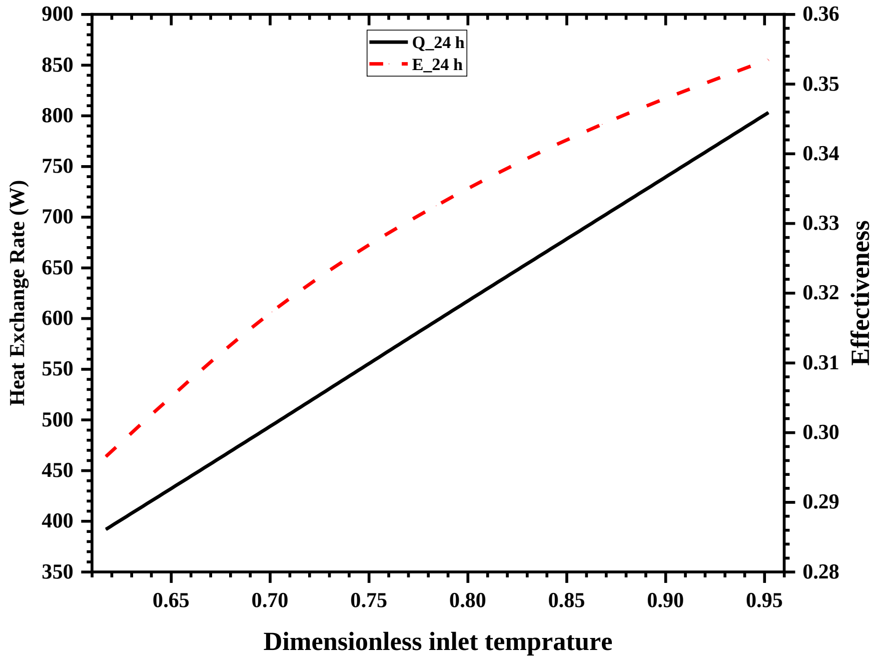

Figure IV.28: Variation of heat exchange rate and effectiveness with operation time at different inlet temperatures.

IV.4.3.3 Effects of pipe diameter

The diameter of the pipe is another parameter that can influence the performance of the GAHE system, therefore five different dimensionless pipe diameters (varied in the range from 0.008 to 0.016) have been considered to evaluate the GAHE performance, while other parameters were kept constant. As shown in Figure IV.29 all curves follow an upward trend with the operation time and difference between them gradually increments. It is noticed that, after 24 h of operation time, T^* outlet was 0.587, 0.632, 0.669, 0.698 and 0.722 for dimensionless pipe diameters of 0.008, 0.01, 0.012, 0.014 and 0.016, respectively. It is derived that, by incrementing dimensionless pipe diameter, the T^* outlet increments so that its value in d^* of 0.016 compared to the d^* of 0.008 is increased to 30 %. This is due to the fact that by incrementing dimensionless pipe diameter the air mass flow rate (keeping constant the ventilation velocity) is incremented, which result in a significant increase of the T^* outlet. Moreover, Contours of the temperature distribution of the HGAHE system after 24 h of operation time at different pipe diameters in 3D view are depicted in Figure IV.30. According to this figure, it is evident that, by incrementing dimensionless pipe diameter, the temperature distribution increases into the backfill material and surrounding soil, therefore the T^* outlet increments.

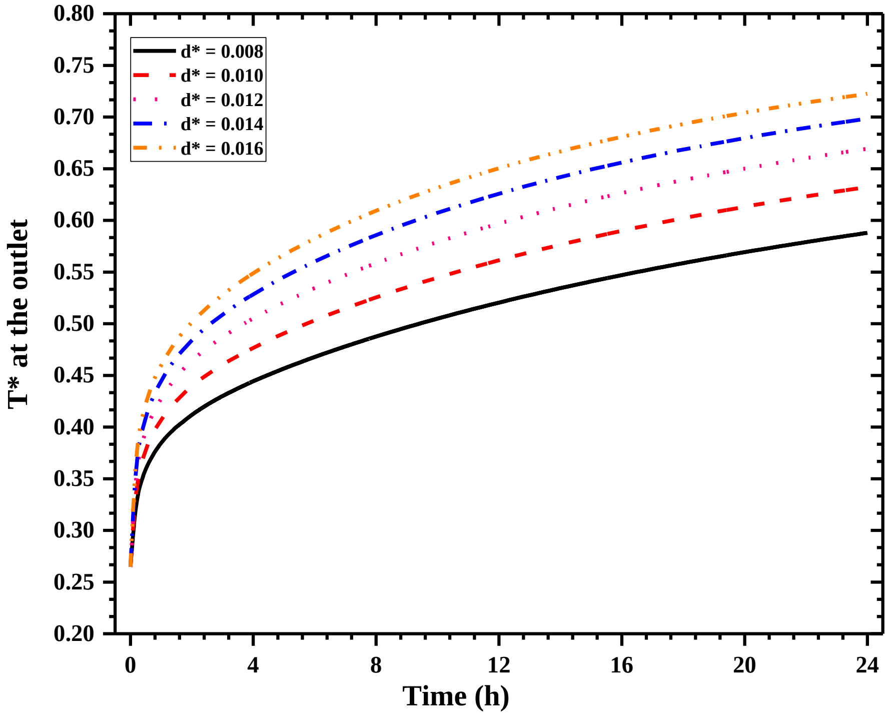

Figure IV.29: Variation of T^* outlet with operation time at different pipe diameters.

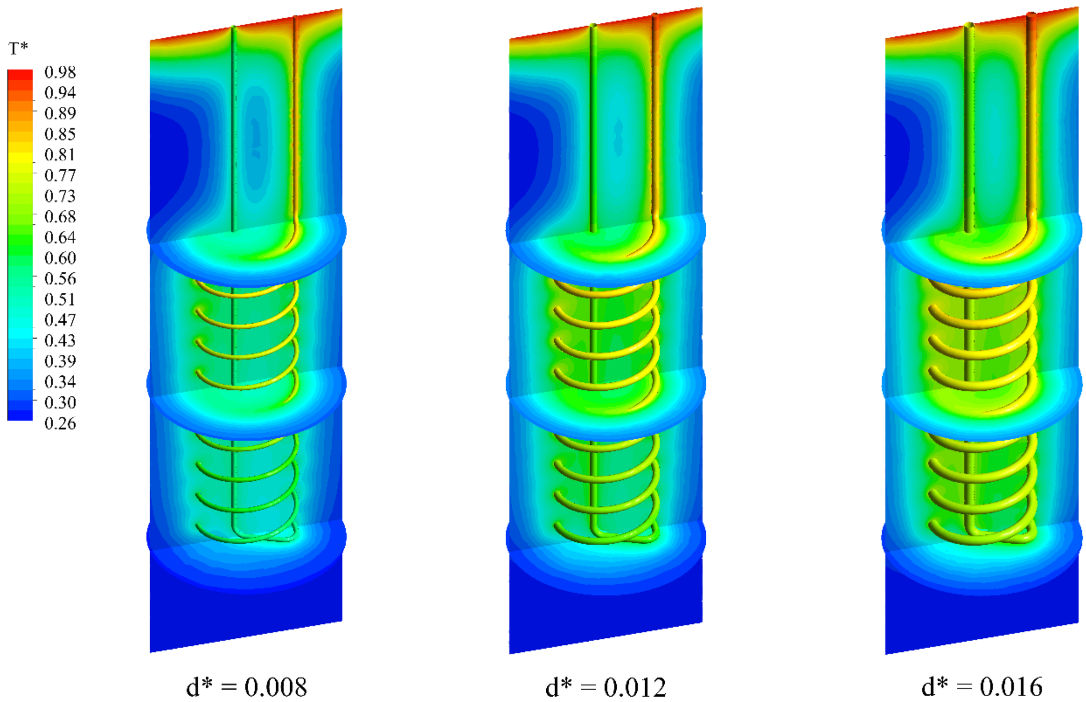

Figure IV.30: Temperature distribution contours of the HGAHE system after 24 h of operation time at different pipe diameters in 3D view.

Figure IV.31 illustrates the heat exchange rate and effectiveness versus the dimensionless pipe diameter after 24 hour of operation time. It can be seen that upon increasing the dimensionless pipe diameter from 0.008, to 0.016, the heat exchange rate raises considerably from 459.4 W to 1159.2 W. However, by raising the dimensionless pipe diameter from 0.008, to 0.016, the effectiveness decreases from 0.45 to 0.28. These findings reveal that, as dimensionless pipe diameter is incremented from 0.008, to 0.016 the heat exchange rate enhanced by 152.3 %, while the effectiveness dropped by 37.7 % only.

Above results can be clarified as follows: the heat exchange rate is related to the mass flow rate and air temperature drop as presented in Eq. (II.1). Thus, by raising d^* from 0.008 to 0.016 (at constant ventilation velocity) the mass flow rate increases from 0.052 kg/s to 0.209 kg/s (301.9 %), whereas the drop in air temperature decreased from 8.7 °C to 5.5 °C (36.7 %). Therefore, the relative increase in mass flow rate is greater than decrement in air temperature drop and consequently raises the heat exchange rate of the GAHE system. For the effectiveness, the reason for the decline can be explained due to the fact that by increasing dimensionless pipe diameter the T^* outlet raises, which yield a reduction in air temperature drop. Thus, based on Eq. (II.5) the effectiveness is decreased.

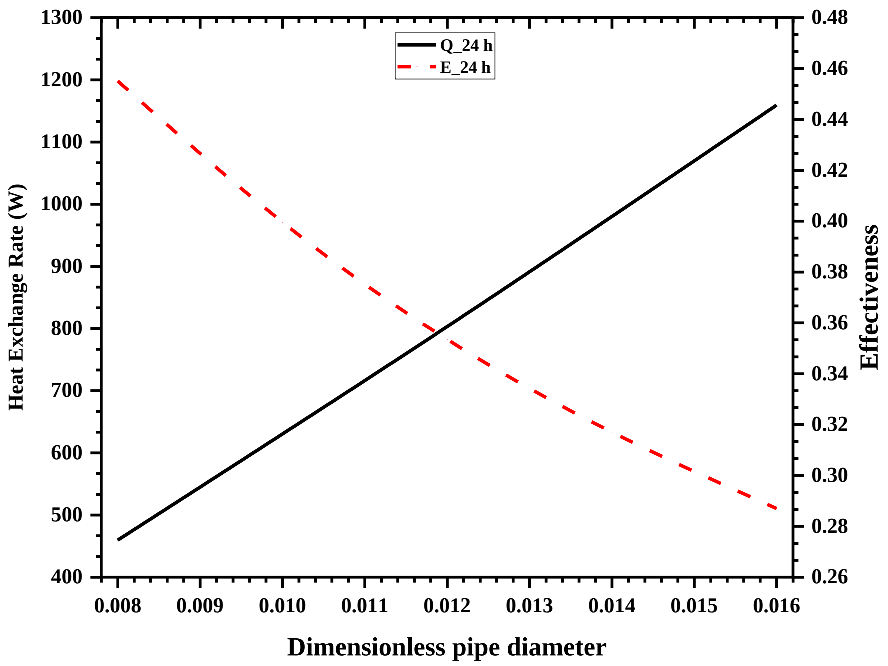

Figure IV.31: Variation of heat exchange rate and effectiveness with operation time at different pipe diameters.

The pressure drop for various dimensionless pipe diameters after 24 hours of operation time is depicted in Figure IV.32. It is observed that, the pressure drop is decreasing with the increase of dimensionless pipe diameter. Based on the obtained numerical results, by raising d^* from 0.008 to 0.016 the pressure drop decreased significantly from 55786.9 Pa to 4609.6 Pa, that is about 12 times reduction. From this, it can be revealed that, dimensionless pipe diameter has a remarkable influence on the pressure drop of the system, Based on Eq. (II.8), it is mentioned that the pressure drop has a reverse relation to the hydraulic diameter of the pipe. Figure IV.32, also shows the pressure drop obtained from the numerical model as well as the pressure drop obtained from some correlations. In comparison with the numerical results, the pressure drop difference with Ju et correlation and Schmidt correlation is ranging from 11.2 % to 36.3 % and from 5.8 % to 41.5 %, respectively. Moreover, comparing the pressure drop of the helical pipe to the straight pipe (as reference) shows that, the pressure drop of the helical pipe is greater than that of the straight pipe for the different dimensionless pipe diameters, furthermore the maximum pressure drop was found at the lowest d^* value i.e. 0.008, where the pressure drop of the helical pipe incremented by about 1.5 times compared to the straight pipe.

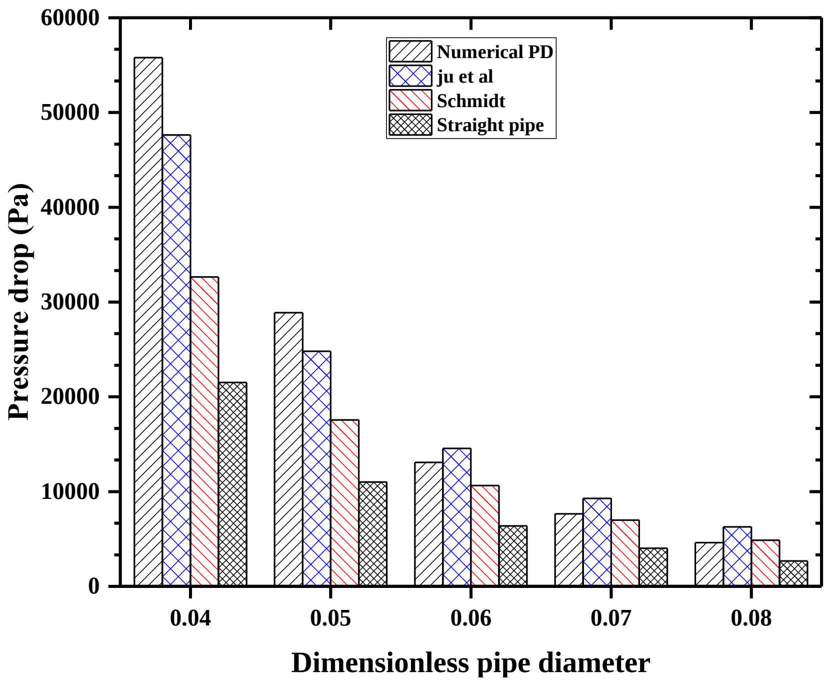

Figure IV.32: Pressure drop for different pipe diameters after 24 h of operation time.

IV.4.3.4 Effects of helical pitch

The length and the surface area of the helical pipe in the borehole depend on the helical pitch size. In order to investigate the effects of helical pitch on the efficiency of the GAHE, performance tests with dimensionless helical pitches of 0.02, 0.04, 0.06, 0.08 and 0.1 were conducted, while other parameters were kept constant. The variation of T^* outlet with operation time for various helical pitches are presented in Figure IV.33. From the figure, it can be seen that T^* outlet of all curves is increased greatly during the first 12 h, but the increasing rate becomes small after 12 h and the differences between curves gradually decreased. This means that T^* outlet can be decreased mostly in the first 12 h of operation time, therefore the heat exchange rate can be improved in the early operation time by reducing the helical pitch. However, after 12 h this change became less and not impressive. Furthermore, it is noticed that, after 24 h of operation time, T^* outlet was 0.622, 0.649, 0.669, 0.691 and 0.705 for dimensionless helical pitches of 0.02, 0.04, 0.06, 0.08 and 0.1, respectively. These results indicate that by increasing helical pitch the T^* outlet is incremented, but this increase is not so significant and the highest and lowest T^* outlet occur in helical pitches of 0.1 and 0.02, respectively. This is caused mostly by the fact that reducing the helical pitch can increment the total length of pipe and hence the heat exchange area between the air and the borehole also increased. Based on these findings, the helical pitch cannot be decreased unlimitedly and should be optimized through considering the total heat exchange rate as well as the available borehole area. Furthermore, Figure IV.34 illustrates the temperature distribution contours of the HGAHE system after 24 h of operation time at different dimensionless helical pitches in 3D view. It can be seen from the figure that, by increasing the P^* the temperature of backfill material and surrounding soil significantly decreases. The reason can be attributed to the fact that with the increase in the helical pitch, the total length of pipe and hence the heat transfer area decreased. Hence, the T^* outlet increments.

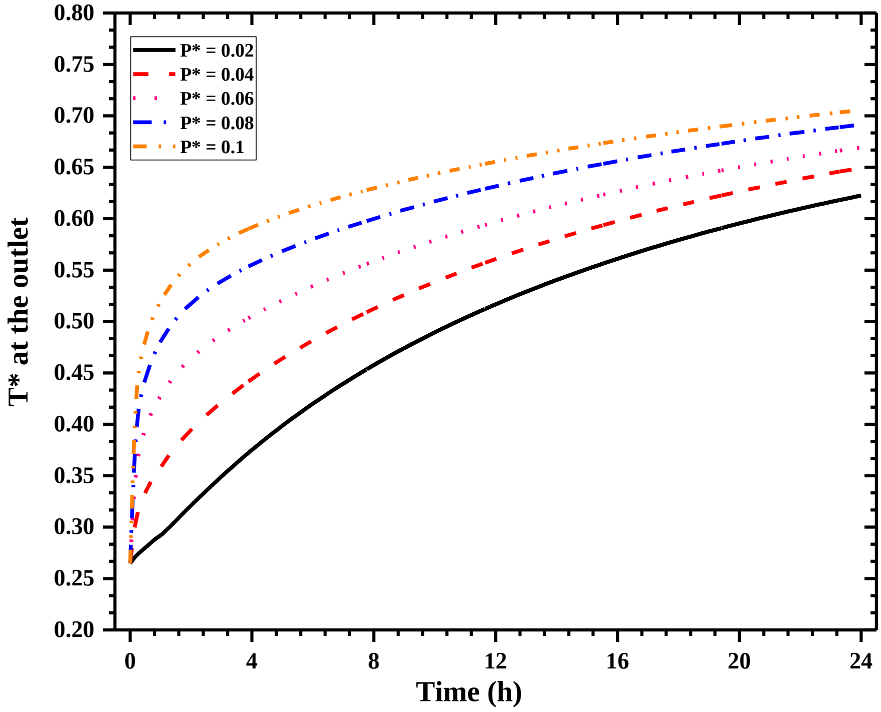

Figure IV.33: Variation of T^* outlet with operation time at different helical pitch values.

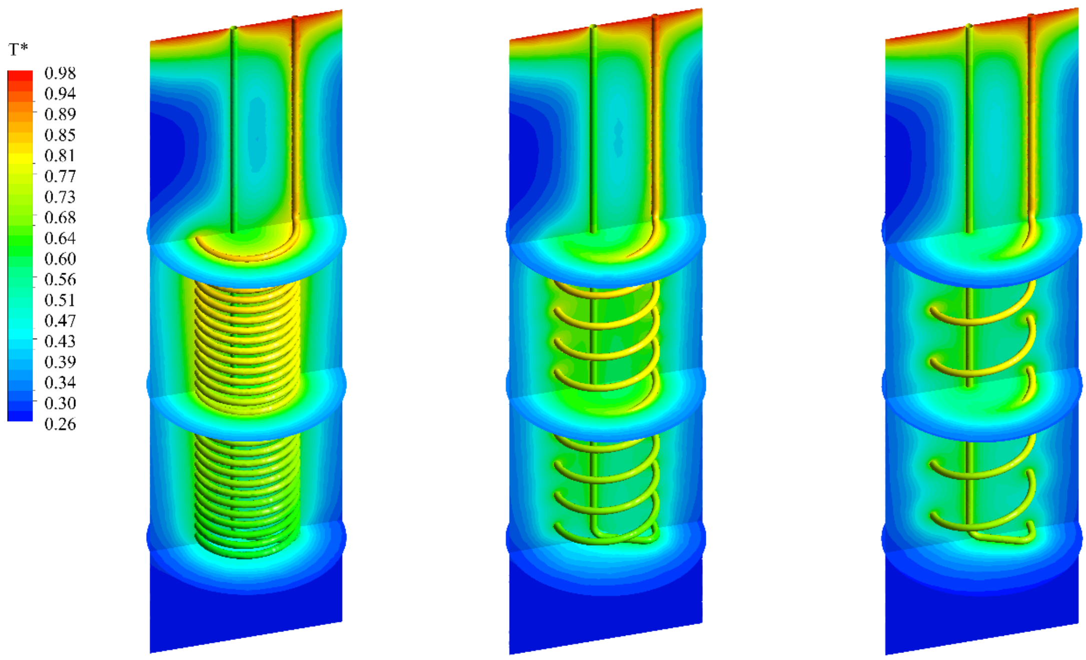

P* = 0.02 P* = 0.06 P* = 0.1

Figure IV.34: Temperature distribution contours of the HGAHE system after 24 h of operation time at different helical pitches in 3D view.

The impact of dimensionless helical pitch on the heat exchange rate and effectiveness of the system also determined and presented in Figure IV.35. From the figure it is observed that after 24 h of operation time, upon increasing P^* from 0.02 to 0.1 the heat exchange rate decreases from 935.8 W to 700.1 W and the effectiveness decreases from 0.41 to 0.31. These results indicate that as the P^* is incremented from 0.02 to 0.1 the heat exchange rate dropped by 25.2 %, whereas the effectiveness decreased by 24.4 % and the reason can be attributed to the fact that, by increasing the dimensionless helical pitch the heat transfer area decreased resulting in incremental in the T^* outlet, hence reducing the heat exchange rate and effectiveness of the GAHE system.

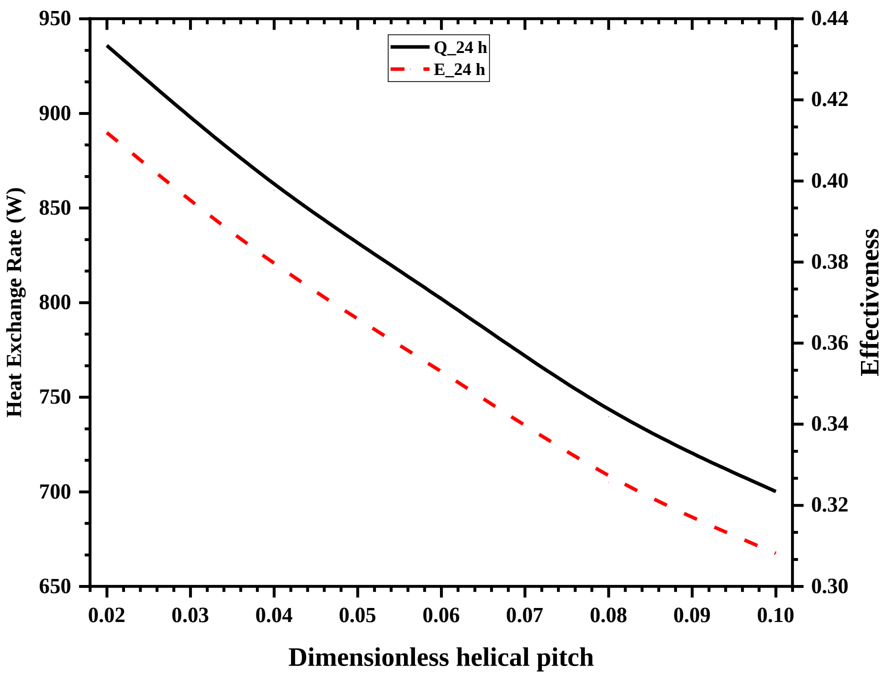

Figure IV.35: Variation of heat exchange rate and effectiveness with operation time at different helical pitches.

The pressure drop for various dimensionless helical pitches after 24 hours of operation time is shown in Figure IV.36. It is evident from the figure that, the pressure drop of the helical pipe decreases with raising its dimensionless helical pitch. According to the pressure drop obtained from the numerical model, the highest pressure drop was found at the minimum P^* value, that is 43665.9 Pa. However, the lowest pressure drop was attained at the maximum P^* value, which is 9778.8 Pa, indicating 5.5 times reduction and reason for that can be justified as follows: by raising dimensionless helical pitch the length of the helical pipe is decreased, therefore the pressure drop is decreased, because as expressed in Eq. (II.8), the pressure drop has a direct relation to the total length of the helical pipe. Furthermore, as illustrates in Figure IV.36, in comparison with the numerical results, the pressure drop difference with Ju et correlation and Schmidt correlation is varying from 3.5 % to 24.1 % and from 9.2 % to 38.3 %, respectively. In addition, the pressure drop of the helical pipe and the straight pipe has been compared which shows that, the pressure drop of the helical pipe is more than that of the straight pipe. Moreover, the pressure drop of the helical pipe at the lowest p^* value has an incremental of 170 % compared to that of the straight pipe.

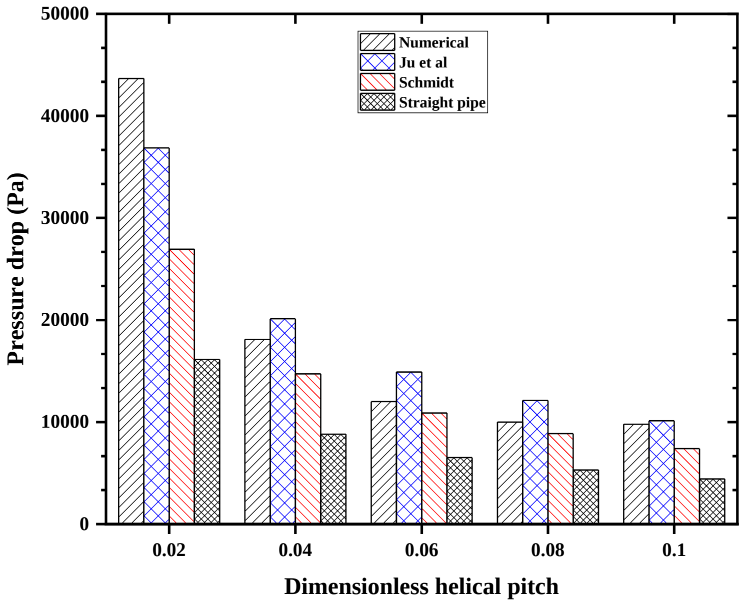

Figure IV.36: Pressure drop for different helical pitches after 24 h of operation time.

IV.4.3.5 Effects of pipe thickness

Another parameter examined in this study is the pipe thickness. In order to further investigate the effects of the pipe thickness on the thermal performance of the GAHE system, five various dimensionless pipe thickness i.e. 0.0002, 0.0004, 0.0006, 0.0008 and 0.001 have been considered, while other parameters were kept constant. Figure IV.37 illustrates the variation of T^* outlet with operation time for different dimensionless pipe thickness. From this figure it can be seen that all curves of the T^* outlet are increasing with the same trend with the operation time. However, the T^* outlet for various dimensionless pipe thickness is not so tangible so that the different percentages of T^* outlet between different dimensionless pipe thickness are not so significant. Moreover, it is also observed that, after 24 h of operation time, T^* outlet was 0.661, 0.665, 0.669, 0.673 and 0.676 for dimensionless pipe thickness of 0.0002, 0.0004, 0.0006, 0.0008 and 0.001, respectively. This result shows that by increasing dimensionless pipe thickness the T^* outlet is decreased, but this reduction is not so important and the lowest T^* outlet and the highest one occur in dimensionless pipe thickness of 0.0002 and 0.001 respectively, while the T^* outlet only increased in dimensionless pipe thickness increment from 0.0002 to 0.001 by 2.2 %. From this, it can be concluded that the change in dimensionless pipe thickness does not so much affect T^* outlet and there will be no dramatic change in the thermal performance of the GAHE system. Figure IV.38 illustrates the temperature distribution contours of the HGAHE system after 24 h of operation time at different dimensionless pipe thickness in 3D view. Similar to the observation made above it is clear from the figure that, increase in dimensionless pipe thickness does not have a considerable effect on temperature distribution into the backfill material and surrounding soil, hence very small change in T^* outlet has been observed.

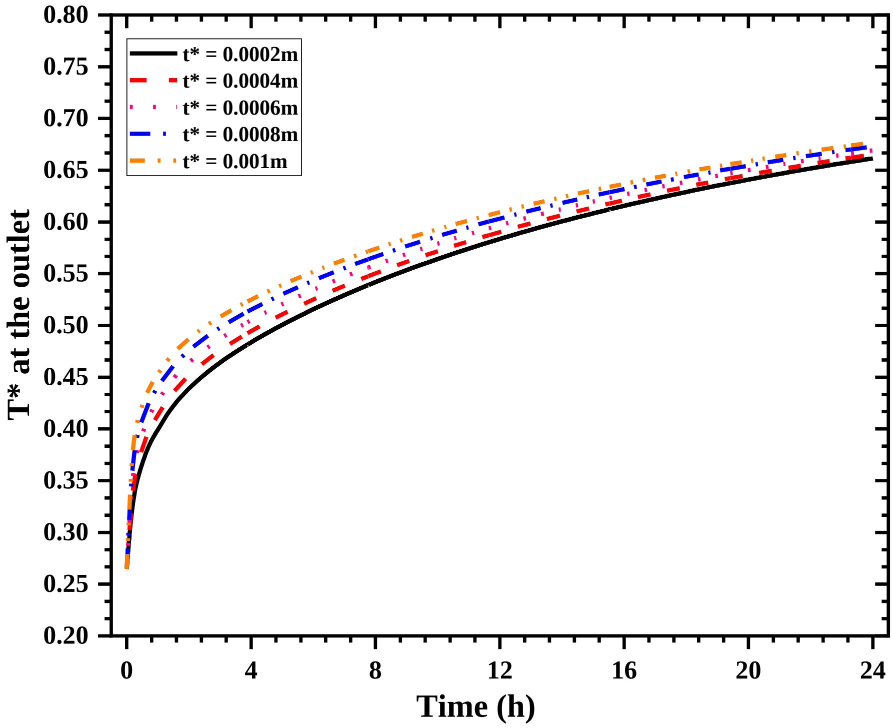

Figure IV.37: Variation of T^* outlet with operation time at different pipe thickness.

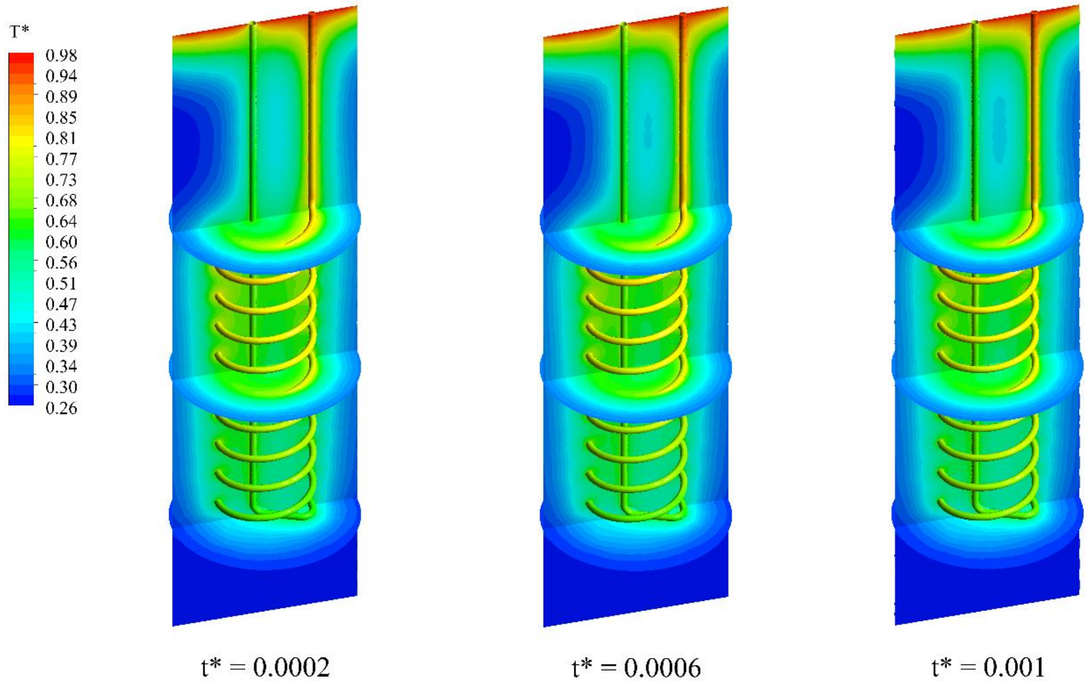

Figure IV.38: Temperature distribution contours of the HGAHE system after 24 h of operation time at different pipe thickness in 3D view.

Moreover, the influence of dimensionless pipe thickness on the heat exchange rate and effectiveness has also been analyzed. From Figure IV.39 it can be seen that, after 24 h of operation time, by raising dimensionless pipe thickness from 0.0002 to 0.001 the heat exchange rate decreases from 825.3 W to 781.6 W only and the effectiveness slightly drops from 0.36 to 0.34. These results indicate that as the dimensionless pipe thickness is raised from 0.0002 to 0.001 the heat exchange rate decreased only by 5.3 %, whereas the effectiveness decreased just by 5.5 %. This suggests that the change in dimensionless pipe thickness has no impressive impact on the thermal performance of GAHE system.

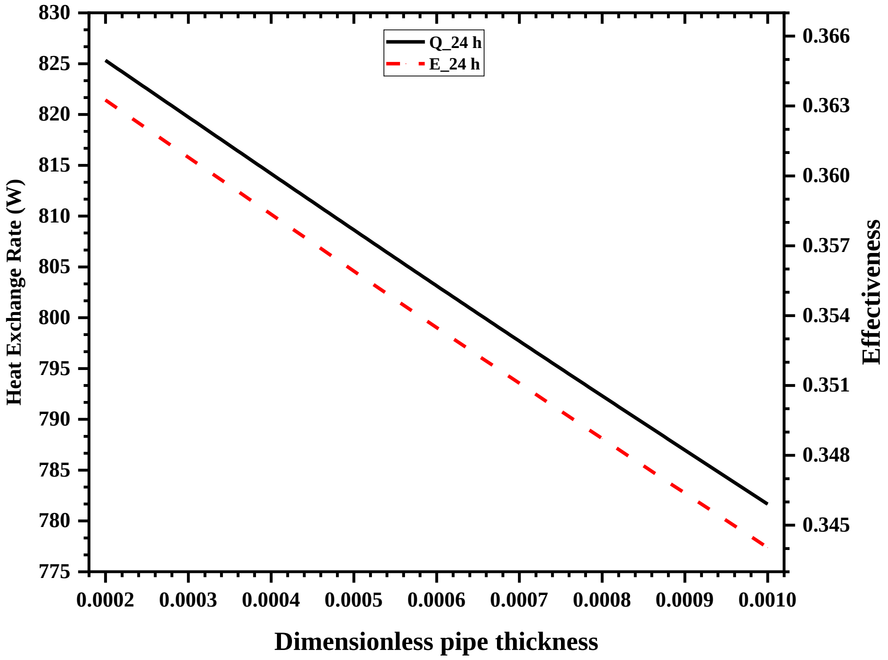

Figure IV.39: Variation of heat exchange rate and effectiveness with operation time at different pipe thickness.

IV.4.3.6 Effects of helical diameter

In this section, the impact of the change in the helical diameter has been investigated by considering five various dimensionless helical diameters i.e. 0.04, 0.06, 0.08, 0.1 and 0.12, while other parameters were kept constant. Figure IV.40 illustrates the variation of T^* outlet with operation time for different dimensionless helical diameters. From this figure, it can be seen that all curves are increasing with the same trend with the operation time. It is also noticed that, after 24 h of operation time, T^* outlet was 0.780, 0.728, 0.669, 0.616 and 0.572 for dimensionless helical diameters of 0.04, 0.06, 0.08, 0.1 and 0.12, respectively. This result shows that, the T^* outlet at D^* of 0.12 compared to D^* of 0.04 is decreased up to 26.6 %. Therefore, the T^* outlet is decremented by increasing dimensionless helical diameter. These findings can be justified as follows, by incrementing the dimensionless helical diameter, the length of the pipe increments and the residence time of air into the pipe increases, which result in more heat transfer between air and borehole and consequently the T^* outlet decreases. Also, contours of the temperature distribution of the HGAHE system after 24 h of operation time at different dimensionless helical diameters in 3D view are demonstrated in Figure IV.41. As shown in this figure, the lower helical diameters, the higher temperature distribution into the backfill material and surrounding soil, Therefore, the T^* outlet is decreased by increasing dimensionless helical diameter as concluded above.

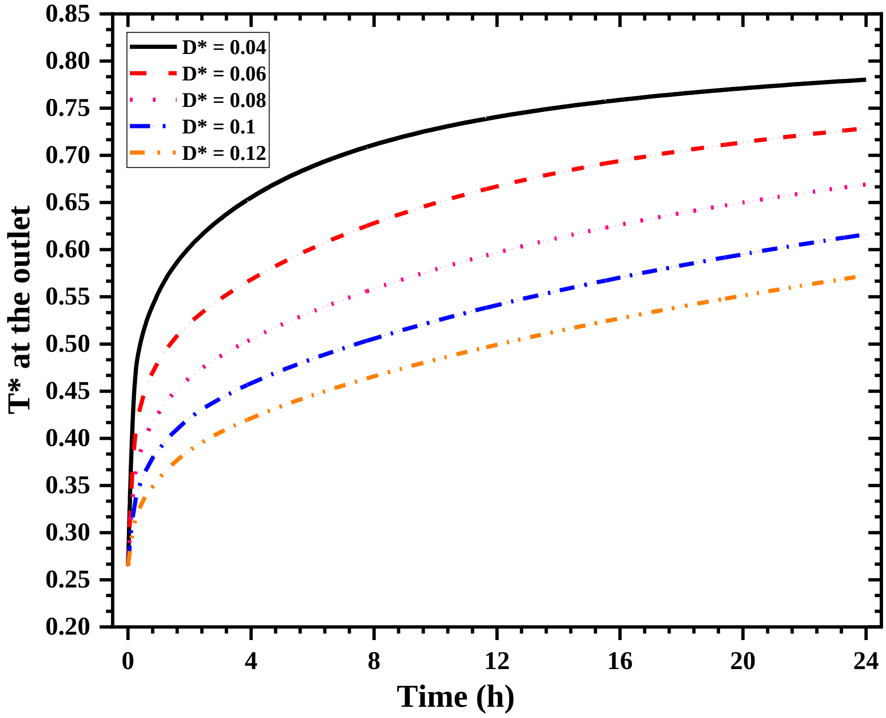

Figure IV.40: Variation of T^* outlet with operation time at different helical diameters.

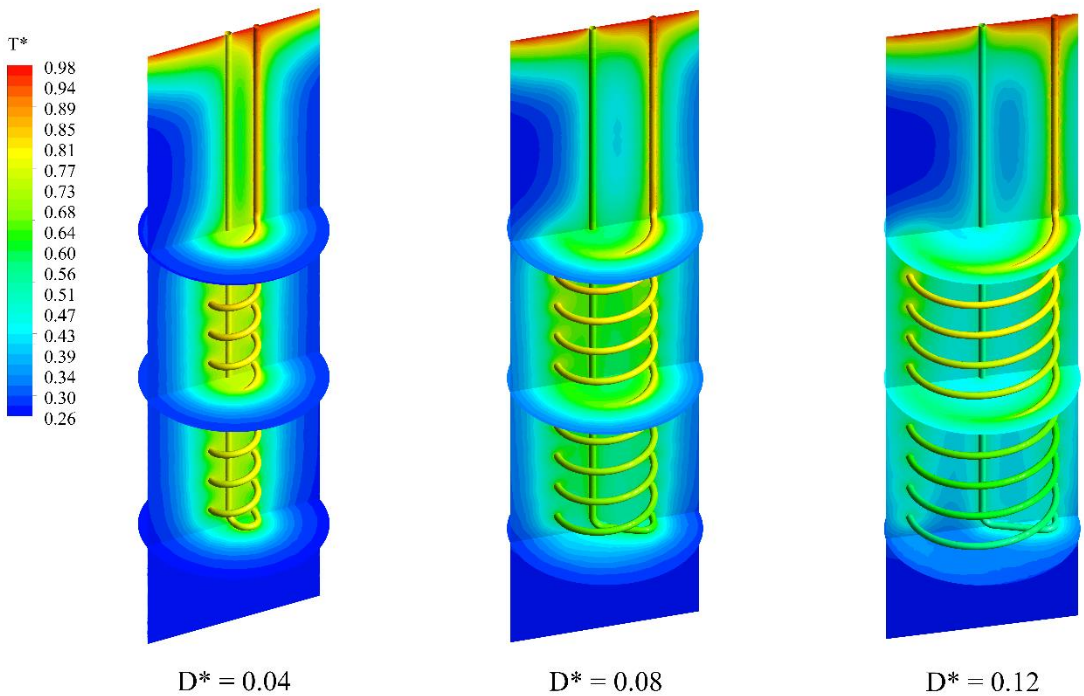

Figure IV.41: Temperature distribution contours of the HGAHE system after 24 h of operation time at different helical diameters in 3D view.

The influence of dimensionless helical diameter on the heat exchange rate and effectiveness of the GAHE system is depicted in Figure IV.42. It can be seen that, after 24 h of operation time, with increasing D^* from 0.04 to 0.12 the heat exchange rate raises from 488.3 W to 1077.1 W and the effectiveness increases from 0.21 to 0.47. From these findings it can be concluded that, as the D^* is incremented from 0.04 to 0.12 the heat exchange rate increments by 120.6 %, whereas the effectiveness augments by 123.8 %, because with increasing the dimensionless helical diameter, the length of the pipe increments and thus, the heat transfer surface augmented which result in decremental of the T^* outlet, hence improving the heat exchange rate and effectiveness of the GAHE.

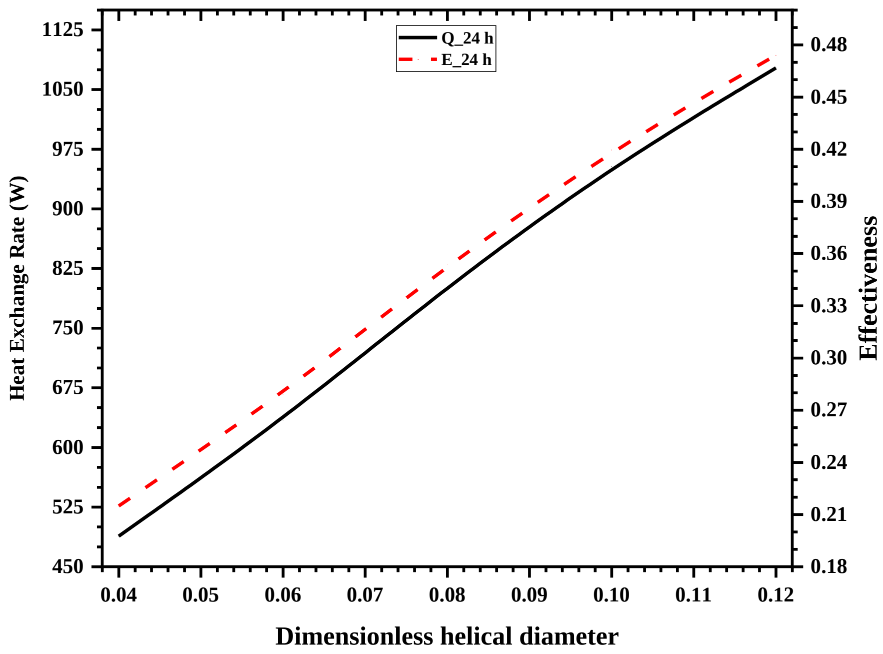

Figure IV.42: Variation of heat exchange rate and effectiveness with operation time at different helical diameters.

The pressure drop for different dimensionless helical diameters after 24 hours of operation time is depicted in Figure IV.43. It is noticed from the figure that, the pressure drop is raising with the increase of dimensionless helical diameter. According to the obtained numerical results, with increasing D^* from 0.04 to 0.12 the pressure drop raises from 9744.7 Pa to 16762.6 Pa. This outcome shows that, the pressure drop at D^* of 0.12 compared to D^* of 0.04 is increased by 72.0 %. Thus, it can be revealed that the dimensionless helical diameter has a considerable effect on the flow pressure drop of the GAHE, this is caused mostly by the fact that as the D^* incremented the length of the helical pipe is increased, thus the pressure drop is raised, because according to Eq. (II.8), the pressure drop has a direct relation to the total length of the helical pipe. In Figure IV.43, the numerical results of the pressure drop have been compared with the results of some correlations. It can be seen that, the highest difference between the numerical results and Ju et correlation is 16.2 %, whereas the highest difference between the numerical results and Schmidt correlation is 20.1 %. Moreover, the pressure drop of the helical pipe was compared to the pressure drop of a straight pipe (as reference). From the figure, it is observed that the pressure drop of the helical pipe is higher than that of the straight pipe. For example, when the D^* is 0.12 the pressure drop of straight pipe and helical pipe is 8830.7 Pa and 16762.6 Pa respectively, suggesting about 150.0 % of pressure drop increase in the helical pipe.

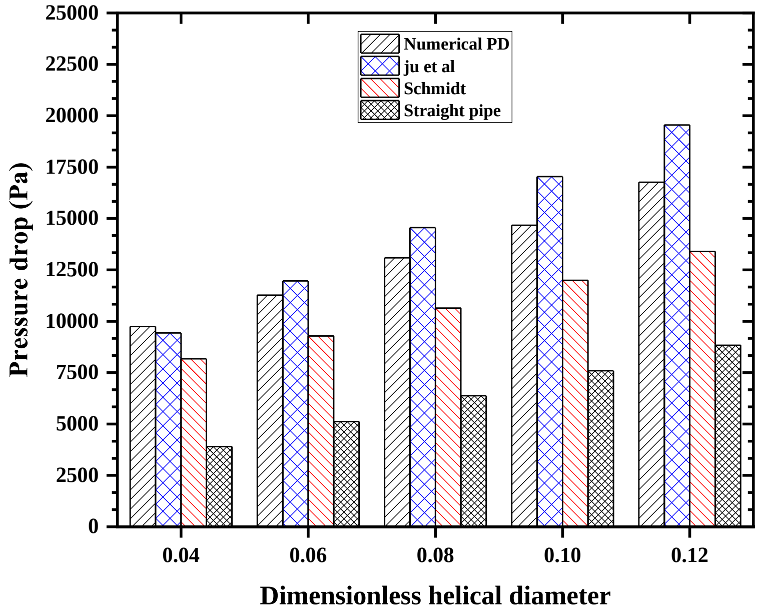

Figure IV.43: Pressure drop for different helical diameters after 24 h of operation time.

IV.4.3.7 Effects of backfill material

The backfill material type is another factor that can influence the performance of the GAHE system. In this study, the impact of the backfill material type with different thermal properties were analyzed, while other parameters were kept constant. Five types of backfill material have been considered, which includes silt loam, sandy, silica sand, concrete and sandy loam. Thermal properties of the used backfill materials are listed in Table IV.8.

Table IV.8: Thermal properties of the used backfill materials.

Material	Density (kg/m^3)	Specific heat (J/kg K)	Thermal conductivity (W/m K)	Thermal effusivity ($W\ s^{1/2}/m^2\ K$)	Ref.
Silt loam	1415	804	0.6	826.19	[112]
Sandy	2050	1840	0.52	1400.51	[66]
Silica sand	2210	750	1.4	1523.31	[90]
Concrete	2500	837	1.63	1846.82	[113]
Sandy loam	2100	1047.6	2.2	2199.98	[112]

The obtained results are presented in Figure IV.44. From the figure, it can be seen that all curves of the T^* outlet are increasing with the operation time for the different types of the backfill material. Furthermore, it is noticed that, after 24 h of operation time, T^* outlet was 0.801, 0.729, 0.706, 0.669 and 0.636 for backfill materials of silt loam, sandy, silica sand, concrete and sandy loam, respectively. These findings shows that the lowest and highest T^* outlet were found for backfill materials of sandy loam and silt loam, respectively. This is could be clarified due to the fact that, the backfill material with a higher thermal effusivity can store more heat and thus the heat exchange rate of the GAHE system can be improved more effectively as shown in Figure IV.45 which illustrates the temperature distribution contours of the HGAHE system after 24 h of operation time at different types of the backfill material in 3D view. Moreover, from Table IV.8 it can be seen that, the backfill material with sandy loam has the highest thermal effusivity, followed by the concrete, silica sand, sandy and the smallest is for the silt loam. These results indicate that by using the sandy loam as backfill material the T^* outlet can be decreased up to 20.6 % compared to a backfill material with silt loam. Therefore, the thermal effusivity of the backfill material has a significant impact on its performance over the operation period.

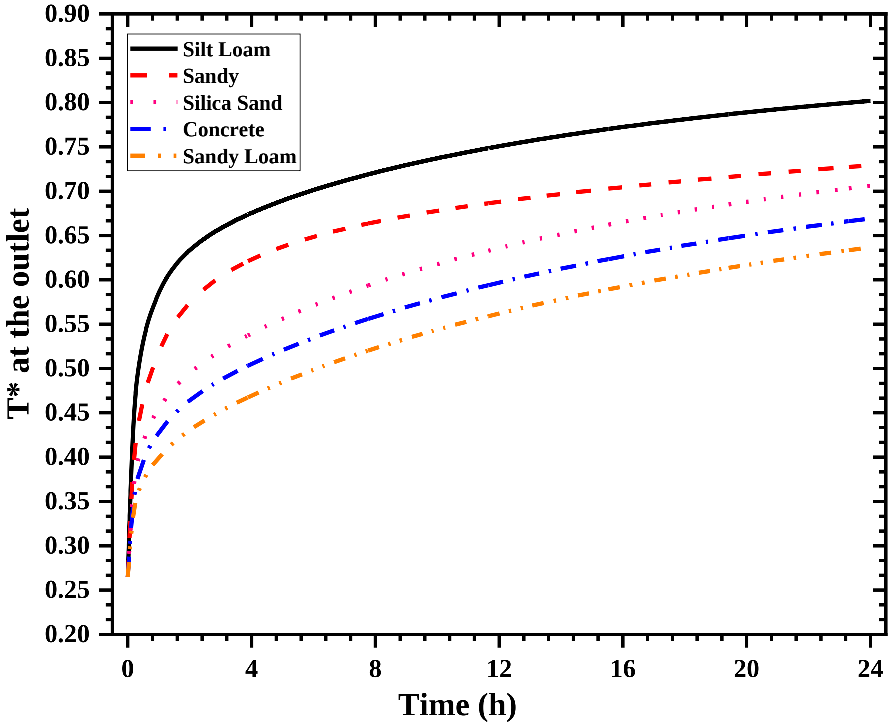

Figure IV.44: Variation of T^* outlet with operation time at different Reynolds number.

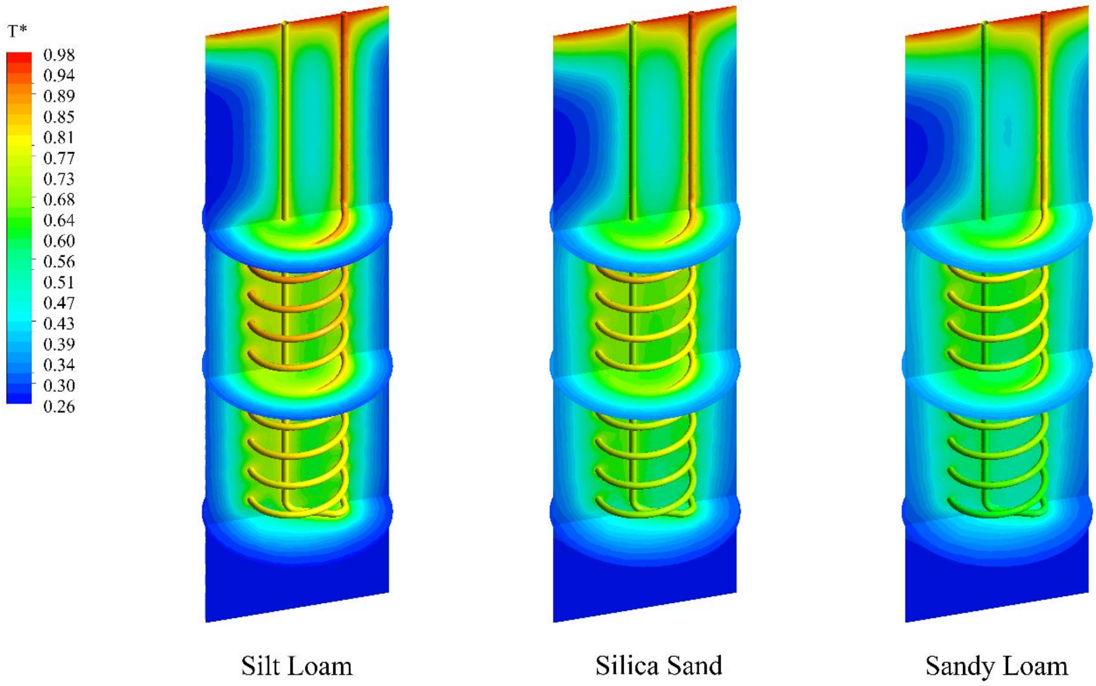

Figure IV.45: Temperature distribution contours of the HGAHE system after 24 h of operation time at different types of the backfill material in 3D view

Figure IV.46 illustrates the heat exchange rate and effectiveness of the system for different backfill material types. It is noticed from the figure that, the silt loam backfill material has the lowest heat exchange rate and effectiveness which is 426.8 W and 0.19, respectively. However, the sandy loam backfill material has the highest heat exchange rate and effectiveness which is 895.6 W and 0.39, respectively. These outcomes suggest that, by using the sandy loam as backfill material compared to the silt loam, the heat exchange rate and effectiveness are significantly enhanced by 109.8 % and 105.3 %, respectively. This is due to the fact that, the silt loam and the sandy loam, respectively have the lowest and highest thermal effusivity. Thus, backfill material with higher thermal effusivity implies more enhancement on the heat exchange rate and effectiveness of the GAHE system.

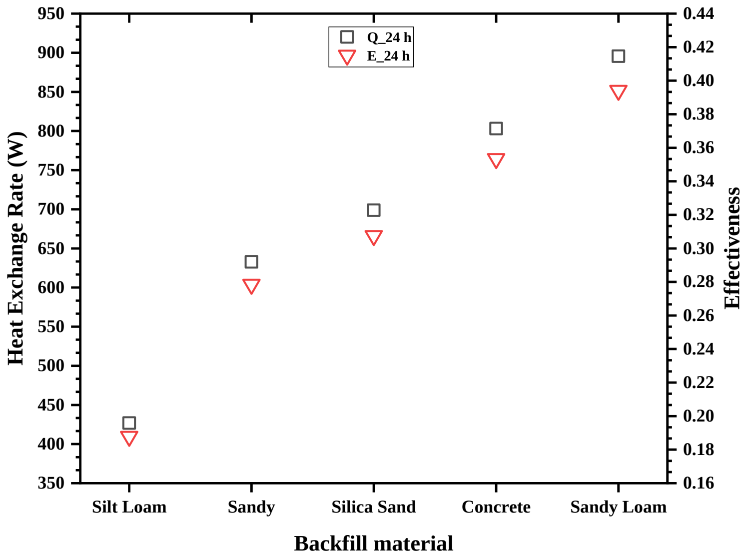

Figure IV.46: Variation of heat exchange rate and effectiveness with operation time at different Reynolds numbers.

IV.4.3.8 Multiple linear regression equation

The Multiple-linear regression has been performed and the suggested model equation from this regression analysis is in the form of equation (IV.2) as follows:

$$T^{*}outlet = 0.6148\,Re + 0.6183\,T^{*}inlet + 0.4465\,d^{*} + 0.2764\,P^{*} + 0.0505\,t^{*} - 0.7016\,D^{*} - 0.3407 \quad \text{(IV.2)}$$

Interpreting the coefficients of (IV.2), and in light of the regression results statistics, where R^2, adjusted R^2, predicted R^2, and a standard error are 0.9652, 0.9652, 0.9651, and 7.789 respectively, indicates a good model prediction. It can also be observed that only the helical diameter has a negative contribution on the outlet temperature, while other parameters have a positive contribution. Moreover, each variable has a different impact on the proposed model equation. Therefore, it is essential to accurately clarify the most effective parameter. As illustrates in Figure IV.47, the helical diameter, inlet temperature and Renolds number are the most effective variables among the other variables in the predicting equation. Findings also reveal that the pipe diameter and pitch size have a moderate impact on thermal performance of the HGAHE system, while the effect of pipe thickness is relatively negligible as aforementioned in subsection 5.5. Further analysis from the proposed model suggested that, while holding all other parameters constant, an increase in the outlet temperature is explained by an increase of 0.614 in Reynolds number, 0.618 °C in inlet temperature, 0.446 m in pipe diameter, 0.276 in pitch size and a decrease of 0.701 m in helical diameter, while the pipe thickness has no impressive impact.

To further assess the performance of the proposed model, a detailed evaluation of its numerical against predictions data is performed and it is found, as expected, to reasonable prediction error, and well explain variations in the target variables considering input variables, specifically, the model explains that variation at 99.1 % out of the total variance in $T^{*}outlet$ presenting a good fit to the data, while the adjusted R^2 was found to be 0.977, slightly lower than R^2 (0.982) indicating a satisfactory performance by the model, additionally, the predicted R^2 of the model was at 0.982 indicating that the model would perform well on unseen dataset. In term of error metrics, it can be seen from the scatter plot of numerical and prediction outlet temperature shown in Figure IV.48, a very good predictive ability is achieved by the model. In addition, the Standard Error of the model was only 0.032, while the RMSE of its predictions was at 0.0284. The MAE and MSE were also indicating good model fit as their attained values were 0.0157 and 0.00081, respectively. The Mean Absolute Percentage Error (MAPE) was well below 5 % (3.588) which demonstrate remarkable forecasting accuracy and close match to numerical data, and hence reflecting the solid performance by the model, its reliability and suitability for practical real-world applications.

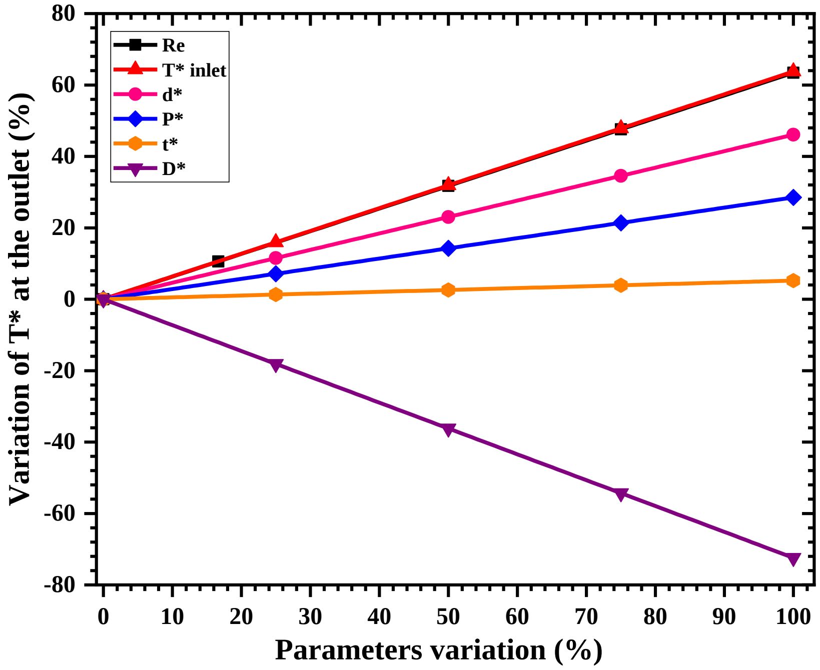

Figure IV.47: Sensitivity analysis of the outlet temperature.

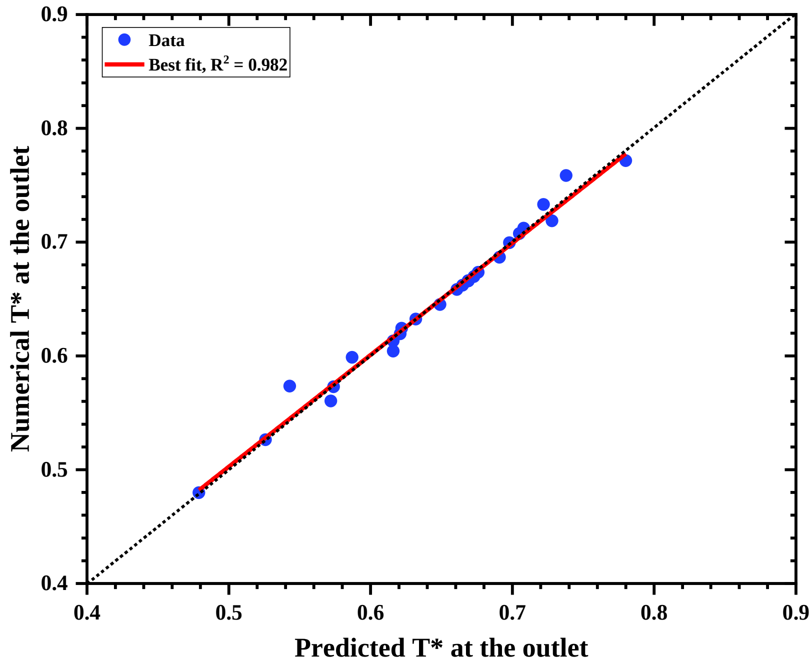

Figure IV.48: Scatter plot of numerical versus predicted outlet temperature.

IV.5 Conclusion

This chapter presented the analysis of the thermal behavior of helical-coil layout GAHE both experimentally and computationally as well as the parametric study results. The key outcomes and findings of the present research work are below. It's important to note that, given the extensive number of concluding remarks, the majority of the conclusions will be consolidated and presented in the overarching general conclusion:

- Temperature drop of air decreases with the operation time and also with increment of air velocity.

- Experimental findings revealed that, the heat exchange rate of the HGAHE system enhanced with incrementing the air temperature drop. The maximum heat exchange rate of 463.4 W is achieved at the highest air temperature drop of 13.3 °C.

- Pressure drop of air flow along the length of pipe increments with raising the airflow velocity. Upon increasing the airflow velocity from 10 to 20 m s^{-1}, the pressure drop increases more than 3 times.

- Increasing the ventilation velocity can increase the outlet air temperature, the heat exchange rate and the pressure drop of the flow inside the pipe, but also result in a decrease in the effectiveness. By raising Reynolds number from 80,000 to 200,000, after 24 h of operation, the outlet air temperature, the heat exchange rate and the pressure drop incremented by 30.3 %, 30.6 % and 465.4 % respectively, while the effectiveness decreased by 49.0 %. Ventilation velocity has a significant impact on the pressure drop compared to the other factors.

- The higher the inlet temperature, the more the outlet air temperature, the heat exchange rate and the effectiveness. With an increase in dimensionless inlet temperature from 0.617 to 0.952, after 24 h of operation the outlet air temperature, the heat exchange rate and the effectiveness increased by 39.6 %, 104.8 % and 16.6 % respectively. Hence, the thermal performance of the GAHE system can be improved effectively through increasing the inlet air temperature.

The study findings suggested that the helical GAHE has a significant potential to minimize the construction cost, decrease the energy consumption and provides efficient heating and cooling for buildings.

GENERAL CONCLUSION

The aim of the present thesis was to obtain a better understanding of the ground air heat exchanger thermal behavior in regard to the helical pipe configuration. The overall goal was sub-divided into a number of specific studies objectives which have been previously detailed.

First of all, bibliographical research on geothermal energy use and up to date technologies around the globe have been conducted and current practices on the Algeria's geothermal resources and the development roadmap have been discussed. Furthermore, extracting geothermal energy by GAHE systems has been performed and the different classification, types, applications and recent research trends of the GAHEs have been discussed, in addition research gab and limitations have been identified. Following this, an experimental set up of the proposed helical configuration of the GAHE has been implemented in order to evaluate its thermal performance experimentally in terms of air temperature drop, heat transfer rate, total thermal resistance, effectiveness, pressure drop and thermal performance derating factor. Later on, the proposed helical shaped GAHE system was also numerically investigated using ANSYS Fluent to analyze the performance of the proposed configuration in terms of air temperature drop obtained, heat exchange rate, distribution of heat into the borehole as well as to investigate the borehole temperature recovery using cold ambient air for a night purging. Moreover, the validated numerical model has been also used to carry out a parametric study to investigate the impact of the various operating and geometric parameters on the thermal performance of the HGAHE system. The obtained results from the experimental and numerical investigations have been presented and discussed in the last section of the thesis. The main key outcomes and findings derived from the present research work can be summarized as follows:

- The outlet air temperature of the HGAHE system is mainly dependent to the inlet temperature. However, the variation in the outlet temperature is much lower due to the large borehole and surrounding ground thermal mass.

- Experimental findings revealed that, the heat exchange rate of the HGAHE system drops with time duration of operation, and enhanced with incrementing velocity of air. The maximum heat exchange rate of 668.9 W was achieved after a period of 1 hour and at the highest air velocity which is 20 m s^{-1}.

- Effectiveness of the HGAHE system decreases with the operation time and diminishes by increasing velocity of air. The highest effectiveness of 0.83 was obtained after a period of 1 hour and at the lowest air velocity of 10 m s^{-1}.

- The thermal performance derating factor (TPDF) increments with the time duration of operation. Furthermore, experiments revealed that, the minimum and maximum decline in the performance of the system is observed with the lowest and highest air velocity of 10 and 20 m s^{-1}, respectively. At air velocity of 20 m s^{-1} the TPDF decreases by 27 % in a period of 3 hours, whereas, it drops by 14 % only at air velocity of 10 m s^{-1}.

- During the cooling mode, the borehole temperature in the axial direction is higher at the upper surface, and then this temperature decrements with the length of the HGAHE because of the high temperature gap between the pipe wall at the upper surface of the borehole and the air, thus this difference is reducing with the HGAHE length. At 0.1 m away from the pipe surface, the borehole temperature at the upper surface is increased by 2.1 °C. However, the borehole temperature at the bottom surface is increased by only 0.5 °C.

- The borehole temperature near the helical pipe surface in the radial direction was strongly influenced by the inlet temperature. This effect was more pronounced in the vicinity of the pipe surface and declined when increasing from the pipe wall. After a period of 15.5 hours, the borehole temperature at the upper surface was increased by 2.1 °C at 0.1 m away from the pipe surface, while the borehole temperature at the upper surface was incremented by only 0.8 °C at 0.2 m away from the pipe surface.

- The analysis of the heat penetration into the borehole implies that the thickness of the affected area keeps incrementing along with the heat exchange between the borehole and air. After 5 hours of operation time, the affected area was 0.27 m, whereas after a period of 10 hours the thickness of the affected area incremented up to 0.3 m.

- When the ambient air temperature drops during the night period, the forced convection between the borehole and air helps the borehole and surrounding ground to restore its cooling ability. At the end of the night purging period, the borehole recovered its cooling ability by 1.0 °C. So, it is recommended to operate the HGAHE system during the night shift for temperature recovery through the night purging phenomena.

- Raising the pipe thickness has no impressive impact on the thermal performance of GAHE system. By increasing the dimensionless pipe thickness from 0.0002 to 0.001 the outlet air temperature, the heat exchange rate and the effectiveness incremented only by 2.2 %, 5.3 % and 5.5 % respectively.

- By incrementing the helical diameter, the outlet air temperature decrease. However, as the helical diameter increases, the heat exchange rate, the effectiveness and the pressure drop increase.

- As the pipe diameter increments, the outlet air temperature and the heat exchange rate increase while the effectiveness and the pressure drop of the flow inside the pipe decrease. With an increase in dimensionless pipe diameter from 0.008 to 0.016, after 24 h of operation the outlet air temperature and the heat exchange rate increased by 30 % and 152.3 % respectively, but the effectiveness of the HGAHE system and the pressure drop of the flow inside the pipe decrease by 37.7 % and 91.7 % respectively.

- Due to the spiral geometry, the pressure drop of the helical pipe was higher than that of the straight pipe. As an example, at Reynolds number of 200,000 the pressure drop increased about 116.9 % in the helical pipe.

- The backfill material has a significant influence on the thermal performance of the GAHE system. Using a backfill material of sandy loam with higher thermal effusivity compared to the silt loam, the heat exchange rate and effectiveness can significantly improve by 109.8 % and 105.3 %, respectively.

- The proposed model equation based on multiple regression, was in good agreement with the results of numerical model, confirming its ability to accurately predict the performance of the HGAHE system.

- The study findings suggested that the helical-coil pipe pattern can be used efficiently where area of land is insufficient for construction of longer tunnels. The main benefits of using the helical-coil pipe configuration are that it augments the heat exchange rate per unit area of operation and allows placing a much longer pipe into a smaller area. Hence, it has a significant potential to minimize the construction cost.

Recommendation and perspective

The research outcomes reported within the scope of the present thesis have highlighted several potential areas for future research works. Applying the findings of this study, the following suggestions for future developments have been identified.

- First and foremost, it is suggested that measured data from the experimental set up should be continued for the longest possible period. The value of the data-base will increase with time, thus, long-term behavior of the HGAHE system can be investigated at the monitoring site.

- If long-term experimental data and adequate simulation machines are available, a strong transient numerical model can be developed, which will allow for accurate long-term predictions and decision-making.

- The present study showed that the helical pipe layout of GAHE system could be effectively used for building cooling and heating applications. Moreover, the performance of HGAHE system can be enhanced by considering the obtained results from this work as a valuable guidance for the design of HGAHE systems.

- A detailed, comprehensive study may be carried out in future to look on the techno-economic analysis of using helical-coil pipe configuration as well as to investigate the thermal performance of HGAHE under optimized night purging duration and air flow velocity. A comprehensive study on the techno-economic analysis of using helical-coil pipe layout may be executed in future to assess the sustainability of this configuration for refreshing buildings in the Sahara of Algeria.

- There were some differences and fragmentation between the data given in the previous published papers on Algeria geothermal domain. This could lead to uncertainty and doubts about the reliability of sources of data, which is a common problem as elsewhere. We, thus, believe that the information in the presented Algeria geothermal energy review would help to decrease the contrast and gap in geothermal data of the country. Yet, valid documented sources for the country geothermal energy should be provided.

REFERENCES

1. Stocker, T.F., et al., Climate Change 2013: The Physical Science Basis. Contribution of Working Group I to the Fifth Assessment Report of the Intergovernmental Panel on Climate Change, 1535 pp. 2013, Cambridge Univ. Press, Cambridge, UK, and New York.

2. Pachauri, R.K., et al., Climate change 2014: synthesis report. Contribution of Working Groups I, II and III to the fifth assessment report of the Intergovernmental Panel on Climate Change. 2014: IPCC, Geneva, Switzerland, 151 pp.

3. REN21, Renewables 2018 global status report. renewable energy policy network for the 21st century. 2018, REN21 secretariat, Paris.

4. REN21, Renewables 2016 global status report. renewable energy policy network for the 21st century. REN21 secretariat, Paris, 2016.

5. Saiah, S.B.D. and A.B. Stambouli, Prospective analysis for a long-term optimal energy mix planning in Algeria: Towards high electricity generation security in 2062. Renewable and Sustainable Energy Reviews, 2017. 73: p. 26-43.

6. Dickson, M.H. and M. Fanelli, What is geothermal energy. Istituto di Geoscienze e Georisorse-CNR, Pisa, Italy, 2004.

7. Dickson, M.H. and M. Fanelli, Geothermal energy: utilization and technology. 2013: Routledge.

8. Hepbasli, A. and L. Ozgener, Development of geothermal energy utilization in Turkey: a review. Renewable and Sustainable Energy Reviews, 2004. 8(5): p. 433-460.

9. Hepburn, B.D.P., An investigation of the behaviour of the ground in response to energy extraction. PhD thesis. 2013, Cardiff University, Cardiff, UK.

10. Stefansson, V. World geothermal assessment. in Proceedings world geothermal congress. 2005.

11. Lund, J.W. and T.L. Boyd, Direct utilization of geothermal energy 2015 worldwide review. Geothermics, 2016. 60: p. 66-93.

12. Melikoglu, M., Geothermal energy in Turkey and around the World: A review of the literature and an analysis based on Turkey's Vision 2023 energy targets. Renewable and Sustainable Energy Reviews, 2017. 76: p. 485-492.

13. Bertani, R., Geothermal power generation in the world 2010–2014 update report. Geothermics, 2016. 60: p. 31-43.

14. Valdimarsson, P. Geothermal power plant cycles and main components. in Short course on geothermal drilling, resource development power plants. 2011.

15. DiPippo, R., Geothermal power plants: principles, applications, case studies and environmental impact. 2012: Butterworth-Heinemann.

16. Meng, N., et al., Techno-economic performance comparison of enhanced geothermal system with typical cycle configurations for combined heating and power. Energy Conversion and Management, 2020. 205: p. 112409.

17. Zarrouk, S.J. and H. Moon, Efficiency of geothermal power plants: A worldwide review. Geothermics, 2014. 51: p. 142-153.

18. Moya, D., O.C. Akinsipe, and P. Kaparaju, Various cycle configurations for geothermal power plants, in Thermodynamic Analysis and Optimization of Geothermal Power Plants. 2021, Elsevier. p. 3-15.

19. Moya, D., C. Aldás, and P. Kaparaju, Geothermal energy: Power plant technology and direct heat applications. Renewable and Sustainable Energy Reviews, 2018. 94: p. 889-901.

20. Gondal, I.A., S.A. Masood, and M. Amjad, Review of geothermal energy development efforts in Pakistan and way forward. Renewable and Sustainable Energy Reviews, 2017. 71: p. 687-696.

21. Somogyi, V., V. Sebestyén, and G. Nagy, Scientific achievements and regulation of shallow geothermal systems in six European countries–A review. Renewable and Sustainable Energy Reviews, 2017. 68: p. 934-952.

22. Noorollahi, Y., et al., The effects of ground heat exchanger parameters changes on geothermal heat pump performance–A review. Applied Thermal Engineering, 2018. 129: p. 1645-1658.

23. Agrawal, K.K., et al., The state of art on the applications, technology integration, and latest research trends of earth-air-heat exchanger system. Geothermics, 2019. 82: p. 34-50.

24. Stambouli, A.B., et al., A review on the renewable energy development in Algeria: current perspective, energy scenario and sustainability issues. Renewable and Sustainable Energy Reviews, 2012. 16(7): p. 4445-4460.

25. Saibi, H. Geothermal Resources in Algeria. in Proceedings of the 2015 World Geothermal Congress, Melbourne, Australia. 2015. International Geothermal Association, 10 p.

26. Energy, M.o., Renewable energies and energy efficiency development program in Algeria. Ministry of Energy. [Online: http://www.energy.gov.dz]. Algers, Algeria, 2011.

27. Energy, M.o., Renewable energies and energy efficiency development program in Algeria. Ministry of Energy. [Online: http://www.energy.gov.dz]. 2016, Algers, Algeria.

28. Abada, Z. and M. Bouharkat, Study of management strategy of energy resources in Algeria. Energy Reports, 2018. 4: p. 1-7.

29. Bouraiou, A., et al., Status of renewable energy potential and utilization in Algeria. Journal of Cleaner Production, 2020. 246: p. 119011.

30. Corner, R., H. Fersoy, and V. Crespi, Integrated agri-aquaculture in desert and arid lands-Learning from case studies from Algeria, Egypt and Oman. Vol. No. 1195. 2020: Fisheries and Aquaculture Circular.

31. Boudries, R. and R. Dizene, Potentialities of hydrogen production in Algeria. International Journal of Hydrogen Energy, 2008. 33(17): p. 4476-4487.

32. Ouali, S., et al., The exploitation of hydrogen sulfide for hydrogen production in geothermal areas. International Journal of Hydrogen Energy, 2011. 36(6): p. 4103-4109.

33. Gouareh, A., et al., GIS-based analysis of hydrogen production from geothermal electricity using CO2 as working fluid in Algeria. International Journal of Hydrogen Energy, 2015. 40(44): p. 15244-15253.

34. Bendaikha, W., S. Larbi, and M. Bouziane, Feasibility study of hybrid fuel cell and geothermal heat pump used for air conditioning in Algeria. International Journal of Hydrogen Energy, 2011. 36(6): p. 4253-4261.

35. Bendaikha, W. and S. Larbi, Hybrid fuel cell and geothermal resources for air-conditioning using an absorption chiller in Algeria. Energy Procedia, 2012. 28: p. 190-197.

36. Salhi, K., M. Korichi, and K.M. Ramadan, Thermodynamic and thermo-economic analysis of compression–absorption cascade refrigeration system using low-GWP HFO refrigerant powered by geothermal energy. International Journal of Refrigeration, 2018. 94: p. 214-229.

37. Mahmoudi, H., et al., Application of geothermal energy for heating and fresh water production in a brackish water greenhouse desalination unit: A case study from Algeria. Renewable and Sustainable Energy Reviews, 2010. 14(1): p. 512-517.

38. Saibi, H., Geothermal resources in Algeria. Renewable and Sustainable Energy Reviews, 2009. 13(9): p. 2544-2552.

39. Fekraoui, A. Geothermal activities in Algeria. in Proceedings of the 2010 World Geothermal Congress, Bali, Indonesia. 2010.

40. Ouali, S., Contribution à l'étude de quelques réservoirs géothermiques en Algérie. PhD thesis. 2015, University of Science and Technology Houari Boumedienne, USTHB, Algers, Algeria.

41. Bordoloi, N., et al., An intense review on the latest advancements of Earth Air Heat Exchangers. Renewable Sustainable Energy Reviews, 2018. 89: p. 261-280.

42. Agrawal, K.K., et al., A review on effect of geometrical, flow and soil properties on the performance of Earth air tunnel heat exchanger. Energy Buildings, 2018. 176: p. 120-138.

43. Yildiz, A., O. Ozgener, and L. Ozgener, Exergetic performance assessment of solar photovoltaic cell (PV) assisted earth to air heat exchanger (EAHE) system for solar greenhouse cooling. Energy Buildings, 2011. 43(11): p. 3154-3160.

44. Kaushal, M., Geothermal cooling/heating using ground heat exchanger for various experimental and analytical studies: Comprehensive review. Energy Buildings, 2017. 139: p. 634-652.

45. Ozgener, O., L. Ozgener, and D.Y. Goswami, Seven years energetic and exergetic monitoring for vertical and horizontal EAHE assisted agricultural building heating. Renewable Sustainable Energy Reviews, 2017. 80: p. 175-179.

46. Bisoniya, T.S., A. Kumar, and P. Baredar, Experimental and analytical studies of earth–air heat exchanger (EAHE) systems in India: a review. Renewable Sustainable Energy Reviews, 2013. 19: p. 238-246.

47. Agrawal, K.K., et al., Effect of different design aspects of pipe for earth air tunnel heat exchanger system: A state of art. International Journal of Green Energy, 2019. 16(8): p. 598-614.

48. Agrawal, K.K., et al., Computational Fluid Dynamics Simulation Based Comparison of Different Pipe Layouts in an EATHE System for Cooling Operation. Journal of Thermal Science Engineering Applications, 2019. 11(5).

49. Majumdar, M., Energy-efficient buildings in India. 2001: The Energy and Resources Institute (TERI).

50. Sharan, G., H. Prakash, and R. Jadhav, Performance of Greenhouse Coupled to Earth-Tube-Heat-Exchanger in Closed-Loop Mode. 2004.

51. Elminshawy, N.A., et al., Performance of PV panel coupled with geothermal air cooling system subjected to hot climatic. Applied Thermal Engineering, 2019. 148: p. 1-9.

52. Vidhi, R., D. Goswami, and E. Stefanakos, Parametric study of supercritical Rankine cycle and earth-air-heat-exchanger for low temperature power generation. Energy Procedia, 2014. 49: p. 1228-1237.

53. Vidhi, R., D.Y. Goswami, and E. Stefanakos, Supercritical Rankine cycle coupled with ground cooling for low temperature power generation. Energy Procedia, 2014. 57: p. 524-532.

54. Barakat, S., et al., Enhancement of gas turbine power output using earth to air heat exchanger (EAHE) cooling system. Energy conversion management, 2016. 111: p. 137-146.

55. Mathur, A., et al., CFD analysis of EATHE system under transient conditions for intermittent operation. Energy Buildings, 2015. 87: p. 37-44.

56. Mathur, A., et al., Transient effect of soil thermal diffusivity on performance of EATHE system. Energy Reports, 2015. 1: p. 17-21.

57. Kaushal, M., et al., Finite volume and response surface methodology based performance prediction and optimization of a hybrid earth to air tunnel heat exchanger. Energy Buildings, 2015. 104: p. 25-35.

58. Nazer-Nejad, M., M.R. Saffarian, and M. Behbahani-Nejad, Investigating the possibility of using the underground tunnel for air-conditioning in Tehran. Journal of the Brazilian Society of Mechanical Sciences Engineering, 2018. 40: p. 1-10.

59. Ralegaonkar, R., M. Kamath, and V. Dakwale, Design and development of geothermal cooling system for composite climatic zone in India. Journal of The Institution of Engineers : Series A, 2014. 95: p. 179-183.

60. Mathur, A., et al., Investigation of soil thermal saturation and recovery under intermittent and continuous operation of EATHE. Energy Buildings, 2015. 109: p. 291-303.

61. Mathur, A., A.K. Surana, and S. Mathur, Numerical investigation of the performance and soil temperature recovery of an EATHE system under intermittent operations. Renewable Energy, 2016. 95: p. 510-521.

62. Rouag, A., A. Benchabane, and C.-E. Mehdid, Thermal design of Earth-to-Air Heat Exchanger. Part I a new transient semi-analytical model for determining soil temperature. Journal of Cleaner Production, 2018. 182: p. 538-544.

63. Agrawal, K.K., et al., Experimental study to investigate the effect of water impregnation on thermal performance of earth air tunnel heat exchanger for summer cooling in hot and arid climate. Renewable Energy, 2018. 120: p. 255-265.

64. Agrawal, K.K., et al., Effect of soil moisture contents on thermal performance of earth-air-pipe heat exchanger for winter heating in arid climate: In situ measurement. Geothermics, 2019. 77: p. 12-23.

65. Agrawal, K.K., R. Misra, and G.D. Agrawal, Improving the thermal performance of ground air heat exchanger system using sand-bentonite (in dry and wet condition) as backfilling material. Renewable Energy, 2020. 146: p. 2008-2023.

66. Benrachi, N., et al., Numerical parametric study of a new earth-air heat exchanger configuration designed for hot and arid climates. International Journal of Green Energy, 2020. 17(2): p. 115-126.

67. Ramírez-Dávila, L., et al., Numerical study of earth-to-air heat exchanger for three different climates. Energy buildings, 2014. 76: p. 238-248.

68. Fazlikhani, F., H. Goudarzi, and E. Solgi, Numerical analysis of the efficiency of earth to air heat exchange systems in cold and hot-arid climates. Energy conversion management, 2017. 148: p. 78-89.

69. Menhoudj, S., et al., Study of the energy performance of an earth—Air heat exchanger for refreshing buildings in Algeria. Energy Buildings, 2018. 158: p. 1602-1612.

70. Amanowicz, Ł., Influence of geometrical parameters on the flow characteristics of multi-pipe earth-to-air heat exchangers–experimental and CFD investigations. Applied Energy, 2018. 226: p. 849-861.

71. Zeng, C., et al., Thermal and infrared camouflage performance of earth-air heat exchanger for cooling an underground diesel generator room for protective engineering. Sustainable Cities Society, 2019. 47: p. 101437.

72. Agrawal, K.K., et al., Thermal performance analysis of slinky-coil ground-air heat exchanger system with sand-bentonite as backfilling material. 2019. 202: p. 109351.

73. Yusof, T., et al., The thermal characteristics and performance of a ground heat exchanger for tropical climates. Renewable Energy, 2018. 121: p. 528-538.

74. Mathur, A., et al., Comparative study of straight and spiral earth air tunnel heat exchanger system operated in cooling and heating modes. Renewable Energy, 2017. 108: p. 474-487.

75. Ahmed, S., et al., Parametric study on thermal performance of horizontal earth pipe cooling system in summer. Energy Conversion Management, 2016. 114: p. 324-337.

76. Benhammou, M., B. Draoui, and M. Hamouda, Improvement of the summer cooling induced by an earth-to-air heat exchanger integrated in a residential building under hot and arid climate. Applied Energy, 2017. 208: p. 428-445.

77. Benhammou, M. and B. Draoui, Parametric study on thermal performance of earth-to-air heat exchanger used for cooling of buildings. Renewable Sustainable Energy Reviews, 2015. 44: p. 348-355.

78. Jamshidi, N. and N. Sadafi, An evaluation for spiral coil type earth-air heat exchanger at different climate conditions. Energy Sources, 2019: p. 1-18.

79. Liu, Z., et al., Numerical modeling and parametric study of a vertical earth-to-air heat exchanger system. Energy, 2019. 172: p. 220-231.

80. Mathur, A. and S. Kumar, Thermal performance and comfort assessment of U-shape and helical shape earth-air heat exchanger in India. Energy Built Environment, 2021.

81. Rana, M., M.M. Nuhash, and A.A. Bhuiyan, A CFD modelling for optimizing geometry parameters for improved performance using clean energy geothermal ground-to-air tunnel heat exchangers. Case Studies in Thermal Engineering, 2024. 53: p. 103867.

82. Boughanmi, H., et al., Evaluation of soil thermal potential under Tunisian climate using a new conic basket geothermal heat exchanger: Energy and exergy analysis. Applied Thermal Engineering, 2017. 113: p. 912-925.

83. Dehghan, B., Performance assessment of ground source heat pump system integrated with micro gas turbine: Waste heat recovery. Energy Conversion and Management, 2017. 152: p. 328-341.

84. Bezyan, B., S. Porkhial, and A.A. Mehrizi, 3-D simulation of heat transfer rate in geothermal pile-foundation heat exchangers with spiral pipe configuration. Applied Thermal Engineering, 2015. 87: p. 655-668.

85. Khezzani, B. and S. Bouchemal, Variations in groundwater levels and quality due to agricultural over-exploitation in an arid environment: the phreatic aquifer of the Souf oasis (Algerian Sahara). Environmental Earth Sciences, 2018. 77(4): p. 1-18.

86. Ghodbane, M., et al., A numerical simulation of a linear Fresnel solar reflector directed to produce steam for the power plant. Journal of Cleaner Production, 2019. 231: p. 494-508.

87. Jakhar, S., et al., Thermal performance investigation of earth air tunnel heat exchanger coupled with a solar air heating duct for northwestern India. Energy Buildings, 2015. 87: p. 360-369.

88. Belatrache, D., S. Bentouba, and M. Bourouis, Numerical analysis of earth air heat exchangers at operating conditions in arid climates. International journal of hydrogen energy, 2017. 42(13): p. 8898-8904.

89. Javadi, H., et al., Performance analysis of helical ground heat exchangers with different configurations. Applied Thermal Engineering, 2019. 154: p. 24-36.

90. Javadi, H., et al., Thermal analysis of a triple helix ground heat exchanger using numerical simulation and multiple linear regression. Geothermics, 2019. 81: p. 53-73.

91. Miyara, A., Thermal performance and pressure drop of spiral-tube ground heat exchangers for ground-source heat pump. Applied Thermal Engineering, 2015. 90: p. 630-637.

92. Ju, H., et al., Hydraulic performance of small bending radius helical coil-pipe. Journal of Nuclear Science Technology, 2001. 38(10): p. 826-831.

93. Rhinehart, R.R., Nonlinear regression modeling for engineering applications: modeling, model validation, and enabling design of experiments. 2016: John Wiley & Sons.

94. Rosiek, S., J. Alonso-Montesinos, and F. Batlles, Online 3-h forecasting of the power output from a BIPV system using satellite observations and ANN. International Journal of Electrical Power & Energy Systems, 2018. 99: p. 261-272.

95. Alcañiz, A., et al., Trends and gaps in photovoltaic power forecasting with machine learning. Energy Reports, 2023. 9: p. 447-471.

96. Gentle, J.E., W.K. Härdle, and Y. Mori, Springer Handbooks of Computational Statistics. 2012.

97. Pawlowski, A., et al. Application of time-series methods to disturbance estimation in predictive control problems. in 2010 IEEE International Symposium on Industrial Electronics. 2010. IEEE.

98. Holman, J.P. and W.J. Gajda, Experimental methods for engineers. vol. 2, McGrawHill, New York, 1994, 1994.

99. ANSYS, ANSYS Fluent theory guide. https://www.ansys.com.

100. Wendt, J.F., Computational fluid dynamics: an introduction. 2008: Springer Science & Business Media.

101. Blasius, H., Das Aehnlichkeitsgesetz bei Reibungsvorgängen in Flüssigkeiten, in Mitteilungen über Forschungsarbeiten auf dem Gebiete des Ingenieurwesens: insbesondere aus den Laboratorien der technischen Hochschulen. 1913, Springer Berlin Heidelberg: Berlin, Heidelberg. p. 1-41.

102. Xiao, Y., et al., Experimental study of two-phase frictional pressure drop of steam-water in helically coiled tubes with small coil diameters at high pressure. Applied Thermal Engineering, 2018. 132: p. 18-29.

103. Ju, H., et al., Hydraulic performance of small bending radius helical coil-pipe. Journal of Nuclear Science and Technology, 2001. 38(10): p. 826-831.

104. Schmidt, E.F., Wärmeübergang und druckverlust in rohrschlangen. Chemie Ingenieur Technik, 1967. 39(13): p. 781-789.

105. ANSYS, ANSYS Fluent Theory Guide. ANSYS Inc ed. 2018.

106. Bansal, V., et al., Transient effect of soil thermal conductivity and duration of operation on performance of Earth Air Tunnel Heat Exchanger. Applied Energy, 2013. 103: p. 1-11.

107. Misra, R., et al., Numerical investigation of dynamic interaction of earth Aair tunnel heat exchanger with surrounding soil during continuous and intermittent operation in winter. International Journal of Engineering Technology Science and Research, 2017. 4(3): p. 333-344.

108. Agrawal, K.K., R. Misra, and G.D. Agrawal, To study the effect of different parameters on the thermal performance of ground-air heat exchanger system: In situ measurement. Renewable Energy, 2020. 146: p. 2070-2083.

109. Misra, R., et al., Transient analysis based determination of derating factor for earth air tunnel heat exchanger in summer. Energy Buildings, 2013. 58: p. 103-110.

110. Misra, R., T.K. Aseri, and V. Bansal. CFD analysis of thermal influence zone of earth air tunnel heat exchanger under transient conditions. in Proceedings of BS2015: 14th Conference of International Building Performance Simulation Association, Hyderabad, India. 2015.

111. Al-Ajmi, F., D. Loveday, and V.I. Hanby, The cooling potential of earth–air heat exchangers for domestic buildings in a desert climate. Building and Environment, 2006. 41(3): p. 235-244.

112. Hacini, K., et al., Efficiency assessment of an earth-air heat exchanger system for passive cooling in three different regions: The Algerian case. FME Transactions, 2021. 49(4): p. 1035-1046.

113. Carotenuto, A., et al., Energy piles for ground source heat pump applications: comparison of heat transfer performance for different design and operating parameters. Applied Thermal Engineering, 2017. 124: p. 1492-1504.

114. Ouali, S., et al., Cartographie et caractérisation des ressources géothermiques de l'Algérie. Revue des Energies Renouvelables, 2018. 21(1): p. 54-61.

115. Bahri, F. and H. Saibi, Characterization, classification, and determination of drinkability of some Algerian thermal waters. Arabian Journal of Geosciences, 2011. 4(1-2): p. 207-219.

116. Kedaid, F.Z., Database on the geothermal resources of Algeria. Geothermics, 2007. 36(3): p. 265-275.

117. Fekraoui, A., Geothermal resources in Algeria and their possible use. Geothermics, 1988. 17(2-3): p. 515-519.

118. Saibi, H., et al., Progress of geothermal development in Algeria. Journal of the Geothermal Research Society of Japan, 2006. 28(4): p. 383-397.

119. Himri, Y., et al., Review and use of the Algerian renewable energy for sustainable development. Renewable and Sustainable Energy Reviews, 2009. 13(6-7): p. 1584-1591.

120. Bellache, O., et al. Geothermal heating of greenhouses in southern Algeria. in Proceedings of the World Geothermal Congress 1995, Florence, Italy. 1995.

121. Freeston, D.H., Direct uses of geothermal energy 1995. Geothermics, 1996. 25(2): p. 189-214.

122. Fekraoui, A. and M. Abouriche. Algeria country update report. in Proceedings of the World Geothermal Congress 1995, Florence, Italy. 1995.

123. Fekraoui, A. and F.Z. Kedaid. Geothermal resources and uses in Algeria: A country update report. in Proceedings of the World Geothermal Congress 2005, Antalya, Turkey. 2005.

124. Lund, J.W., D.H. Freeston, and T.L. Boyd, Direct application of geothermal energy: 2005 worldwide review. Geothermics, 2005. 34(6): p. 691-727.

125. Lund, J.W., D.H. Freeston, and T.L. Boyd, Direct utilization of geothermal energy 2010 worldwide review. Geothermics, 2011. 40(3): p. 159-180.

126. Lund, J.W. and D.H. Freeston, World-wide direct uses of geothermal energy 2000. Geothermics, 2001. 30(1): p. 29-68.

127. Moummi, N., et al., Le rafraîchissement par la géothermie: étude théorique et expérimentale dans le site de Biskra. Revue des Energies Renouvelables, 2010. 13(3): p. 399-406.

128. Lekhal, M.C., et al., Thermal performance of a residential house equipped with a combined system: A direct solar floor and an earth–air heat exchanger. Sustainable Cities and Society, 2018. 40: p. 534-545.

129. Benzaama, M., et al., Experimental and numerical analysis of the energy performance of a water/soil exchanger coupled to a cooling floor for North Africa. Geothermics, 2019. 80: p. 8-19.

130. Atia, A., et al., A Review of Studies on Geothermal Energy System Applied on Sub-Saharan Climate Regions. Water and Energy International, 2017. 60(5): p. 63-68.

131. Hadjadj, A., et al., Air Velocity Effect on Geothermal Helicoidally Water-Air Heat Exchanger under El Oued Climate-Algeria. Thermal Science Engineering Progress, 2020: p. 100548.

132. Sakhri, N., et al., Study of Heat and Mass Transfer Through an Earth to Air Heat Exchanger Equipped with Fan in South West of Algeria. International Journal of Heat and Technology, 2019. 37(3): p. 689-695.

APPENDICES

Appendix A

A review on geothermal energy use in Algeria

1. Geothermal locations

Table A1: Physicochemical data of some hot springs of northern Algeria [114, 115].

Hot spring	Province	Temp (°C)	TDS (mg/l)	Flow rate (l/s)	Water type
Ouled Aich unit	Batna	35	7143	4	Na-Cl
Sillel	Bejaia	46	2221	10	Na-Cl
Chegua	Biskra	50	6210	20	Na-Cl
Boughrara	Tlemcen	43	398	6.5	Mg-Cl
Charef	Djelfa	42	1670	38	Ca-Cl
Sidi Aisa	Saida	44.5	2502	5	Na-SO_4
Touansa	Medea	22	8970	5	Na-SO_4
Delaa	Msila	42	1980	25	Na-SO_4
Bouhanifia	Mascara	66	2012	23	Na-Cl
Sidi Trad	El Tarf	63	542	1.8	Na-Cl
Sidi Slimane	Tissemsilt	42	2374	5	Na-Cl
Elssalhine	Khenchela	70	2082	60	Na-Cl
Serghine	Tiaret	40	4400	12	Na-Cl
Righa	Ain Defla	68	2466	2.5	Ca-SO_4
Ksena	Bouira	60	3520	50	Na-Cl

Table A2: Physicochemical data of some drilled wells in southern Algeria [114].

Well name	Province	Temp (°C)	TDS (mg/l)	Flow rate (l/s)	Water type
H011-516	El Oued	65	1970	197	Na-SO_4
J0010-583	Ouargla	51	1620	120	Ca-SO_4
J0011-94	Ouargla	60	1760	150	Ca-SO_4
L011-11	Ouargla	48	3333	22	Na-SO_4
H008-59	Laghouat	34	2300	12	Ca-SO_4
I009-55	Ghardaia	41	1569	160	Na-Cl
G009-109	Biskra	53	2822	100	Ca-Cl

Table A3. Characteristics of geothermal regions in Algeria [33, 38, 40, 116].

Characteristics	North-West	North-East	South
Geological unit	Alpine Domain	Alpine Domain	Saharan Platform
Formation	Tlemcenian dolomites	Carbonate formations	Albian sandstone
Highest spring Temp (°C)	66	98	60
Reservoir depth (m)	500 – 1000	1000 – 3000	1000 – 2700
Average reservoir thickness (m)	500	700	600
Geothermal Gradient (°C/km)	25 – 43	30 – 60	30 – 50
Reservoir Temp (°C)	66 – 125	84 – 150	50 – 120
pH value	Near-neutral	Near-neutral	Near-neutral
Mean TDS (g/l)	0.4 – 4.1	0.6 – 2.2	1 – 3.5
Heat discharge (MW_t)	60	79	503

2. Literature review on geothermal energy development in Algeria

Table A4. Historical development of geothermal energy in Algeria.

Year	Notes	Ref.
Before 1962	• Geothermal springs were used only for bathing and swimming in the ancient Roman pools.	[117]
1967	• Geothermal exploration program was started-up by the national company Sonatrach.	[117, 118]
1978 - 1979	• The first geophysical prospection in the northeastern part of the country. • The first geothermal well was drilled in Guelma area.	[117]
1980 - 1982	• Geothermal exploration program was conducted focusing on the Constantinois Oriental area. • The national company Sonelgaz conducted geothermal identification studies in the eastern and northern regions of the country. • An inventory of more than 200 hot springs was counted in Algeria.	[118, 119]
1983	• Geothermal resources activities have been continued by the Algerian Centre of Renewable Energies Development and the program has been extended to the entire northern part of the country	[118]
1992	• The first installation of greenhouse heating system for 18 greenhouses with a total area of 7,200 m^2 using the Albian geothermal water in Ouargla and Touggourt regions.	[120, 121]
1995	• Updated inventory with more than 240 identified thermal springs in the country.	[121, 122]
2005	• An investigation was carried out through the recorded 240 hot springs and all were identified as low enthalpy resources with maximum reservoir temperature of 120 °C. • Geothermal space heating was first installed in Hammam Bouhnifia and Hammam Meskhoutine.	[123, 124]
2008	• The first fish farms were installed in Saida, Ouargla and Ghardaia locations.	[39, 125]
2010	• The first residential geothermal heat pump system was installed in a primary school of Saida city. • Starting the installation of the first binary cycle power plant in Guelma region.	[39, 125]
2015	• The first air conditioning system was installed in Algeria.	[11, 25]
2018	• The updated inventory identified more than 282 hot springs in the country.	[114]

Table A5. The share of various categories of direct-use geothermal capacity in Algeria for the period 1995–2015.

Capacity, MW_t	2015	2010	2005	2000	1995
Bathing and swimming	44.37	55.47	60.9	97.7	97.7
Greenhouse heating	0	0	2.3	2.3	2.3
Space heating	1	1.4	0.1	0	0
Fish farming	9.02	9.8	0	0	0
Heat pumps	0.17	0.17	0	0	0
Air conditioning	0.08	0	0	0	0
Total	54.64	66.84	63.3	100	100
Ref.	[11]	[125]	[124]	[126]	[121]

3. Geothermal energy utilization in Algeria

Table A6. Main characteristics of the major spas [25, 39, 123].

Spas	T (°C)	TDS (mg/l)	Flow rate (l/s)	Therapeutic utilization
Meskhoutine	98	1600	80	Rheumatism, neurology, breath, arthritis
Guergour	44	3543	30	Rheumatism, arthritis
Bouhanifia	68	1400	9	Rheumatism, arthritis, digestive
Bouhadjar	65	3100	10	Rheumatism, neurology, digestive, arthritis
Boughrara	37	398	7	Rheumatism, urology, arthritis
Righa	68	2400	8	Rheumatism, arthritis
Chiguer	35	3200	5	Rheumatism, arthritis
Elssalhine	43	2082	65	Rheumatism, arthritis, skin treatment
Zalfana	42	1650	–	Rheumatism, neurology, breath, arthritis

Table A7. Characteristics of the geothermal heat exchangers installed for studies in Algerian universities.

Location	Year built	System technical specification	Ref.
Biskra	2010	Earth to air horizontal heat exchanger; pipe length: 60 m; material: PVC; burial depth: 3 m; pipe diameter: 0.11 m.	[127]
Oran	2013	Earth to air horizontal heat exchanger; pipe length: 120 m; material: zinc; burial depth: 3 m; pipe diameter: 0.12 m.	[128]
Oran	2014	Water to soil heat exchanger coupled with a cooling floor; the system consists of two galvanized steel water tanks with a volume of 2 m^3 each and located at a 2 m shallow depth.	[129]
Oran	2015	Two earth to air horizontal heat exchangers, first one with zinc material and second one with PVC material, both exchangers have the same configuration; pipe length: 20 m; burial depth: 2 m; pipe diameter: 0.12 m.	[69]
El Oued	2017	Water to air helical heat exchanger; pipe length: 30 m; burial depth: from 2 to 5 m.	[130, 131]
Bechar	2018	Earth to air heat exchanger; pipe length: 66 m; material: PVC; burial depth: 1.5 m; pipe diameter: 0.11 m.	[132]

Table A8. Geothermal water used for fish farming in Algeria [25].

Geothermal source	Flow rate (l/s)	Inlet T (°C)	Outlet T (°C)
Ain Skhouna hot spring	60	31	20
Ghardaia well	150	28	18
Ouargla well	44	21	17

4. Concluding remarks

Algeria has relatively abundant geothermal resources of low-enthalpy type that are feasible for direct use applications, thus provides a clean energy alternative for reducing fossil fuel dependence and its negative impact on the environment. Algeria is the leading country in the direct utilization of geothermal energy in Africa, as well as among the top five countries in the world for space cooling application. The main findings derived from this review can be summarized as follows:

- Three main geothermal areas have been delineated according to several parameters such as the geological and geophysical considerations where the overall heat discharge was evaluated at 642 MW_t.
- Geothermal water temperatures are in the range of 20–98 °C, demonstrating a significant potential for various geothermal energy applications.
- Based upon the current status, just few geothermal energy applications are used in the country. There are many applications can be realized in Algeria to improve the geothermal energy utilization such as greenhouse heating, industrial processes, drying and snow melting.
- Geothermal area in the Sahara region known as Albian aquifer represents a large potential for the development of different agricultural production.
- Despite the several studies that confirmed and proven technically and economically the feasibility of the GSHPs installation in Algeria, this application is still very limited in the country which represents just 0.31 % from the total geothermal power utilization. However, at the international level, GSHPs have the largest installed capacity worldwide with about 71 % of the installed capacity.
- The helical geothermal heat exchanger configuration provides the highest response in heat exchange rate per unit of application area and its shape allows to decrease the surface of installation. Also, thermal conductivity of backfilling materials can be increased by cement and sand–bentonite mixtures. Hence, these findings can be implemented in the country to enhance the performance of the GSHP
- From the conducted review of the latest technologies of geothermal energy around the world, it is concluded that the Binary Organic Ranking Cycle power plants and advanced geothermal energy conversion systems – hybrid configurations are the most appropriate

technologies for power generation from low-enthalpy geothermal resources such as those in Algeria.

- Advanced geothermal energy technologies for low enthalpy reservoirs are well developed and utilized in Europe and the USA. Thus, similarly to Europe and the USA, massive applications of the advanced technologies are highly recommended in Algeria.
- Algeria has numerous abandoned oil and gas fields, therefore advanced geothermal energy conversion systems – hybrid configurations are recommended for power generation.
- The development of geothermal energy in Algeria is not fast enough due to factors such as laws, regulations and policies, as well as lack of governmental support. If laws and regulations become effective and policy mechanism put in place, the geothermal energy development can rapidly speed up in the country.
- There were some differences and fragmentation between the data given in the previous published papers on Algeria geothermal domain. This could lead to uncertainty and doubts about the reliability of sources of data, which is a common problem as elsewhere. We, thus, believe that the information in this review would help to decrease the contrast and gap in geothermal data of the country. Yet, valid documented sources for geothermal energy should be provided.
- In conclusion, geothermal energy is a clean, reliable and environmentally friendly source, which can contribute to social sustainable development and help to protect the global environment. Therefore, government initiatives and efforts are important to emphasize and encourage the exploration, exploitation and development of geothermal resources in the country.

Appendix B

1. Experimental location

Figure B1: Location of the experimental area.

2. Error analysis of second experiment

The uncertainties in experimentation are conducted to estimate potential error associated using various instruments during experimental measurements, which can be determined by the fraction of the measurement device lowest count and minimal parameter reported rate [98]. In this research work, the uncertainties in the experiment are evaluated, the least recorded values for temperature and velocity are 24 °C (i.e. the lowest soil temperature throughout the depth of the borehole while evaluating the mean soil temperature) and 10 m s^{-1}, respectively. Lowest count of measurement devices of temperature and velocity are 0.1 °C and 0.1 m s^{-1}, respectively. Therefore, maximum error in temperature of air and flow velocity measurement is estimated as ± 0.41 % and ±1.0 %, respectively.

3. Mesh schematic of the parametric study model

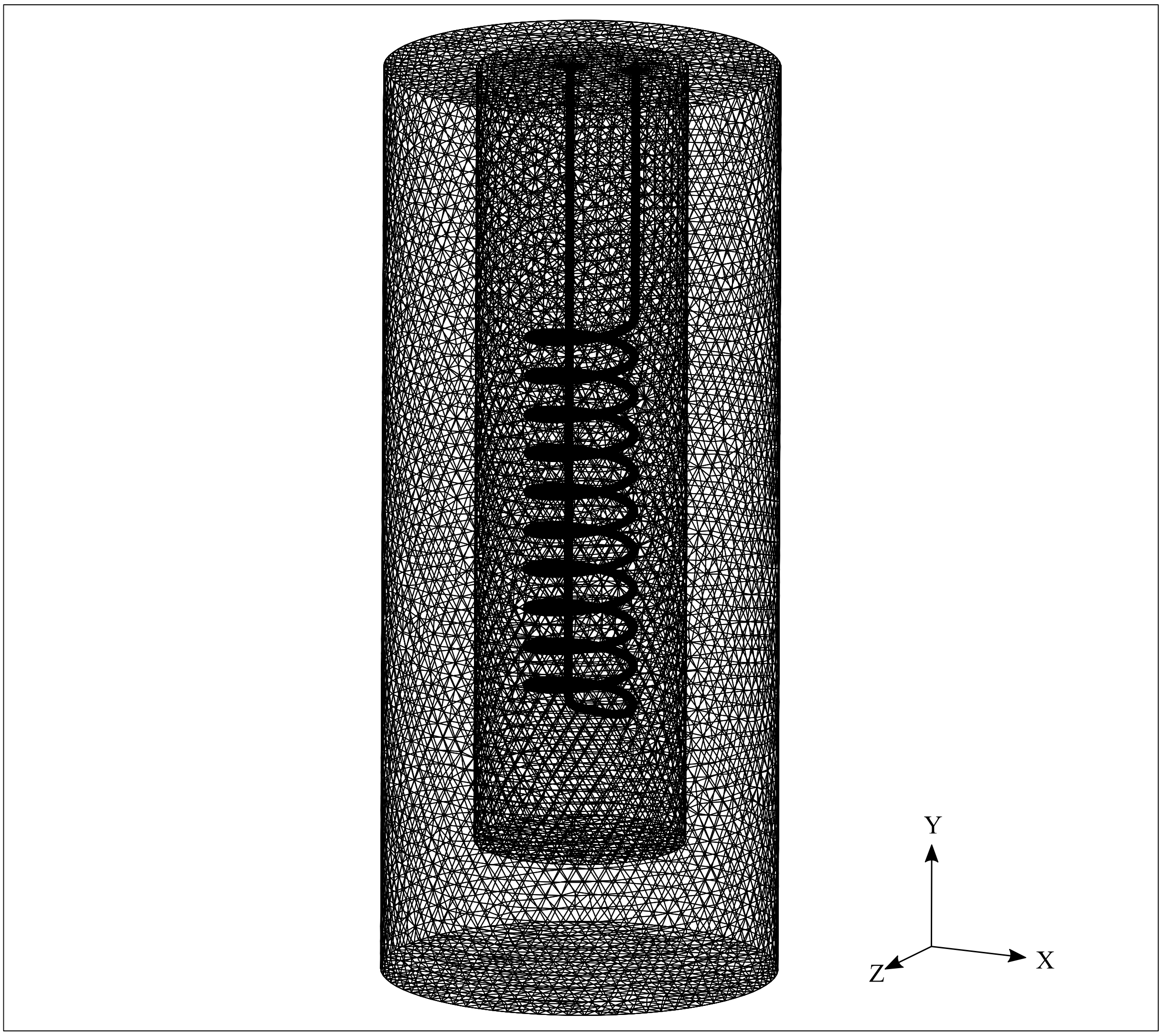

Figure B2: Mesh schematic of the HGAHE system.

Appendix C

Scientific production

- **Publication**

1. Lebbihiat N, Atia A, Arıcı M, Meneceur N. "Geothermal energy use in Algeria: A review on the current status compared to the worldwide, utilization opportunities and countermeasures". Journal of Cleaner Production, 2021: p. 126950.

2. Lebbihiat, N., Atia A, Arıcı M, Meneceur N, Hadjadj A, Chetiuoi Y. "Thermal performance analysis of helical ground-air heat exchanger under hot climate: In situ measurement and numerical simulation". Energy Journal, 2022: p. 124429.

3. Lebbihiat, N., Atia A, Arıcı M, Meneceur N. "Thermal performance of helical ground air heat exchanger under Saharan climate conditions: an experimental study". Journal of Thermal Analysis Calorimetry, 2023: p. 1-13.

4. Hadjadj A, Benhaoua B, Atia A, Khechekhouche A, Lebbihiat N, Rouag A. " Air Velocity Effect on Geothermal Helicoidally Water-Air Heat Exchanger under El Oued Climate -Algeria". Thermal Science and Engineering Progress Journal, 100548, 2020.

5. Keddouda, A., Ihaddadene R, Boukhari A, Atia A, Arıcı M, Lebbihiat N, Ihaddadene R. "Solar photovoltaic power prediction using artificial neural network and multiple regression considering ambient and operating conditions". Energy Conversion Management, 2023. 288: p. 117186.

- **International communication**

1. Lebbihiat N, Atia A, Keddouda A, Menaceur N, " Thermal performance evaluation of spiral earth-air heat exchanger for summer cooling" 1st International Conference on Optoelectronic, Materials & Renewable Energy ICOMRE'22, El Oued December 2022.

2. Lebbihiat N, Atia A, Menaceur N, " Experimental and numerical analysis of helical geothermal heat exchanger operating in hot climates" International Pluridisciplinary PhD Meeting (IPPM'20) 1st Edition «IPPM-20», El Oued Février 2020.

3. Lebbihiat N, Atia A, Hadjaj A, " Geothermal energy development and future possible applications in Algeria" International Symposium on Technology & Sustainable Industry Development «ISTSID-19», El Oued Février 2019.

4. Lebbihiat N, " Modeling and Optimization of Geothermal Heat Exchanger Performances under Sub-Saharan Climate Region -Algeria-". Successful participation in "My Thesis in 200 s Competition". International Symposium on Technology & Sustainable Industry Development «ISTSID-19», El Oued Février 2019.

- **National communication**

1. Lebbihiat N, Atia A, Hadjaj A, Guerrah A, Megdoud S, Chtioui Y, "Exploitation de l'Énergie Géothermique au Niveau de la Région d'El Oued" Séminaire national sur la technologie des matériaux et applications «SNTMA-18», El Oued Février 2018.

2. Lebbihiat N, Atia A, " Modeling and Optimization of Geothermal Heat Exchanger Performances under Sub-Saharan Climate Region -Algeria-" Les premiers Journées Doctorial de la faculté de Technologie sur La Méthodologie d'Elaboration d'une Thèse et d'une Publication en Doctorat «METPD-18», Mars 2018.

Thème de Thèse: Modélisation et optimisation de performance de l'échangeur de chaleur géothermique sous le climat de la région subsaharienne - Algérie -

Résumé

L'échangeur de chaleur air sol (GAHE) système géothermique est couramment utilisé pour exploiter l'énergie propre et renouvelable pour le refroidissement et le chauffage des bâtiments. Dans cette étude, une revue de la littérature sur les pratiques et les technologies de l'énergie géothermique en Algérie et dans le monde entier a été menée. Ainsi, des contre-mesures et des solutions pour promouvoir le développement et l'utilisation de l'énergie géothermique dans le pays sont abordées. De plus, selon la littérature, la configuration hélicoïdale du GAHE nécessite un espace au sol limité et une longueur de tranchée moindre pour l'installation de longs tuyaux. Par conséquent, les performances thermiques de l'échangeur air sol hélicoïdal (HGAHE) ont été analysées expérimentalement dans des conditions climatiques sahariennes pendant la saison estivale. Un tuyau flexible en PVC d'un diamètre de 0,06 m et d'une longueur de 30 m a été disposé selon une disposition en hélice pour concevoir le HGAHE et il est inséré dans un puits de 5 m de profondeur. De plus, un modèle numérique transitoire a été développé et validé par rapport aux données expérimentales pour étudier la pénétration de la chaleur dans le puits. De plus, le modèle numérique a également été utilisé pour étudier l'impact de différents paramètres opérationnels et géométriques importants. Les résultats expérimentaux ont montré que le facteur de dégradation des performances thermiques (TPDF) augmente avec l'augmentation du temps de fonctionnement et de la vitesse de l'air. Après 3 heures de fonctionnement, le TPDF le plus élevé est atteint à 0,27 avec une vitesse de 20 m s^{-1}, tandis que le TPDF le plus bas est observé à 0,14 pour une vitesse de 10 m s^{-1}. Les résultats numériques ont révélé que la distribution de la température du puits dans la direction radiale diminue rapidement avec la distance par rapport à la surface du tuyau. De plus, l'étude paramétrique a indiqué que le diamètre hélicoïdal, la température d'entrée et la vitesse de ventilation sont les paramètres les plus efficaces, tandis que le diamètre du tuyau et le pas hélicoïdal ont un impact modéré sur les performances thermiques du système HGAHE. En outre, l'augmentation de l'effusivité thermique du matériau de remplissage peut améliorer le taux de transfert de chaleur et l'efficacité du système. En plus des résultats numériques, une méthode de régression multiple a été utilisée pour proposer un modèle efficace pour prédire le comportement thermique du système HGAHE.

Mots clés : Énergie géothermique, Taux de transfert de chaleur, Efficacité, CFD, Système HGAHE, Climat saharien.

عنوان الأطروحة: نمذجة وتحسين أداء المبادل الحراري الأرضي تحت ظروف المناخ الصحراوي – الجزائر –

ملخص

نظام التبادل الحراري هواء أرض (GAHE) المعروف أيضًا بنظام الطاقة الجيوحرارية يستخدم بشكل شائع لاستغلال الطاقة النظيفة والمتجددة لتبريد وتدفئة المباني. في هذه الدراسة، تم إجراء إستعراض للمراجع حول ممارسات وتقنيات الطاقة الجيوحرارية في الجزائر وحول العالم. وبالتالي، تم التطرق إلى التدابير والحلول لتعزيز تطوير واستخدام الطاقة الجيوحرارية في البلاد. علاوة على ذلك، وفقًا للمراجع، فإن الشكل اللولبي لنظام GAHE يتطلب مساحة أرض محدودة وطول خندق أقل لتثبيت الأنابيب الطويلة. لذلك، تم تحليل الأداء الحراري لنظام التبادل الحراري هواء أرض اللولبي (HGAHE) تجريبيًا تحت ظروف المناخ الصحراوي خلال فصل الصيف. تم ترتيب أنبوب PVC مرن بقطر 0.06 متر وطول 30 متر على شكل لفائف لتصميم HGAHE وتم إدخاله في بئر بعمق 5 أمتار. بالإضافة إلى ذلك، تم تطوير نموذج عددي إعتمادا على البيانات التجريبية لفحص إنتشار الحرارة في البئر. علاوة على ذلك، تم استخدام النموذج العددي أيضًا للتحقيق في تأثير مختلف العوامل التشغيلية والهندسية الهامة. تشير النتائج التجريبية إلى أن معامل تقليل الأداء الحراري (TPDF) يزيد مع زيادة وقت التشغيل وسرعة الهواء. بعد 3 ساعات من وقت التشغيل، تم الحصول على أعلى TPDF بواقع 0.27 مع سرعة 20 مترًا في الثانية، في حين يُلاحظ أدنى TPDF تم الحصول عليه هو 0.14 بسرعة 10 مترًا في الثانية. كشفت النتائج العددية عن أن توزيع حرارة البئر في الاتجاه الشعاعي ينخفض بسرعة مع البعد عن سطح الأنبوب. بالإضافة إلى ذلك، أشارت الدراسة الإحصائية إلى أن القطر اللولبي ودرجة الحرارة الداخلة وسرعة الهواء هي العوامل الأكثر فعالية، في حين أن قطر الأنبوب والمسافة بين لفتين له تأثير معتدل على الأداء الحراري لنظام HGAHE. وعلاوة على ذلك، يمكن زيادة الفاعلية الحرارية لمواد التعبئة الخلفية لتعزيز معدل تبادل الحرارة وفعالية النظام. جنبًا إلى جنب مع النتائج العددية، تم استخدام طريقة الانحدار المتعدد لاقتراح نموذج فعال لتنبؤ السلوك الحراري لنظام HGAHE.

كلمات مفتاحية : الطاقة الجيوحرارية، معدل تبادل الحرارة، الفاعلية، ديناميكا الموائع العددية، نظام HGAHE، مناخ صحراوي.

Thesis Title: Modeling and optimization of geothermal heat exchanger performance under Sub-Saharan climate region - Algeria -

Abstract

The ground air heat exchanger (GAHE) geothermal system is commonly used to exploit clean and renewable energy for cooling and heating buildings. In this study, literature review on the geothermal energy practices and technologies in Algeria and around the globe has been conducted. Thus, countermeasures and solutions to promote the development and utilization of geothermal energy in the country are addressed. Furthermore, according to the literature the helical configuration of GAHE requires a limited ground space and lesser trench length for installing long pipes. Therefore, thermal performance of helical ground air heat exchanger (HGAHE) has been experimentally analyzed under Saharan climate conditions during summer season. A flexible PVC pipe with a diameter of 0.06 m and a length of 30 m has been arranged as a helical-coil layout to design the HGAHE and it is inserted into a borehole of 5 m depth. Besides, a transient numerical model has been developed and validated against the experimental data to investigate the heat penetration into the borehole. Moreover, the numerical model has also been employed to investigate the impact of different important operating and geometric parameters. The experimental finding acknowledged that, thermal performance derating factor (TPDF) increments with increasing the operation time and air velocity. After 3 hours of operation time, the highest TPDF is attained as 0.27 with a velocity of 20 m s^{-1}, whereas the lowest TPDF is observed as 0.14 for a velocity of 10 m s^{-1}. Numerical results revealed that, the borehole temperature distribution in the radial direction decreases rapidly with the distance away from the pipe surface. In addition, the parametric study indicated that, the helical diameter, inlet temperature and ventilation velocity are the most effective parameters, whereas the pipe diameter and pitch size have a moderate impact on thermal performance of the HGAHE system. Furthermore, increasing the thermal effusivity of backfill material can enhance the heat exchange rate and effectiveness of the system. Along with the numerical results, multiple regression method has been used to propose effective model to predict thermal behavior of the HGAHE system.

Keywords: Geothermal energy, Heat exchange rate, Effectiveness, CFD, HGAHE system, Saharan climate.

Journal of Cleaner Production 302 (2021) 126950

Contents lists available at ScienceDirect

Journal of Cleaner Production

journal homepage: www.elsevier.com/locate/jclepro

Review

Geothermal energy use in Algeria: A review on the current status compared to the worldwide, utilization opportunities and countermeasures

Nacer Lebbihiat [a, *], Abdelmalek Atia [a], Müslüm Arıcı [b], Noureddine Meneceur [a]

[a] University of El Oued, LEVRES Laboratory, Faculty of Technology, 39000, El Oued, Algeria
[b] Kocaeli University, Engineering Faculty, Mechanical Engineering Department, 41001, Kocaeli, Turkey

ARTICLE INFO

Article history:
Received 26 June 2020
Received in revised form
20 March 2021
Accepted 30 March 2021
Available online 2 April 2021

Handling editor: Mingzhou Jin

Keywords:
Algeria
Geothermal energy
Current status
Sustainable development
Renewable energy
Heat pump

ABSTRACT

The main objective of this review paper is to present the historical development, current utilization, practices and opportunities of geothermal energy in Algeria. Algeria has relatively abundant geothermal resources of low-enthalpy type that could form part of the total energy network of the country. Algeria is the leading country of the direct use of geothermal energy in Africa with a total amount reaching 54.64 MW_t installed thermal power, and also among the first five countries in the world in air conditioning application. The main utilization field of geothermal energy in Algeria is balneology, which accounts for about 82% of the total geothermal power utilization, the remaining 18% of the energy is consumed for other purposes such as space heating, heat pumps and fish farming. In this study, the existing literature and current practices of the Algeria's geothermal resources are reviewed and it is revealed that geothermal energy development remained almost stagnant over the past two decades in Algeria although there is a large potential and resources available in the country. Furthermore, geothermal energy use and latest technologies around the world have been summarized. This study elucidates the influencing factors in the development of geothermal energy in Algeria and suggests the development roadmap and a number of measures that can enhance the development of this significant energy source.

Contents

* Corresponding author.
E-mail address: lebbihiat-nacer@univ-eloued.dz (N. Lebbihiat).

https://doi.org/10.1016/j.jclepro.2021.126950
0959-6526/

Energy 254 (2022) 124429

Contents lists available at ScienceDirect

Energy

journal homepage: www.elsevier.com/locate/energy

Thermal performance analysis of helical ground-air heat exchanger under hot climate: In situ measurement and numerical simulation

Nacer Lebbihiat [a,*], Abdelmalek Atia [a], Müslüm Arıcı [b], Noureddine Meneceur [a], Abdessamia Hadjadj [a], Youcef Chetioui [a]

[a] University of El Oued, LEVRES Laboratory, Faculty of Technology, 39000, El Oued, Algeria
[b] Kocaeli University, Engineering Faculty, Mechanical Engineering Department, 41001, Kocaeli, Turkey

A R T I C L E I N F O

Article history:
Received 23 December 2021
Received in revised form
23 April 2022
Accepted 30 May 2022
Available online 1 June 2022

Keywords:
HGAHE system
Heat exchange rate
Cooling
Borehole temperature
Transient thermal performance
Arid climate

A B S T R A C T

The ground air heat exchanger (GAHE) is a promising passive approach for cooling and heating buildings. In this study, thermal performance of helical ground air heat exchanger (HGAHE) has been experimentally assessed in summer season for arid climate. The findings revealed that, the outlet air temperature of the HGAHE is strongly dependent on the inlet air temperature. Furthermore, the air temperature drop and the heat exchange rate as high as 13.3 °C and 463.4 W respectively, are attained at the highest inlet temperature of 41.0 °C. Besides, a transient numerical model was established and validated through the experimental data to investigate the heat penetration into the borehole. The results acknowledge that, the borehole temperature distribution in axial direction is higher at the upper surface and then decreases with the HGAHE length. In the other hand, the borehole temperature distribution in the radial direction reduces rapidly with the distance away from the pipe surface. Moreover, when the ambient air temperature during the night shift is lower than the borehole temperature, the forced convection which helps to take the heat away via purge air circulating into the HGAHE pipe allowed the borehole to restore its cooling ability.

1. Introduction

The worldwide total population growth along with the annual raise in the energy usage, as well as the global warming generated from burning of fossil fuel resources, calls for more efficient energy use and leads to sustainable development. In this context, renewable resources appeared to be one of the most energy efficient and productive alternatives [1,2]. In recent years, attempts have been made to establish alternative sources of energy to supply the building's cooling and heating needs. One of the best possible solutions as alternative energy is to utilize geothermal resources, which is classified as one of the world's most efficient and effective sustainable energy. It is green, renewable, appropriate for energy storage and accessible throughout the day. Geothermal energy could be harnessed via the earth air heat exchanger systems (EAHE) [3].

Ground air heat exchanger (GAHE) can be deployed to cool or warm air for building air conditioning, therefore decreasing the energy requirement for ventilation purposes passively and contribute in more cleaner built environment. The GAHEs use the earth's undisturbed temperature as a heat source. When air passes across the ducts, thermal energy is transmitted from air to ground or from ground to air depends to the air temperature relative to the soil temperature which remains more than the outdoor air temperature during winter, and lower in summer, for air heating/cooling based on the seasonal energy needs [4,5]. Many researchers have conducted experimental or numerical modeling analysis to access the thermal efficiency of GAHE systems. Mihalakakou [6] assessed the efficiency of EAHE device experimentally as well as via mathematical modeling. Al-Ajmi et al. [7] investigated the cooling capability of GAHE for buildings air conditioning under Saharan climate. Givoni [8] evaluated the potential of the EAHE system under arid climate. Findings revealed that, the system could be improved by using different ground cooling techniques to decrease the natural underground temperature such as shading and surface treatment with pebbles and plants.

Bansal et al. [9,10] analyzed the performance of EAHE connected to a room and showed that the change in EAHE tube material has

* Corresponding author.
E-mail address: lebbihiat-nacer@univ-eloued.dz (N. Lebbihiat).

https://doi.org/10.1016/j.energy.2022.124429
0360-5442/

Journal of Thermal Analysis and Calorimetry (2023) 148:5819–5831
https://doi.org/10.1007/s10973-023-12085-5

Thermal performance of helical ground air heat exchanger under Saharan climate conditions: an experimental study

Nacer Lebbihiat[1] · **Abdelmalek Atia**[1] · **Müslüm Arıcı**[2] · **Noureddine Meneceur**[1]

Received: 4 April 2022 / Accepted: 12 March 2023 / Published online: 9 April 2023

Abstract

In the present research paper, the thermal performance of helical ground air heat exchanger (HGAHE) has been experimentally analyzed under Saharan climate conditions during summer season. A flexible PVC pipe with a diameter of 0.06 m and a length of 30 m has been arranged as a helical-coil layout to design the HGAHE, and it is inserted into a borehole of 5 m depth. The study acknowledges that a drop as high as 11.0 °C in air temperature can be achieved with an air velocity of 10 m s^{-1} and an inlet air temperature of 38 °C. The study also revealed that, by incrementing the air velocity from 10 to 20 m s^{-1}, the heat exchange rate of the HGAHE system increases by 158% after 3 h of operation time; however, the efficiency of the HGAHE decreases by 21.51%. Moreover, thermal performance derating factor (TPDF) increments with increasing the operation time and air velocity. After 3 h of operation time, the highest TPDF is attained as 0.27 with a velocity of 20 m s^{-1}, whereas the lowest TPDF is observed as 0.14 for a velocity of 10 m s^{-1}.

Keywords HGAHE · Helical pipe · Heat exchange rate · Effectiveness · Cooling · Saharan climate

List of symbols

A	Surface area, m^2
C_p	Air specific heat, J kg^{-1} K^{-1}
E	Effectiveness
ρ	Density, kg m^{-3}
d	Pipe diameter, m
D	HGAHE diameter, m
f	Friction factor
f_c	Friction factor for curved pipe
f_s	Friction factor for straight pipe
L	Length of PVC pipe, m
$\dot{m}$	Air mass flow rate, kg s^{-1}
ΔP	Pressure drop, Pa
$\dot{Q}$	Heat exchange rate, W
R	Total thermal resistance, °C m W^{-1}
Re	Reynolds number
T	Temperature, °C
U	Overall heat transfer coefficient, W m^{-2} °C^{-1}
V	Airflow velocity, m s^{-1}
Z	HGAHE depth, m

Subscripts

act	Actual
avg	Average
h	Hour
i	Inlet
max	Maximum
s	Soil
o	Outlet

Abbreviations

CFD	Computational fluid dynamics
EAHE	Earth air heat exchanger
EPAHE	Earth pipe air heat exchanger
GAHE	Ground air heat exchanger
GHE	Ground heat exchanger
HGAHE	Helical ground air heat exchanger
TPDF	Thermal performance derating factor

✉ Nacer Lebbihiat
lebbihiat-nacer@univ-eloued.dz

1 LEVRES Laboratory, Faculty of Technology, University of El Oued, 39000 El Oued, Algeria

2 Mechanical Engineering Department, Engineering Faculty, Kocaeli University, 41001 Kocaeli, Turkey

Introduction

Nowadays, discussions on global warming, energy security, depletion of fossil fuels at a higher rate and economic growth call for a more sustainable development to reduce the energy usage and pollution rates in the buildings sector [1,

Thermal Science and Engineering Progress 20 (2020) 100548

Contents lists available at ScienceDirect

Thermal Science and Engineering Progress

journal homepage: www.elsevier.com/locate/tsep

Air velocity effect on the performance of geothermal helicoidally water-air heat exchanger under El Oued climate, Algeria

Abdessamia Hadjadj[a,*], Boubaker Benhaoua[a,b], Abdelmalek Atia[c], Abderrahmane Khechekhouche[a,b], Nacer Lebbihiat[c], Amar Rouag[d]

[a] University of El Oued, VTRS Laboratory, 39000 El Oued, Algeria
[b] University of El Oued, UDERZA Unit, 39000 El Oued, Algeria
[c] University of El Oued, LEVRES Laboratory, 39000 El Oued, Algeria
[d] University of Ouargla, LENREZA Laboratory, 30000 Ouargla, Algeria

ARTICLE INFO

Keywords:
Air velocity
Geothermal energy
Thermal efficiency
Water well
Water–air helical heat exchanger

ABSTRACT

This paper investigates experimentally the effect of air velocity on the performance of a water–air helical heat exchanger (HWAHE) in the region of El-Oued, located in the southeast of Algeria. The HWAHE made of PVC piping with 30 m of length and 0.06 m of diameter was immersed into the bottom of a water well at 5 m depth. In addition, a theoretical model was developed to determine the evolution of the air temperature inside the HWAHE as function of the main operating parameters. Results showed that the maximum heat exchange reached nearly 418 W at 10 m/s of air velocity while the maximum of temperature gap between the inlet and the outlet air was 14.1 °C. The HWAHE efficiency decreased with the increase of the air velocity. The efficiency of heat exchanger was obtained to be 82%, 81% and 80% for the average velocity value of 10, 15 and 20 m/s, respectively. According to the obtained results, the HWAHE presented in this paper may be used for cooling and heating of buildings or greenhouses in the southeastern Algeria.

1. Introduction

Algeria has a great potential for renewable energy including geothermal energy, which can be utilized to provide space heating/cooling and even electricity [1–3]. The achievement of indoor thermal comfort and the minimizing energy consumption in buildings are a key challenge in desert climates [4,5]. The geothermal energy system is an environmentally friendly and inexpensive technique that is influenced by the temperature difference T_{in} and T_{out} at the level of the PVC pipe or the heat exchanger. Like any other energy system, the geothermal energy also is influenced by the solar energy [6,7]. Many studies noted that beyond 3 m depth, the temperature can be considered almost constant [8–10]. In the studies of [11–14], numerical simulations and experimentations were performed, and different parameters such as air flow, depth of burial, length and diameter were taken in consideration to calculate the energy performance of earth air heat exchanger (EAHE). The performance of a conventional air/water heat pump system with that of a geothermal heat pump system was compared experimentally in [15,16]. Comparing the two systems, the results show that the geothermal system could save 43% of the energy consumed by the traditional system during the heating period (winter) and 37% during the cooling period (summer).

Many researchers are interested in the development of the EAHEs. Some research has shown the importance of coupling the EAHE to building for air conditioning and found that the temperature at the outlet of the EAHE is very acceptable to provide comfortable indoor environment [17–19]. An experimental and theoretical study was performed to indicate the influence of the burial depth in the ground, length, diameter of exchanger and flow velocity on the performance of geothermal energy in [20]. A transient one-dimensional heat transfer model, for predicting the effect of the operating parameters on the performances of the EAHE was developed in [21,22]. A conic basket ground heat exchanger (CBGHE) coupled to a geothermal heat pump was utilized for greenhouse cooling and it was found that the use of this geometric form of the exchanger provides good results [23–27].

The aim of our study is to reduce the consumption of electric energy used for air conditioning in the buildings in the El Oued region by using renewable energy available in the area, which is geothermal energy. An experimental study was performed with a helicoidally water–air heat exchanger (HWAHE) to select the most appropriate air flow rate for the utilization of geothermal energy effectively. The novelty of this work is the use of abundant wells in the region of El Oued to refresh or heat

* Corresponding author.
E-mail address: hadjadjabdessami@gmail.com (A. Hadjadj).

https://doi.org/10.1016/j.tsep.2020.100548
Received 16 August 2019; Received in revised form 9 April 2020; Accepted 10 April 2020
2451-9049/

Energy Conversion and Management 288 (2023) 117186

Contents lists available at ScienceDirect

Energy Conversion and Management

journal homepage: www.elsevier.com/locate/enconman

Solar photovoltaic power prediction using artificial neural network and multiple regression considering ambient and operating conditions

Abdelhak Keddouda [a,b,*], Razika Ihaddadene [a], Ali Boukhari [c], Abdelmalek Atia [d], Müslüm Arıcı [e,f], Nacer Lebbihiat [d], Nabila Ihaddadene [a]

[a] University of M'Sila, Faculty of Technology, Department of Mechanical Engineering, 28000 M'Sila, Algeria
[b] Laboratory of Materials and Mechanics of Structure L.M.M.S, University of M'Sila, Algeria
[c] UDERZA Unit, Faculty of Technology, University of El Oued, 39000 El Oued, Algeria
[d] LEVRES Laboratory, Faculty of Technology, University of El Oued, 39000 El Oued, Algeria
[e] Kocaeli University, Faculty of Engineering, Department of Mechanical Engineering, 41001 Kocaeli, Turkey
[f] International Joint Laboratory on Low-Carbon and New-Energy Nexus Research and Development, Kocaeli University, 41001 Kocaeli, Turkey

ARTICLE INFO

Keywords:
Photovoltaic
ANN
Power output
Module temperature
Regression

ABSTRACT

This paper proposes artificial neural network (ANN) and regression models for photovoltaic modules power output predictions and investigates the effects of climatic conditions and operating temperature on the estimated output. The models use six days of experimental data creating a large dataset of 172,800 × 7. After data preprocessing, the appropriate attributes were selected as inputs and taken into account as features; solar irradiation, ambient air and module temperature, wind speed, and relative humidity, while the power generation as a target. In light of these data, the effect of training algorithm on the predictive performance of the ANN model was investigated. Results show that solar irradiation, ambient and module temperatures are key factors in predicting PV module power generation, as these variables are strongly correlated with PV power output. Moreover, the Levenberg-Marquardt algorithm was found to be the best training procedure. The ANN model demonstrated higher accuracy than the developed multiple linear regression models. However, the proposed Rational-Power-Law (RPL) and Power-Law (PL) models were able to capture the nonlinearity in the system, as assessed by coefficient of determination (R^2) and the Mean Absolute Error (MAE), and successfully supplied a very high level of precision. The ANN, and both RPL and PL models provided comparable performance, attaining an R^2 of 0.997, 0.998 and 0.996, and a MAE of 1.998, 1.156, and 1.242, respectively, when compared to experimental results. Furthermore, models proposed in this study were evaluated and compared with others available in literature and have demonstrated superior performance and better accuracy.

1. Introduction

Photovoltaic (PV) technology is one of the most convenient methods that affords the possibility to produce one of the most suitable and desired forms of energy, that is electricity, directly from the sun light. However, in terms of performance, this technology still does not provide that much of great deal, and that is the focus of science and engineering nowadays. The efficiency of this conversion process is influenced by a number of climatic and environmental factors, including solar radiation, wind speed, ambient temperature, humidity, and dust, all of which have an impact on the power generated by a PV panel [1–3]. The power output is a key factor for the reliability and stability of energy systems, as well as from an economical point of view. However, complexities and nonlinearity arise for that prediction, due to the fact that the relation between PV power production and those unpredictable and/or mostly correlated ambient conditions such as wind speed have essentially a non-deterministic character. Whenever working on forecasting and prediction problems, regression and statistical analysis are more likely to be encountered, besides to machine learning and data science. This fact is owed to advances in those sciences, in data collection and storage techniques, and to modern computing power. To address the difficulties of forecasting PV power generation and overcome its stochastically and uncontrollability nature due to fluctuations and uncertainty in solar irradiation [4], researchers and engineers are more and more taking advantage of recent innovations in machine learning, data science and

* Corresponding author at: University of M'Sila, Faculty of Technology, Department of Mechanical Engineering, 28000 M'Sila, Algeria.
E-mail address: abdelhak.keddouda@univ-msila.dz (A. Keddouda).

https://doi.org/10.1016/j.enconman.2023.117186
Received 8 March 2023; Received in revised form 26 April 2023; Accepted 11 May 2023
Available online 18 May 2023
0196-8904/